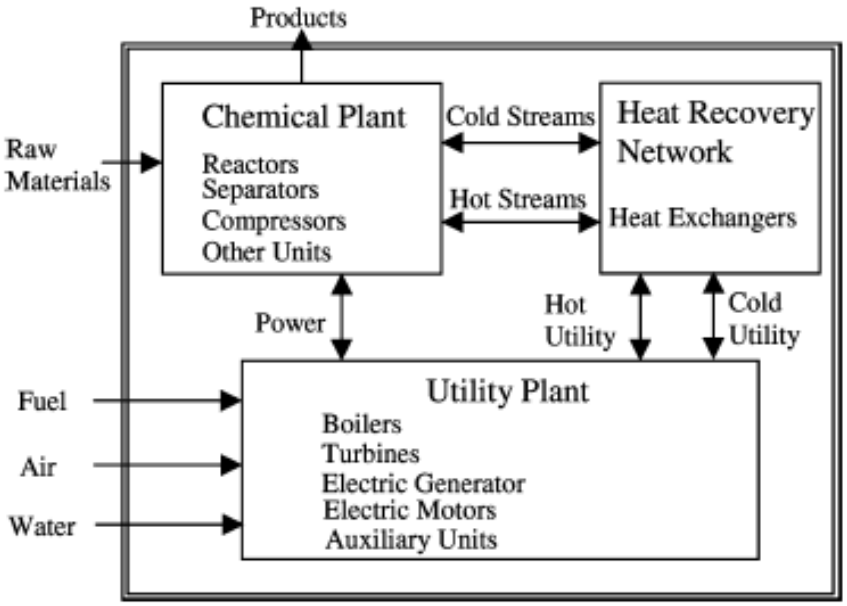

Figure 1: Total processing system.

heat exchangers, aims to recover heat from hot streams to heat cold streams. Maximizing heat recovery in the heat recovery network can bring down both energy consumption and consequently flue gas emission from the utility plant. Therefore, reduction in energy consumption requires the optimization of the heat recovery network, i.e. heat exchanger networks. Advanced heat exchanger technologies can improve the efficiency of heat exchanger networks. Such technologies include compact heat exchangers, multi-stream heat exchangers, heat transfer enhancement, mini- and micro-heat exchangers, etc. [4]. Using these technologies, current processes can be improved and the final energy demands can be reduced.

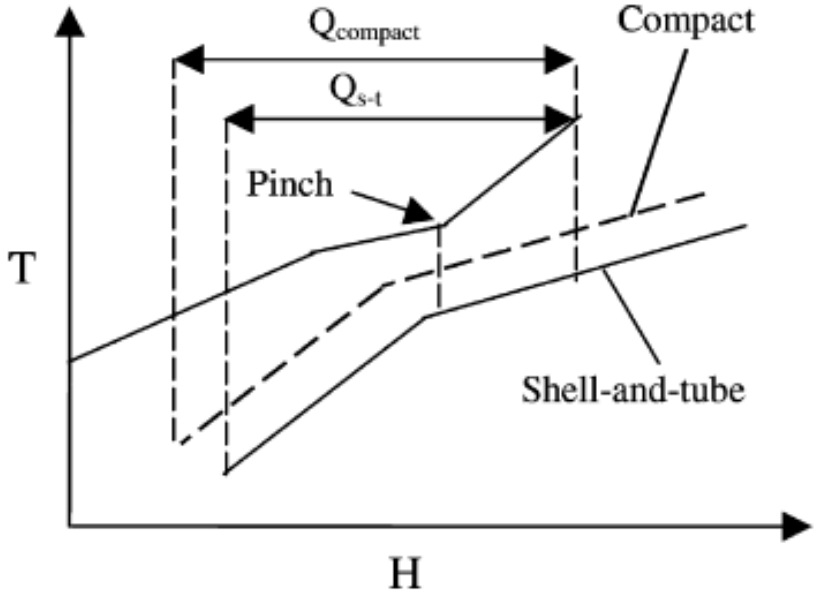

Figure 2: Composite curves.

3 Improved efficiency of energy conversion

There are many ways to improve the efficiency of thermal power plants, but heat transfer and heat exchangers play a significant role in all means. This can be highlighted by considering as an example a power plant that uses gas turbines. The original Brayton cycle for the power plant only needs a compressor, a combustion chamber and a power turbine; this concept can be found in any textbook on thermodynamics, e.g. Cengel and Boles [9]. However, the thermal efficiency is usually very low in such systems, and improvements can be made by employing the concept of intercooling, recuperation (regeneration) and reheating. Such a flow sheet is illustrated in Fig. 3, and the corresponding thermodynamic cycle is shown in Fig. 4. Two stages of gas compression are provided to reduce the power consumption for compression due to the lower inlet temperature of the gas in the second compression stage by using an intercooler. Because the compression power required is reduced, the net power output is certainly increased. The concept of recuperation is the utilization of energy in the turbine exhaust gases to heat the air entering the combustion chamber, thus saving a certain amount of fuel in the combustion process. This will certainly increase the overall thermal efficiency as well. In addition, the turbine output can be increased by dividing the expansion into two or more stages, and reheating the gas to the maximum permissible temperature between the stages. Although the power output is improved, the cost of additional fuel will be heavy unless a heat exchanger is also employed. These concepts can be also seen in the thermodynamic cycle in Fig. 4. The cycle 1-2-3-4-1 corresponds to the simple Brayton cycle. The cycle 9-11-12-2 represents the intercooling and the cycle 15-14-13-4 represents the reheating. The cycles 4-7-12-5 and 4-6-2-5 represent recuperation in the case of intercooling and no intercooling, respectively. This concept has already been incorporated in some real gas turbines, e.g. LMS100 from GE makes use of an intercooler, Mercury 50 from Solar Turbine makes use of a recuperator and GT24/26 from ASLTOM uses sequential combustion. These features significantly increase the efficiency of gas turbines, and a great deal of work has been done for the design of reliable heat exchangers that are operated at higher temperatures.

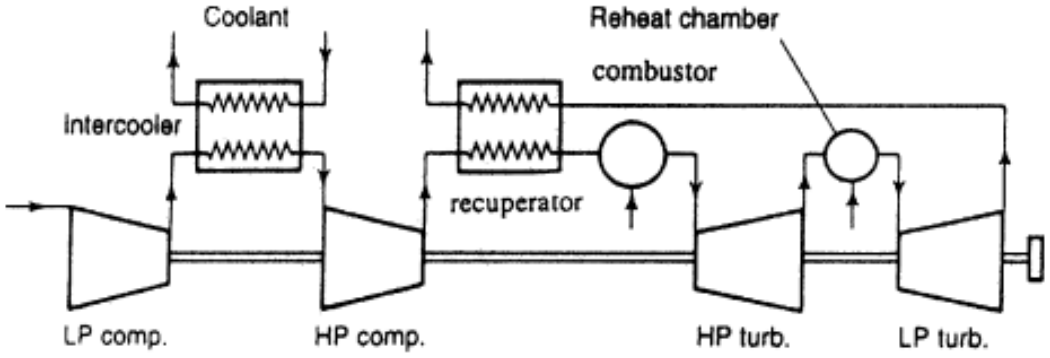

Figure 3: Power plant with intercooler, recuperator and reheater.

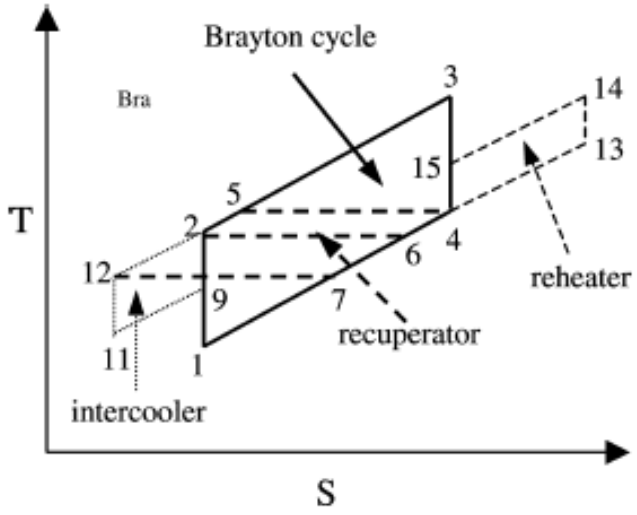

Figure 4: Thermodynamic cycle of a gas turbine power plant with intercooler, recuperator and reheater.

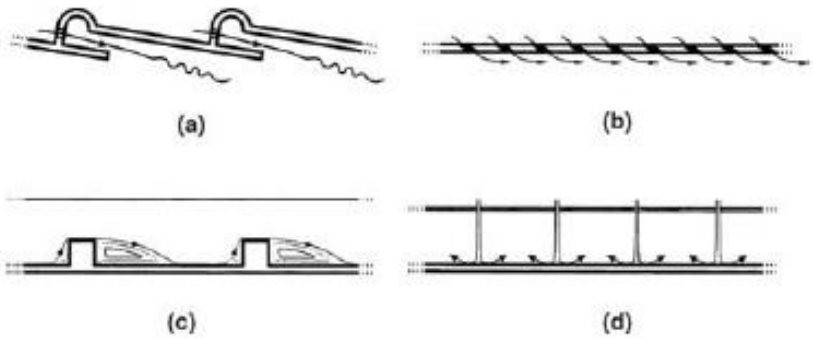

Figure 5: Cooling concepts of combustion chamber: (a) Film cooling; (b) Transpiration cooling; (c) Enhanced convective cooling; (d) Impingement cooling.

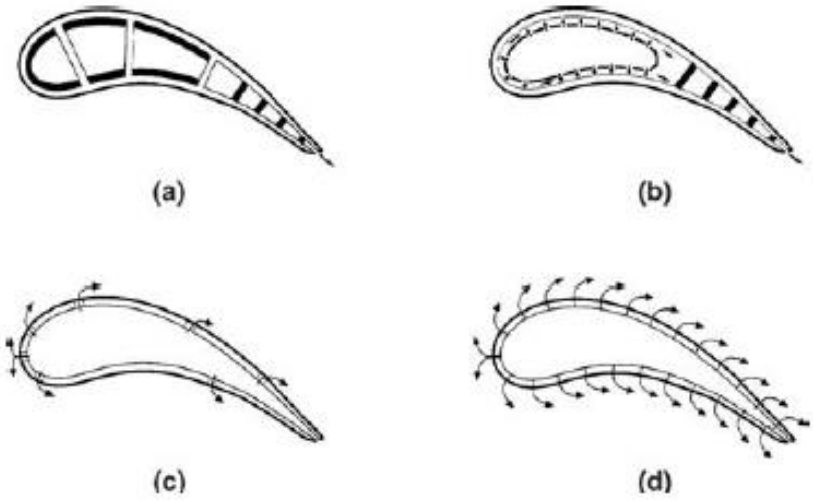

Figure 6: Cooling concepts of gas turbine blade: (a) convection cooling; (b) impingement cooling; (c) film cooling; (d) transpiration cooling.

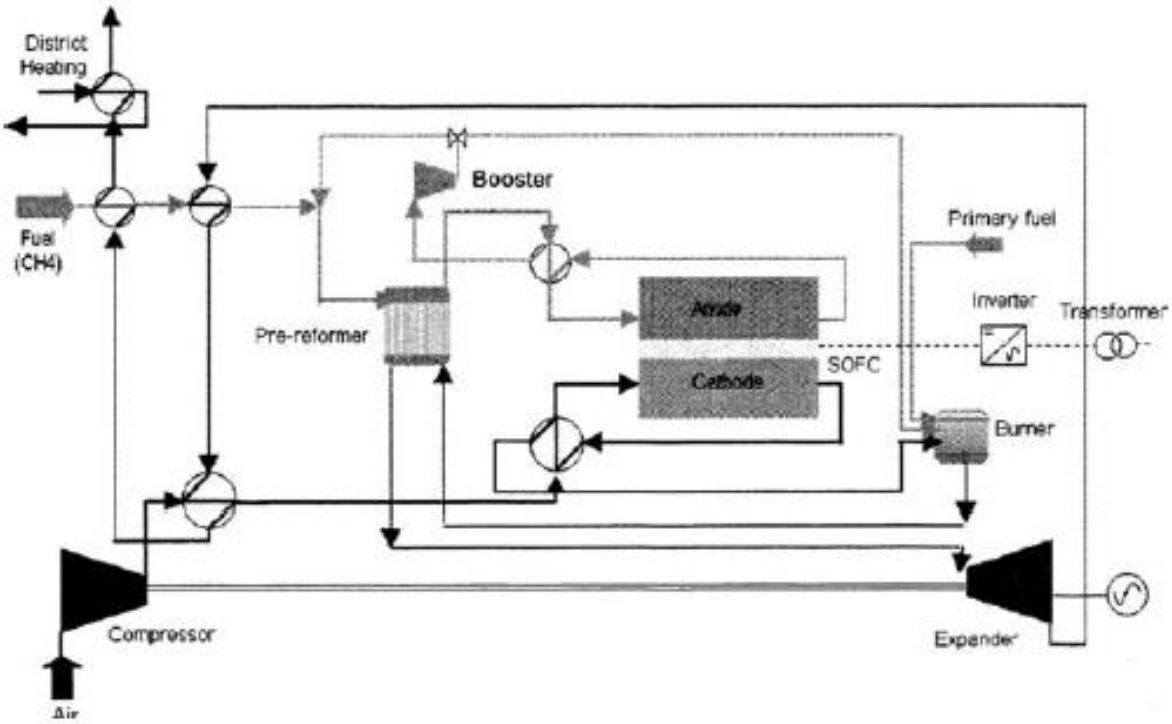

Figure 7: Reference fuel cell and gas turbine system layout [11].

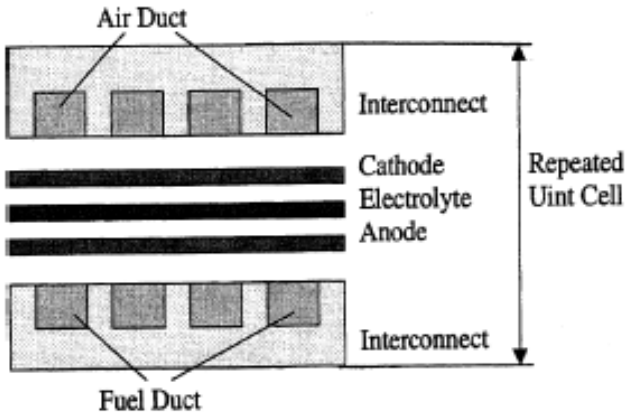

Figure 8: Structure of a unit of a fuel cell.

The above analysis demonstrates that high efficiency of power conversion can be reached with the help of relevant heat transfer and heat exchanger technologies. Therefore, attempts to provide compact, efficient heat transfer methods and heat exchangers and at the same time allowing a cheap and relatively simple manufacturing technique are real challenges for research.

4 Use of renewable energy

Hydropower, biomass, wind and solar energy are regarded the most important renewable and sustainable energy sources. Hydropower is, of course, dependent on the earth's contour, and it is not substantial for those countries with flat earth surface. Biomass appears to be an attractive option for many countries, and technologies for the conversion of biomass into electricity and heat are highly similar to the technologies for other solid fossil fuels. Wind and solar energies are strongly fluctuating sources, but they are very clean, with no pollutant emissions and have received great attention. In these renewable energy systems, heat transfer and heat exchangers play an important role as in those systems described earlier.

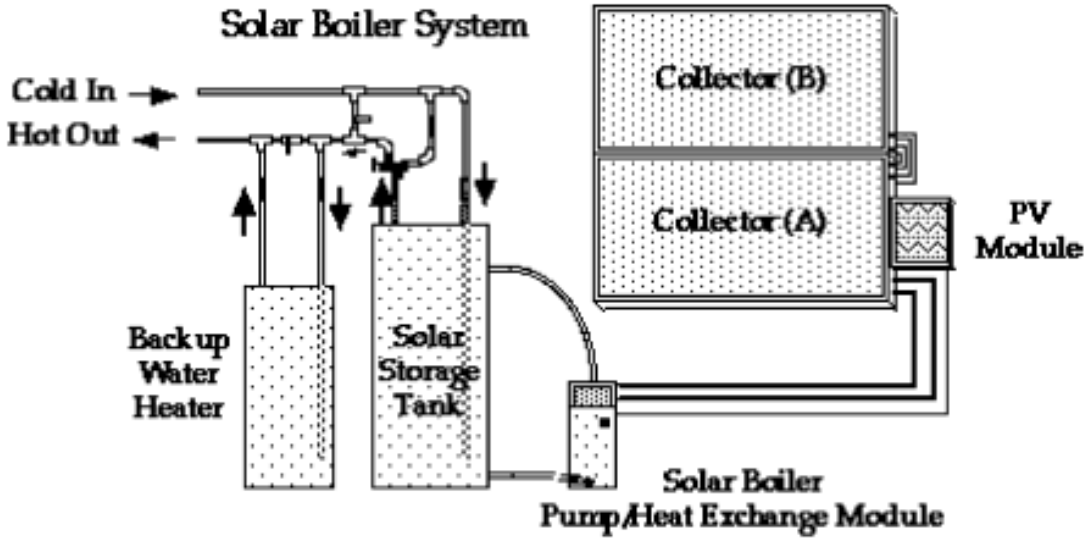

Figure 9: A solar energy system (from Solar-Works Inc.).

5 Reduction of emission and pollutant

Heat transfer and heat exchangers are also important in reducing emissions and pollutants. As illustrated earlier, they play an important role in the development of sustainable energy systems. The reduction of final energy consumption means less prime energy (e.g. fossil fuels) consumption, which results in overall reduction in emissions and pollutants. Improved efficiency of power plants certainly also reduces the primary energy consumption as well as the consequent emissions. Alternative fuels like biofuels (including biomass and waste utilization) are said to be neutral in terms of CO_2. The other renewable energy sources – solar, hydropower and wind – simply are clean enough and no emissions exist at all. In addition, by considering the pressure drop and associated pressure losses (work loss) in the heat transfer processes and attempting to reduce it, the consumption of electricity will be decreased, which is also beneficial. Therefore, heat transfer and heat exchangers are important for the protection of the environment, with regard to their role in the development of sustainable energy system.

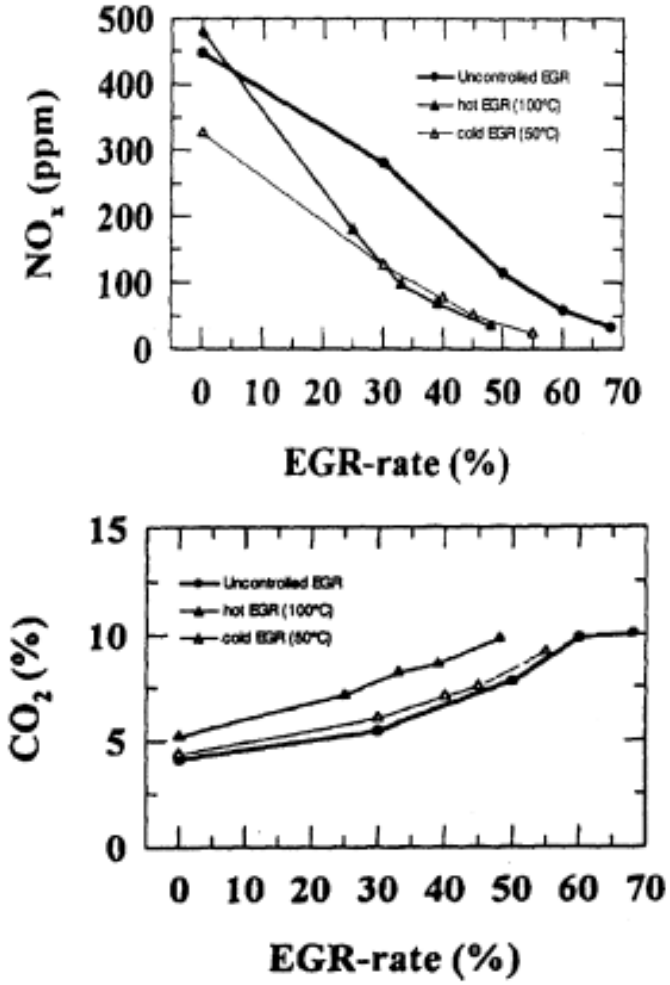

Figure 10: Effect of cooled EGR on NO_x and CO_2 emissions [12].

6.2 High temperature heat exchangers

High temperature heat exchanger technology has become important for improving the performance of power generation. There is a need to develop various type of high temperature heat exchangers in different applications such as hydrogen production, reforming process of solid oxide fuel cells, generation of high temperature gas, low emission power plants. In this section, monolithic heat exchangers are considered and some specific problems are addressed.

6.2.1 Monolithic exchangers

6.2.1.1 Ceramic monolith structures Ceramic monolith structures are used in the industry today and they are produced in large numbers by using the extrusion technique. They are unibody structures composed of interconnected repeating cells or channels (Figs. 17 and 18). They are increasingly under development and evaluation for many new reactor applications [14, 15], e.g. chemical process and refining industries, catalytic combustion, low emission power plants. However, monoliths are mainly used where only one fluid flows through all the channels. An example is the monolithic exhaust structure in automotive applications. In endothermic and slow reactions such as steam reforming of hydrocarbons, large amounts of heat are needed to maintain reaction rates. If the catalysts were deposited on tubes, usage of monoliths would be more efficient, leading to greater reaction rates and a smaller reactor [16]. Additionally, there would be a great improvement in mechanical integrity. Especially, it would be advantageous if two fluids in monolithic channels can exchange heat and/or mass. The reason why monoliths are not widely used in these applications is because of complex technique for feeding and distributing the two fluids in and out of the channels.

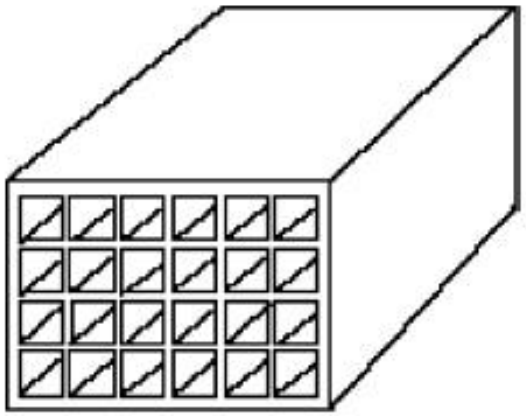

Figure 17: Monolithic 'honeycomb' structure.

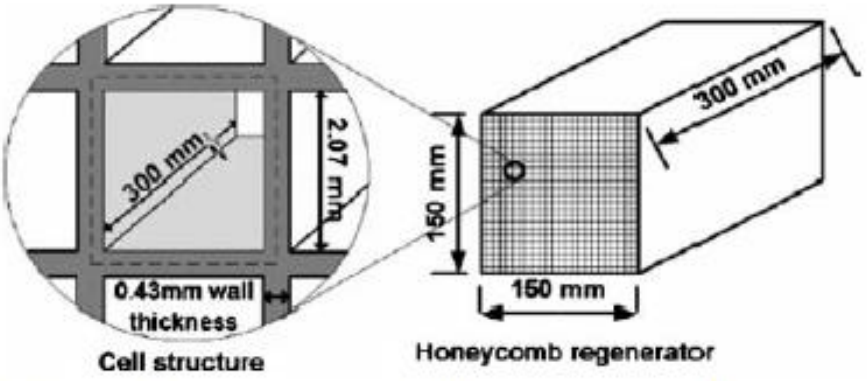

Figure 18: Honeycomb regenerator and dimensions of solid material and flow path. The dashed line binds one symmetrical cell.

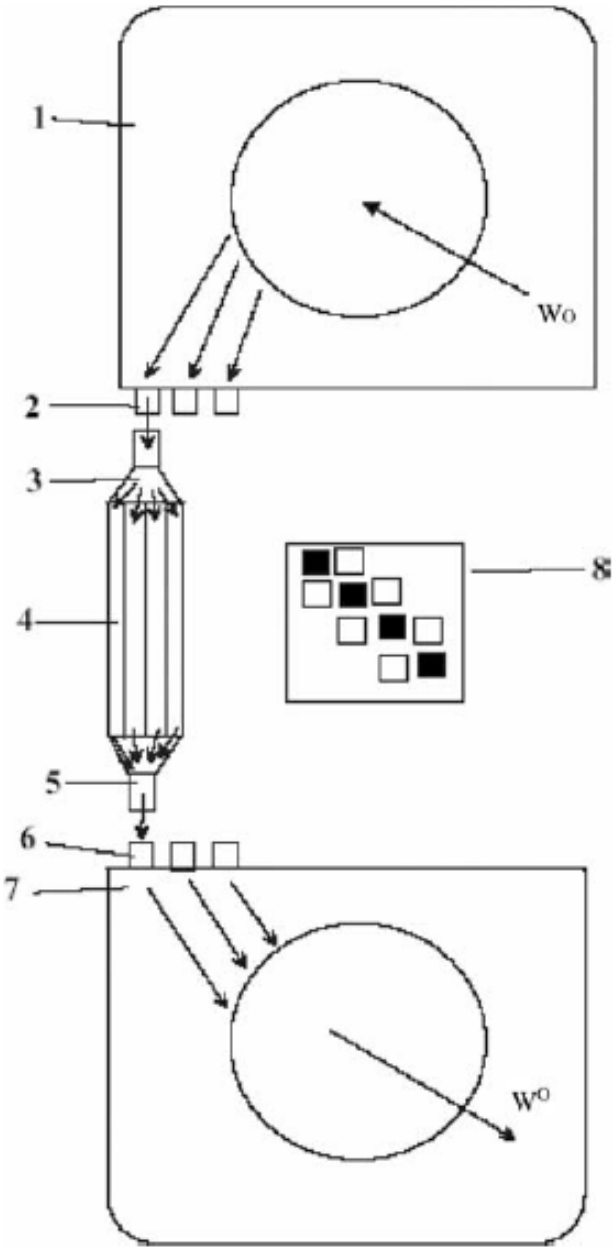

Figure 19: I-type manifold assembly: 1 and 2 – manifold top, 3 – dividing plates, 4 – monolithic channels, 5 – collecting plate, 6 and 7 – manifold bottom, 8 – checkerboard channel arrangement.

6.3 Heat load prediction in combustors

Different phenomena such as complex flow field and heat release by combustion are involved in the heat transfer process in combustion chambers. This section concerns prediction of heat load and wall temperature in a gas turbine combustor by taking different phenomena into account. Two-dimensional axisymmetric models were used to model the flow field and combustion in a premixed combustor with two different cooling schemes. The k–ε turbulence model and Eddy Dissipation Concept were used for modelling turbulent flow and combustion, respectively. In the modelling of heat transfer through the walls, a conjugate heat transfer formulation was applied. The temperatures calculated by the models were compared with experimental data. The results showed that in the mid part of the liner, the prediction of the wall temperature is good, although worse agreement is found in other parts. In addition, radiative heat transfer has been studied. The results showed that radiative heat transfer in simple and ribbed duct cooling schemes can increase the average inner wall temperature up to 33 and 40 K, respectively.

Here computational fluid dynamics (CFD) simulations are used to, first, predict the temperature and heat transfer rate to the combustor wall (called liner wall hereafter) by using a conjugate heat transfer method and, second, study quantities of convective and radiative heat transfer in this type of combustor. The analysis is carried out on a VT4400 LPP combustor developed by Volvo Aero Corporation. A slightly simplified geometry is used to simulate this combustor and some experimental data of inner and outer liner wall temperatures were provided to validate the simulation results.

6.3.2 Governing equations and solution methods

To model the flow field, continuity and Navier–Stokes equations were solved. The turbulence was modelled by solving the transport equations for the turbulent kinetic energy and turbulent dissipation, which are implemented in the standard k–ε model. The summarized governing equations are listed in Table 2.

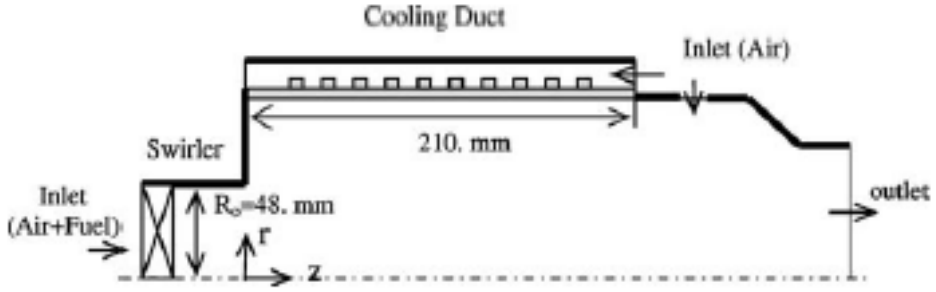

Figure 20: The combustor model for the case of ribbed duct.

Table 2: Governing equations in general form.

$$\frac{\partial(\rho\phi)}{\partial t}+\frac{\partial(\rho U_j\phi)}{\partial x_j}=\frac{\partial}{\partial x_j}\left(\Gamma_\phi\frac{\partial\phi}{\partial x_j}\right)+S_\phi$$

φ	$\Gamma\varphi$	$S\varphi$	Eqn
1	0	0	(2)
U_i	$\mu+\mu_t$	$-\frac{\partial P}{\partial x_i}+\frac{\partial}{\partial x_j}\left((\mu+\mu_t)\left(\frac{\partial U_j}{\partial x_i}-\frac{2}{3}\frac{\partial U_k}{\partial x_k}\delta_{ij}\right)-\frac{2}{3}\rho k\delta_{ij}\right)$	(3)
h	$\mu/Pr+\mu_t/Pr_t$	$\frac{\partial P}{\partial t}-\frac{\partial q_{R,j}}{\partial x_j}$	(4)
Y_α	$\mu/Sc+\mu_t/Sc_t$	$\dot{\omega}_\alpha$	(5)
k	$\mu+\mu_t/\sigma_k$	$P_k-\rho\varepsilon$	(6)
ε	$\mu+\mu_t$	$f_1C_{1\varepsilon}\frac{\varepsilon}{k}P_k-\rho\varepsilon f_2C_{2\varepsilon}\frac{\varepsilon}{k}$	(7)
		$\mu_t=\rho f_\mu C_\mu k^2/\varepsilon$	

Note: The indices in eqn (3) are not correct for the first velocity gradient.

6.3.3 Results and discussion

6.3.3.1 Flow and temperature fields The axial velocity and temperature fields inside the liner and before mixing with the secondary air are shown in Fig. 21. As can be seen, the velocity changes sharply close to the swirler with negative values near the liner wall. The sharp variation is mitigated along the length of the liner. At $z/R_0 = 1.5$ (about 74 mm along the liner), the velocity profile starts to change direction near the wall and therefore a stagnation point is formed. By further increase in z/R_0, the velocity is stabilized in the new direction and its profile in the radial direction will be flattened.

Similar to the velocity field, the temperature field varies sharply close to the swirler. The main reason for the variation is the combustion of fuel in the region

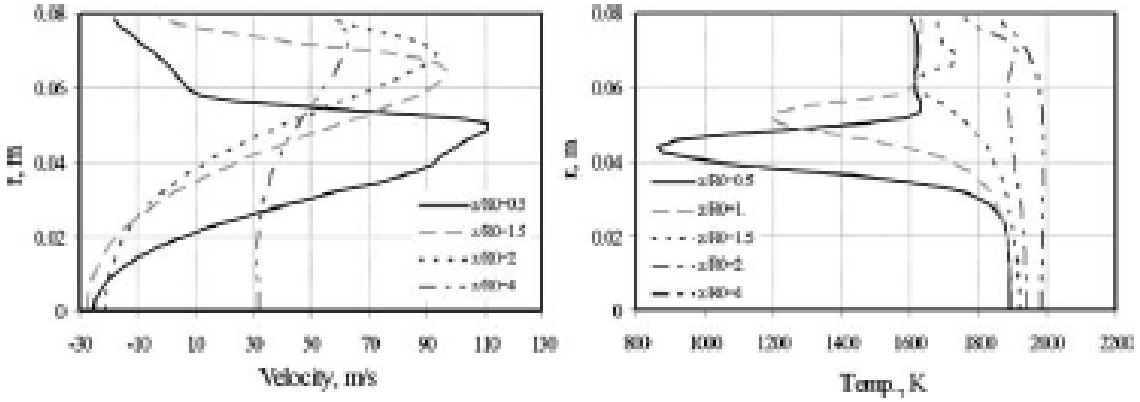

Figure 21: Axial velocity (left) and temperature (right) fields inside the liner, simple cooling duct case, without radiation.

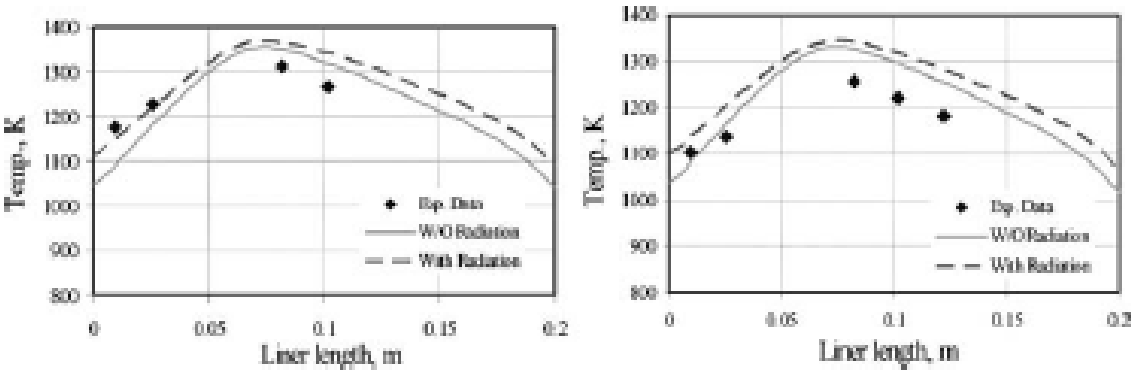

Figure 22: Temperature distribution at inner (left) and outer (right) liner wall in a simple cooling duct.

6.4.1 Types of models

The most common turbulence models for industrial applications are classified as

- zero-equation models,
- one-equation models,
- two-equation models,
- Reynolds stress models,
- algebraic stress models and
- large eddy simulations (LES).

Figure 26: Conjectured flow pattern in a duct with bumps.

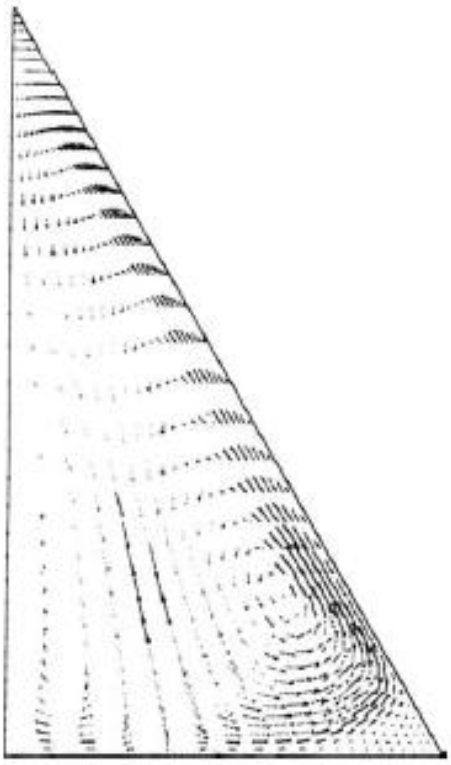

Figure 27: Secondary flow velocity vectors in a cross sectional plane midway over a corrugation element.

CHAPTER 2

Advanced technologies for clean and efficient energy conversion in power systems

A.K. Gupta
Department of Mechanical Engineering,
University of Maryland, College Park, MD, USA.

Abstract

Efficient fossil energy use with low pollution in all kinds of power plants is of growing interest in all industrial sectors. The use of energy is growing steadily by many countries worldwide due to the greater desire to enhance standards of living and increase productivity. Efficient energy use is favorable for better productivity, product quality, costs, and quality of human life but the energy use adversely impacts our environment. During the past decade, energy demands from China and India have grown significantly and are projected to grow even more in the coming decades as they enhance their living standards and productivity. This clearly requires close examination of the available methods of fossil fuel energy conversion as well as advanced methods that will provide increased efficiency and pollution reduction. After a brief review of the historical perspectives on energy conversion, this chapter reviews the various methods used for energy conversion in industrial power plants as well as new innovative methods that are now becoming available with significant fuel saving, compact size of the equipment and low pollution. As an example, high-temperature air combustion technology has seen wider acceptance in many kinds of industrial furnaces, in particular for use in the steel industry and fuel reforming furnaces with demonstrated energy savings of about 30% (on average), about 25% reduction in the size of the equipment (compact size), about 50% reduction in pollution and better quality of the product produced. Such significant energy savings were only dreams of engineers in the past. This technology has been adopted by many countries worldwide. In addition, advanced technologies are developed or being developed for use with coals (and solid fuels) since its cost based on energy content is low compared to gaseous fuels such as natural gas. Several commonly used methods in power generation are presented along with integrated and hybrid systems for increased efficiency.

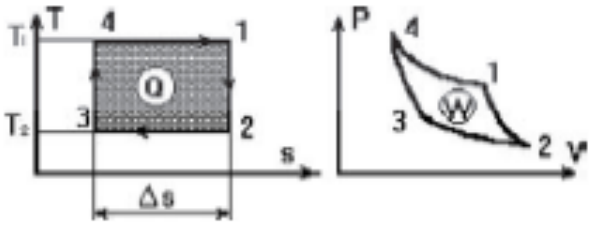

Figure 1: *T*–*S* and *P*–*V* diagrams for the Carnot cycle.

they are today. The progress on technology and industry was slow until a sound knowledge on thermodynamics became established in the 19th century. The development of nuclear power was in the second half of the 20th century based on the theoretical and experimental knowledge gained during the first half of the last century. The Table reveals that fundamental R&D has made a significant impact on the energy conversion needs in a range of areas for power, propulsion and transportation.

2.1 Basic energy conversion concepts

We now consider the basic concept of energy conversion using steam and air as the working media. The Rankine cycle is accepted as the basic standard for steam power plants. Before considering Rankine cycle, we consider Carnot cycle, as this cycle provides maximum possible efficiency. The ideal diesel cycle is a gas cycle and the Carnot cycle is a cycle for all fluids. The Carnot cycle provides the foundation for the second law of thermodynamics and the concept of irreversibility. The temperatures of the heat source and heat sink in this cycle provide thermal efficiency of a reversible cycle. Carnot cycle is hypothetical, as one cannot build a reversible engine. Figure 1 shows Carnot cycle on a *T*–*S* diagram consisting of four processes. Process 1 is reversible adiabatic compression (3-4). Process 2 consists of reversible constant temperature heat addition (4-1). Process 3 consists of reversible adiabatic expansion (1-2).

Finally, the process 4 consists of reversible constant temperature heat rejection (2-3). The thermal efficiency of the Carnot cycle can be determined. One must note that for the reversible case the magnitude of entropy change during heat addition and heat rejection are equal so that $T_H = T_1$ (or T_4) and $T_L = T_2$ (or T_3) since the heat transfer between the heat source and the working fluid occurs at no temperature difference. The Carnot cycle thermal efficiency is given by

$$\eta_{th} = (Q_A - |Q_R|)/Q_A$$

$$= \Delta W_{net}/Q_A$$

$$= T_H(S_2 - S_3) - T_L(S_2 - S_3)/T_L(S_2 - S_3)$$

$$= (T_1 - T_2)/T_1 = 1 - (T_2/T_1)$$

3 Energy and power generation

The amount of energy used as well as the distribution of different kinds of energy used to produce power in the world is given in Fig. 2. Coal oil and gas remain the major sources worldwide. Renewable energy accounts for about 11.5% of the world primary energy and presently provides only about 2.1% of the power generation. Since the amounts of fossil energy available are limited, we must make all the efforts to utilize the available energy at the highest efficiency possible. Most simple cycle power plants have efficiency of the order of about 30–35%. This is because all practical cycles are not reversible and therefore have some efficiency (or entropy production) associated with them. As an example, all turbines and pumps are never isentropic and so we must seek novel means to minimize the isentropic losses. Therefore, a design engineer always has a goal to maximize the efficiencies (or minimize the isentropic losses) by making some modifications to

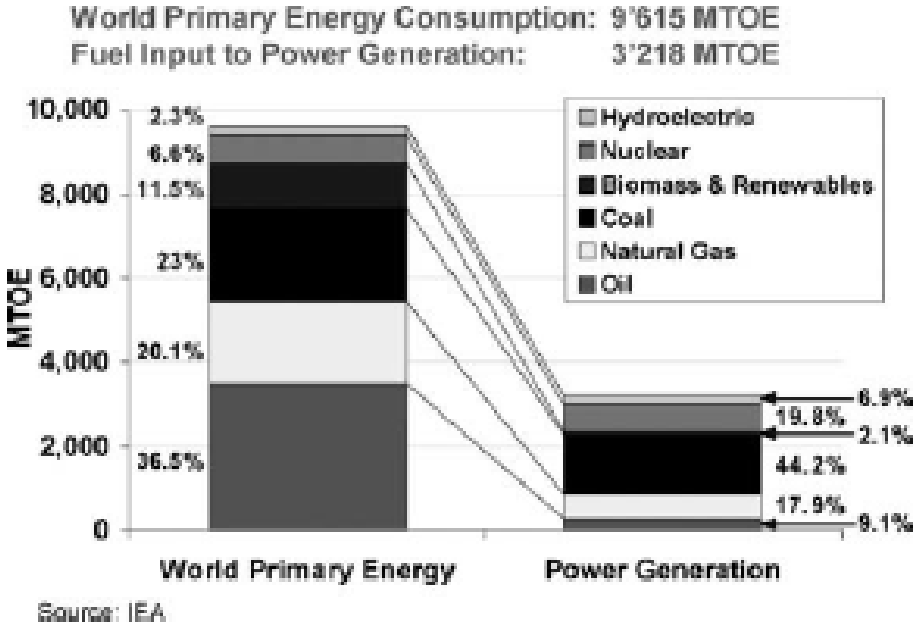

Figure 2: World primary energy into power generation. (Source: IEA.)

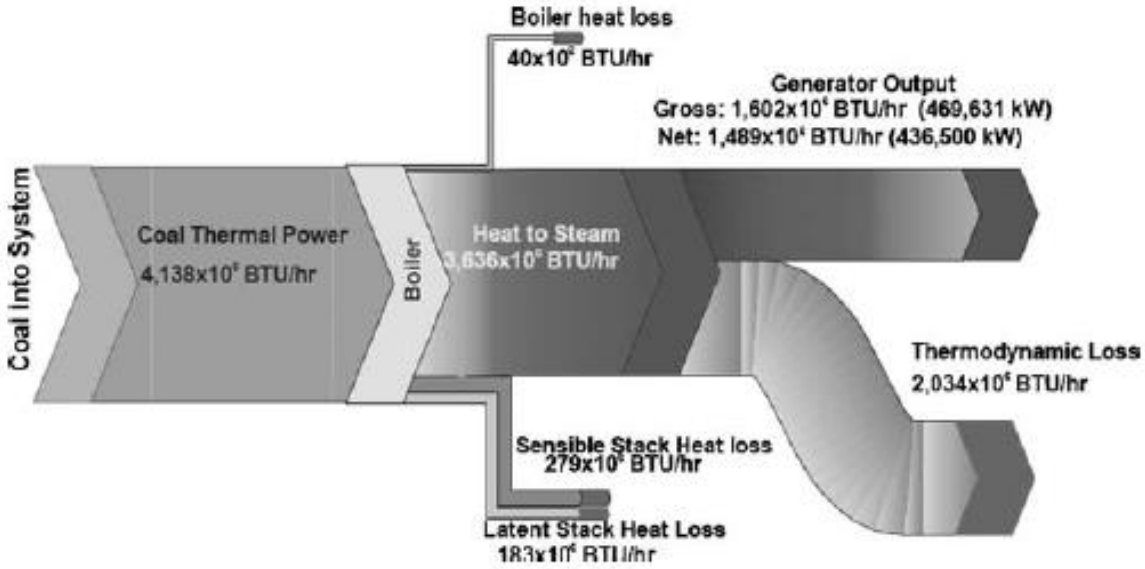

Figure 3: Major thermal energy power usage per unit time from a pulverized coal fired unit with no carbon capture.

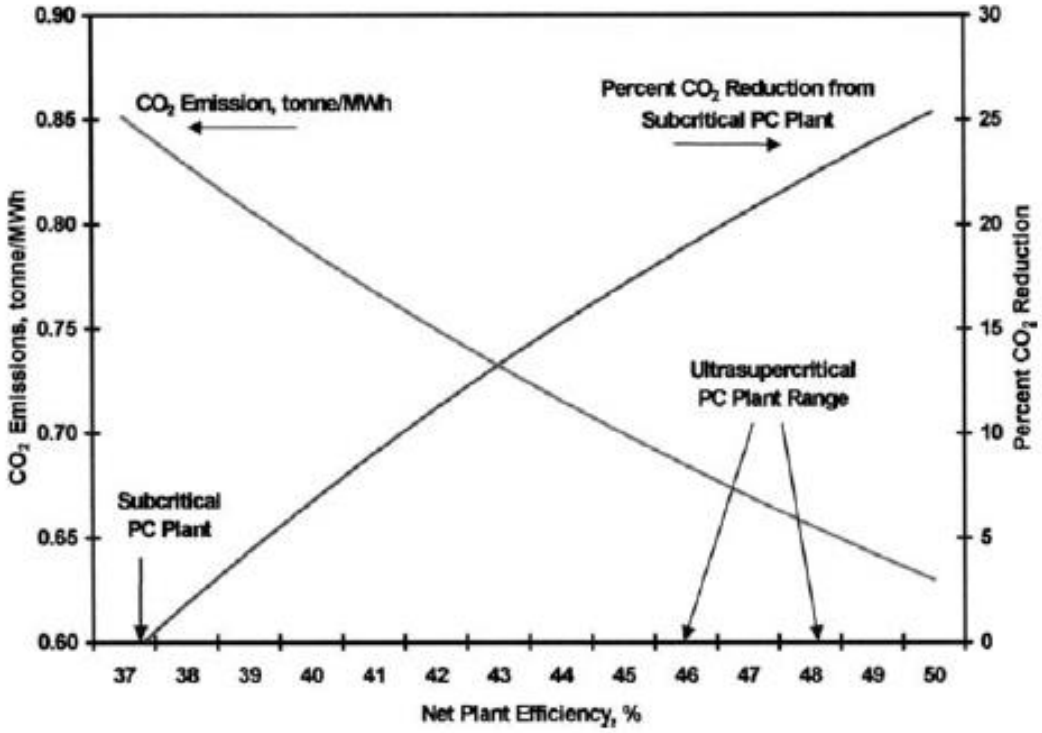

Figure 4: Net plant efficiency vs. carbon dioxide emission (based on firing Pittsburgh #8 Coal) [3]. PC: pulverized coal.

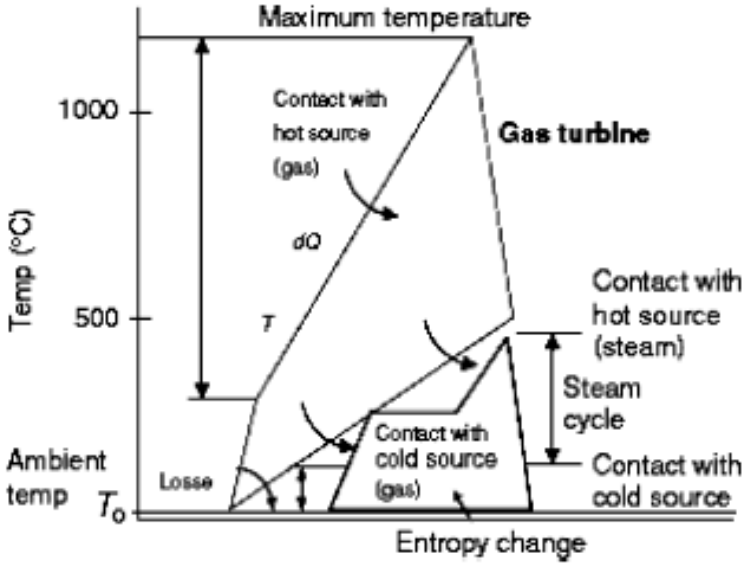

Figure 5: Temperature–entropy (T–S) diagram of combined cycle having Brayton cycle gas turbine and Rankine steam turbine cycle [1].

4.3 Other methods to increase efficiency

The area under the P–V curve (see Figure 1) provides the net power output from the plant. Therefore, operation at higher pressures and heat rejection at lower temperature provides an increase in net power output. In Rankine cycle, this has been used much in the industry. Many of the European power plants operate at supercritical steam temperatures, while the North American plants are typically operated at lower steam temperatures. The increase in power plant efficiency associated with higher pressures and temperatures, as well as reducing the discharge at lower pressures and temperatures, results in higher efficiency. This is illustrated in Fig. 6. Plant operation at higher temperatures and low back pressure can increase the plant efficiency significantly.

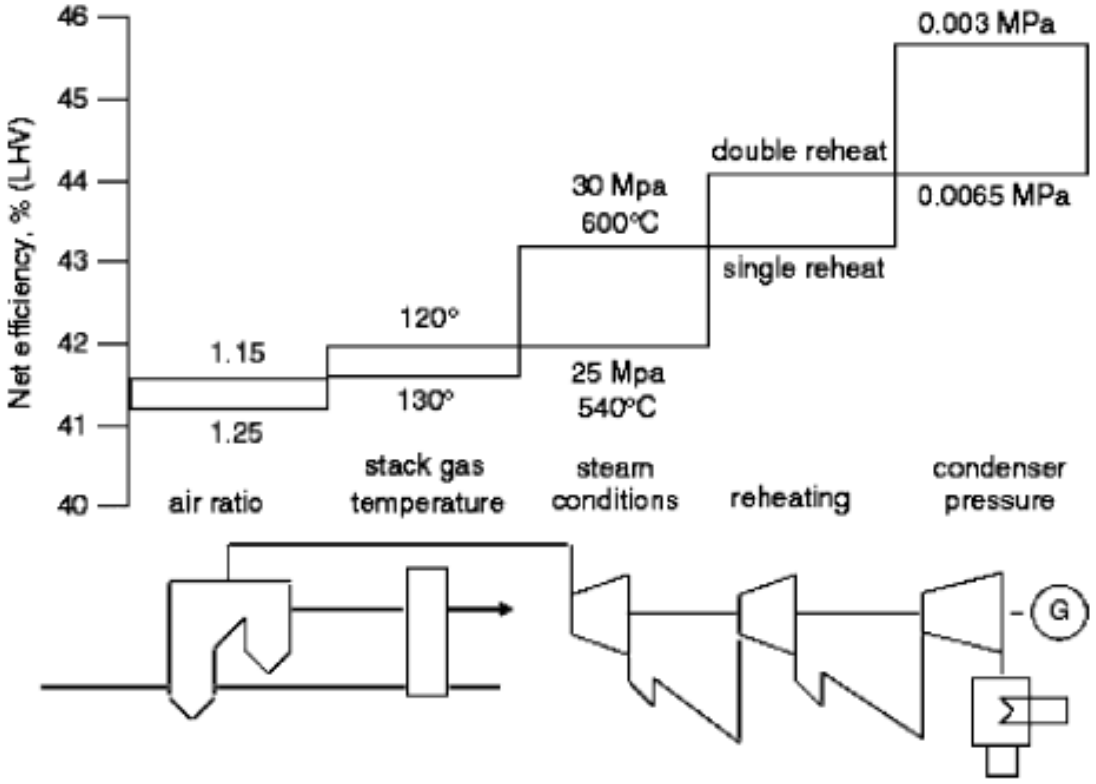

Figure 6: Increase in plant efficiency using various techniques.

4.4 Waste heat recovery for improving efficiency

Plant efficiency increases with decrease in heat losses from the stack, operation at higher temperature and pressures, combined heat and power systems, use of integrated energy conversion systems.

In the combustion zone, not all the heat is used to produce power. In practical power plants, much of the heat is lost via the stack or tail end of the boiler or power plant, see Fig. 7. By utilizing much of this waste heat, significant gains in the thermal efficiency can be obtained. The characteristic efficiency of a power plant is only about 30%.

However, by utilizing the waste heat, significant increase in plant efficiency can be achieved. The extent of waste heat from a plant varies with the type of plant. This is because, for each application, there is certain temperature range of interest, see Fig. 8.

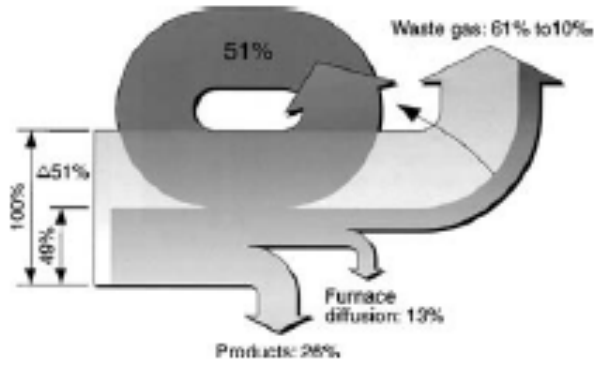

Figure 7: Waste heat from furnaces and potential improvement methodology.

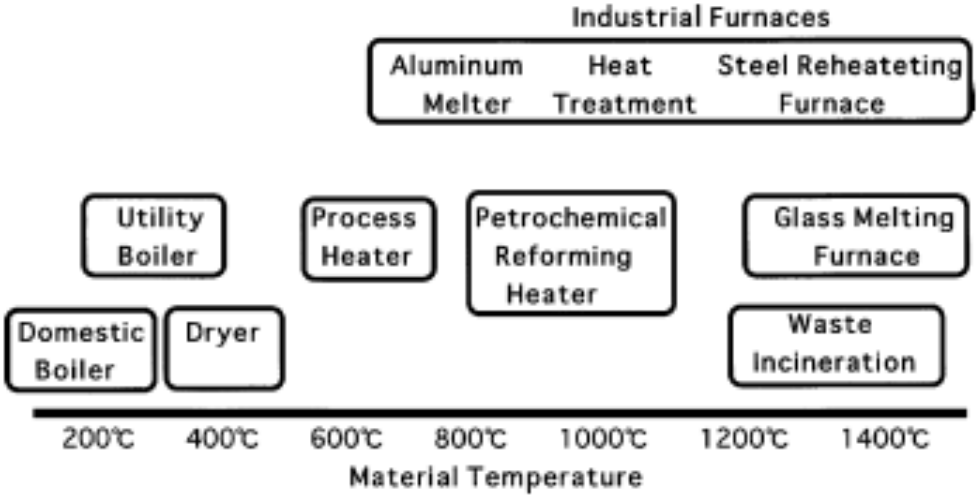

Figure 8: Temperature range of interest for various applications.

5 High temperature air combustion technology

Recent advances on high temperature air combustion (HiTAC), also called colorless distributed combustion or flameless oxidation, have demonstrated significant energy savings, higher and uniform thermal field, lower pollution including noise, and smaller size of the equipment for a range of furnace applications. In HiTAC, combined heat and gas recirculation are used to provide high temperature and low oxygen concentration so as to enlarge and control the flame thermal behavior. This technology has shown promise for much wider applications in various process and power industries, energy conversion and waste to clean fuel conversion. For each application, the flow, thermal and chemical behavior of HiTAC flames must be carefully tailored to satisfy the specific needs. Sample results are given from a few diffusion flames using high temperature combustion air. A specially designed regenerative combustion test furnace facility, built by Nippon Furnace Kogyo, Japan, was used to preheat the combustion air to very high temperatures. The flames with highly preheated combustion air were significantly more stable and homogeneous (both temporally and spatially) compared with the flames with room temperature or moderate temperature combustion air. The global flame features showed the flame color to change from yellow to blue to bluish-green to green to colorless or flameless distributed in the entire combustion zone over the range of conditions examined. In some cases, hybrid color flame was also observed. The flameless or colorless oxidation of the fuel was observed only under certain conditions. Very low levels of NO_x along with negligible levels of CO and hydrocarbons (HC) have been obtained using HiTAC. The thermal and chemical behavior of HiTAC flame depends on air preheats temperature, oxygen concentration of air, fuel chemical property and fuel–air mixture preparation. Waste heat from a furnace in HiTAC technology is retrieved and introduced back into the furnace using a regenerator. These features help save energy, which subsequently also reduce the emission of CO_2 (greenhouse gas) into the environment. Flames with high temperature air provide significantly higher and uniform heat flux than normal air, reduce noise, reduce the equipment size or increase the material throughput for the same size of the equipment. The HiTACHiTAC technology has shown practical demonstration of significant energy savings (up to about 60%), downsizing the equipment (about 25%), pollution reduction (about 50%), and low noise (about 7 dB) in practical systems. Fuel energy savings directly translate into reduction of CO_2 and other greenhouse gases to environment. HiTAC has been used to demonstrate fuel reforming at high efficiency and also clean conversion of wastes to hydrogen-rich syngas and also liquid fuels.

5.2 Benefits of HiTAC technology

5.2.1 Energy saving

HiTAC technology uses regenerative heat exchangers to extract thermal energy from the waste gases in the combustion products. Ceramic honeycomb or balls have been shown to provide good energy storage heat media heat exchangers. Honeycomb type heat exchanger is more effective than ceramic ball type, as this provides larger surface area, low-pressure drop and high efficiency. Exhaust gases from industrial furnaces and processes represent one of the major heat losses from the system. The regenerative media used in the HiTAC devices recovers large amounts of thermal energy from the exhaust gases, which can then be transported back to the combustion zone. The amount of energy recovered translates directly into fuel saving. In the 'High Performance Industrial Furnace Development' project [2, 30], the objective was to demonstrate significant energy savings (about 30%) using regenerative media, reduce physical size of the equipment by about 25%, and pollutants emission reduction (about 50%). Indeed the HiTAC technology has demonstrated average energy savings of about 30% from industrial furnaces. This goal was successfully demonstrated using 167 field demonstration tests [7, 33] with energy savings of 150,000 kiloliters of fuel. Now this technology is used in many countries worldwide.

5.2.2 CO_2 reduction

The role of CO_2 in global warming phenomena is now widely recognized. The demands for reducing CO_2 emission are higher than ever before. All fossil fuels

contain carbon, which generates CO_2 as a byproduct during the combustion of carbon so that any efforts to reduce energy consumption will directly translate into reduction of CO_2 emission. Good correlation between fuel consumption and CO_2 production suggests that CO_2 reduction should be nearly the same as energy saving [33].

5.2.3 NO_x reduction

Emission of NO_x is now known to be responsible for the destruction of ozone layer in the upper atmosphere. In addition, N_2O emission is of concern from combustion systems (for example in low temperature combustion devices, such as fluidized bed, that produce several tens of ppm of N_2O. This gas has 296 times more greenhouse gas potential than CO_2. NO_x (primarily NO and NO_2) involves the complicated reaction mechanisms, which result in accelerating the ozone depletion in the oxygen cycle on earth. Therefore, combustion engineers have focused their attention on developing various strategies to reduce NO_x emission and improve the combustion process. HiTAC is one of the most advanced techniques because of low levels of NO_x formation and emission, significant energy savings and uniform thermal properties in the entire combustion space [7, 22, 24, 33].

5.3 Basic principle of HiTAC technology

5.3.1 Thermodynamic consideration of combustion process

Flame temperature is one of the important factors for considering combustion efficiency and energy conversion efficiency. Weinberg [4] provided the initial concept of excess enthalpy combustion. In his study, limitations on combustion temperature were discussed, including both positive and negative factors associated with combustion temperatures in a certain range. Heat circulation from the exhaust gases, using high-efficiency heat exchanger, was adopted to increase the combustion temperature thus allowing the combustion of low heating value fuels that could otherwise not be combusted without using auxiliary fuel. However, combustion engineers have to pay attention to the upper limit of the combustion temperature because of material constraints used in the equipment and/or pollution formation at higher temperatures, in particular NO_x. Various possibilities on enthalpy intensification have been described [5]. From the economic point of view, it is of course better to use thermal energy generated by combustion process itself to heat-up the oxidant or fuel, which is often of low thermal energy, than via the use of electrical or mechanical energy.

The amount of combustion-generated energy circulated into the combustion process is given as [4]:

$$\int_{T_0}^{T_f} C_p dt = Q_c + Q_a = H_t - H_0$$

where T_f is the final temperature, T_0 is the initial temperature, Q_c is the heat release by chemical energy conversion, Q_a is the energy added, H_t and H_0 are the enthalpies at two states. The circulation part of thermal energy from combustion-generated products will increase the combustion temperature and so the enthalpy of the reaction zone will be above the conventional combustion level. This has resulted in the use of the term called "excess enthalpy combustion."

Increase in thermodynamic efficiency must be coupled with other desirable characteristics, such as low NO_x formation, reliability of the equipment and refractory material, and spatial uniformity of temperature. Nonetheless, the heat circulation and excess enthalpy methods provide new light on next generation of advanced energy conversion technology and combustion chamber design. This method provides new ideas to control temperature in the combustion zone. The method is independent of the fuel composition, and can simultaneously satisfy the demands of high combustion intensity and reduced pollutant formation from fuels, including low-grade fuels.

5.3.2 Basics of excess enthalpy combustion design

Excess enthalpy combustion can be realized by internal or external circulation or their suitable combination. Most designs for internal heat circulation use bluff body, porous media or swirl to the flow. Most of these are aimed at flame stabilization [19] and are very effective. Internal heat circulation relies on heat convection

and species circulation so that pool of hot and active radicals in reaction zone can be maintained, which also assists in flame stabilization.

The external circulation methods use heat exchanger to transfer the thermal energy via conduction between combustion products and solid media so that heat can be exchanged to the cool reactants. Most of the enthalpy contained in hot combustion products can be recirculated back to the combustion process. This allows one to utilize much of the waste energy for flame stabilization.

5.3.3 Excess enthalpy combustion and high temperature air combustion

Thermodynamic considerations suggest that preheating the oxidant to very high temperatures (not fuel due to possible fuel decomposition and safety) increases the cycle thermal efficiency. Air preheats add enthalpy to the combustion zone. From the point of pollutant formation, especially NO_x, high temperature of combustion has been recognized as one of the most important parameters for high levels of NO_x emission. This then requires method to control the emission of NO_x. One method of maintaining the same temperature in the combustion zone is to dilute the incoming combustion air with hot combustion products to cause mild combustion condition. Partial recirculation of hot products into the incoming combustion air dilutes the inlet concentration of oxygen in the air. This diluted air lowers the peak flame temperatures with negligible oxidation of N_2. Further examples of this are given in refs. [5, 7, 20, 33].

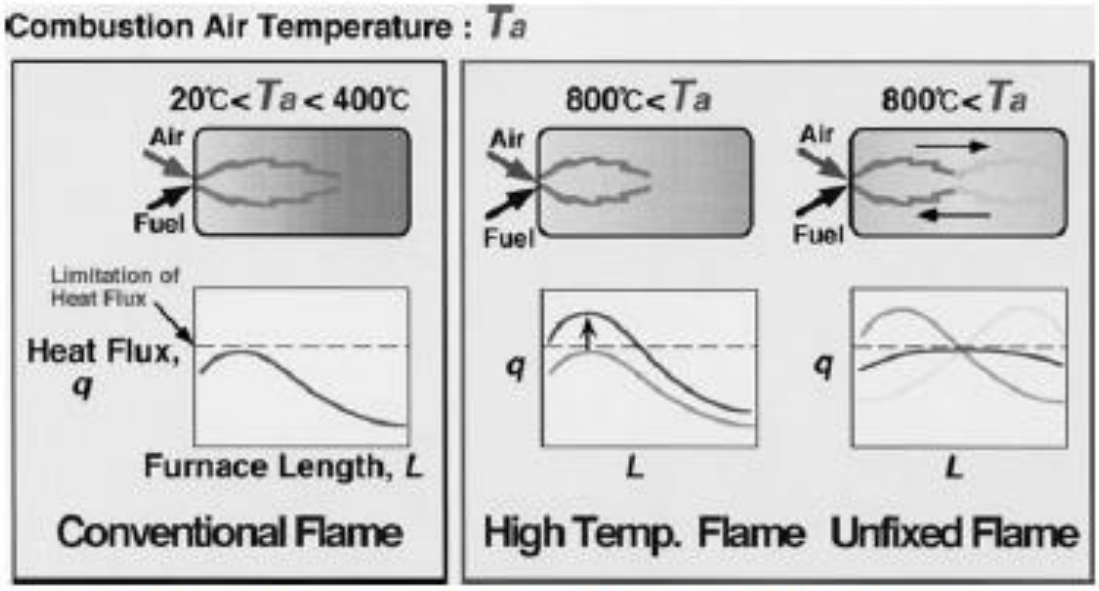

Figure 9: A schematic diagram of flame and heat flux distribution in a furnace with low temperature combustion air, high temperature air, and high temperature and low oxygen concentration air HiTAC condition.

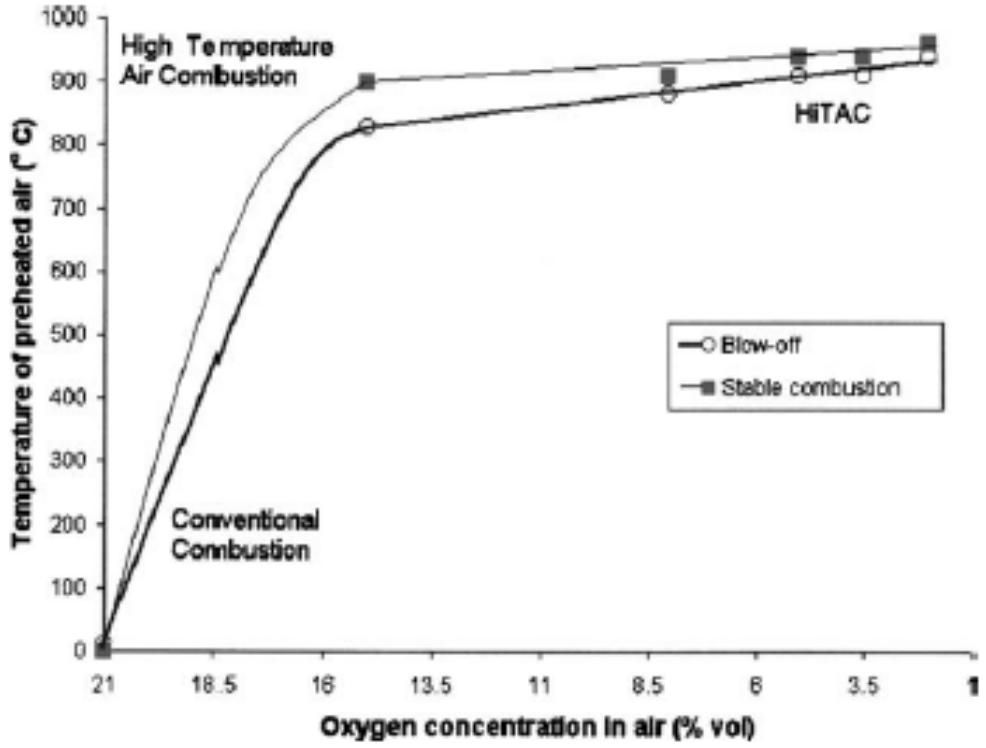

Figure 10: Stability limits of the propane flame as a function of air preheat temperature (heat recirculation) and oxygen concentration in air (flue gas recirculation).

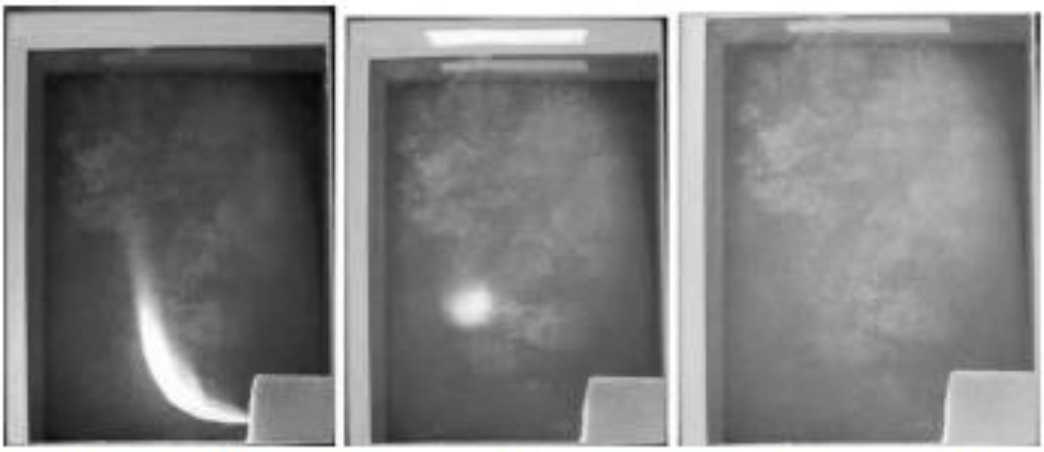

Figure 11: Methane flame photographs with combustion air temperature of 1000°C and oxygen concentrations (from left to right) of 21%, 8% and 2%, respectively. Note the colorless combustion in the extreme right side flame photograph.

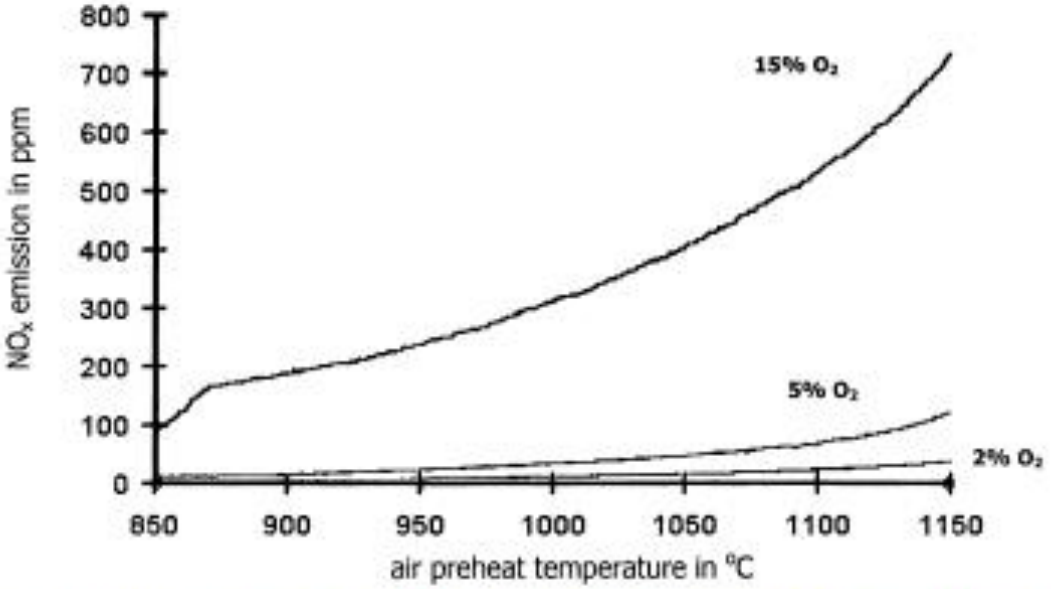

Figure 12: NO_x emission as a function of air-preheat temperature and O_2 concentration in air using propane fuel.

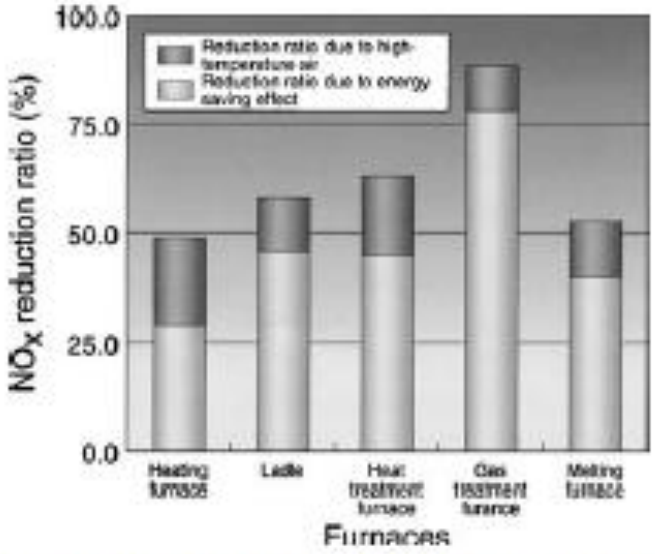

Figure 13: NO_x reduction obtained from the field test demonstration using HiTAC technology.

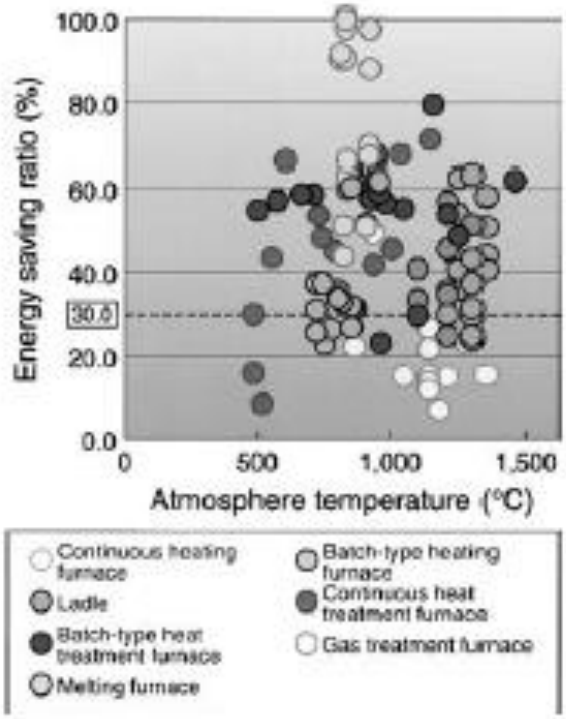

Figure 14: Energy savings demonstrated on different kinds of furnaces.

5.4.3 Energy savings

Field tests demonstrations in actual plants were carried out to determine the extent of energy savings from the use of HiTAC in furnaces. Several different kinds of industrial furnaces were used in the field test demonstration. These field

test demonstrations were carried out on 167 industrial furnaces over a duration of 2 years. The results are shown in Fig. 14. The energy savings are significant and depend on the type of application and furnace. The results clearly show average energy savings of 30% during the time duration. In some cases, nearly 100% energy saving is achieved as in the old furnace the low calorific value fuel gases could not be burnt with the result of nearly 100 energy recovery under HiTAC conditions. As a result of this demonstration, several other countries worldwide have accepted this technology as the most advanced technology demonstrated in the 21st century for significant energy savings and low pollution.

5.6 Waste fuel gasification and fuel reforming using HiTAC

Most of the HiTAC technology efforts have been for furnaces, boilers and waste fuel reforming [33]. Some of the near-term applications include the following:

1. Industrial furnaces used in the steel industry for melting, reheating, heat treatment and soaking, and for process heater, aluminum melters, petrochemical reforming, glass melting, drying, boilers, ceramic heater, and domestic boilers and heater.
2. Waste incineration/waste thermal destruction of solid and liquid wastes including wastes produced from municipal, industrial, yard, chickens, animals and farms. The technology is attractive for gasifying wastes, biomass fuels, and mixed wastes so that the gaseous fuel produced is clean and environmentally benign form of energy. High temperature steam gasification provides further benefits of higher heating value, higher hydrogen content, and high efficiency with minimum residue.
3. Fuel reforming and energy transformation to cleaner fuels for use in fuel cells and other power, propulsion and energy conversion applications.
4. Power production using micro-gas turbines with the combustion of low to medium gas produced from biomass and wastes.
5. Destruction of odors and certain pollutants.

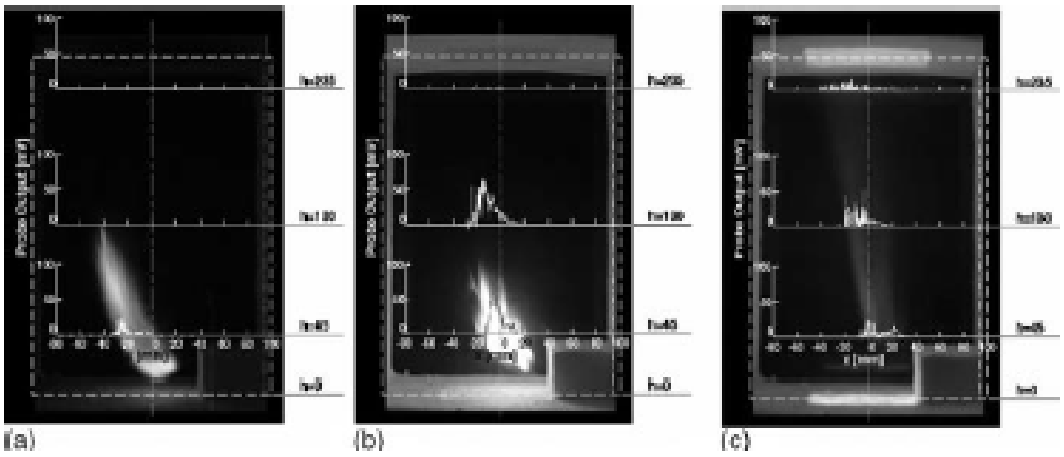

Figure 15: Direct flame photographs and flame ion concentration from (a) ordinary, (b) high temperature and (c) HiTAC flames.

5.6.1 High temperature steam gasification of wastes

The HiTAC technology can also be used to produce very high temperature steam that can be used for coal, biomass and wastes and low grade fuels to produce clean syngas. Under favorable conditions, very high molar concentrations of hydrogen can be produced from biomass and wastes. The tar produced with the use of high temperature steam is minimal. Sample results of the gas composition with paper as the solid fuel are given in Fig. 16. The experimental results provided the influence of elevated gasifying agent temperature on hydrogen yield in the gas composition. In general, the higher the steam temperature, the higher was the amount of hydrogen produced. This trend was true for all the solid fuels examined, including solid wastes, biomass, coal and agricultural wastes (rice husk, rice straw and corn cob). Methane gas production is an important component of syngas in the steam-assisted gasification. Steam gasification at low temperatures favors methane production. In contrast, at high gasification temperatures, hydrogen yield increases as shown in the sample results in Fig. 16. The HiTAC has been successfully demonstrated in Japan on a pilot plant fuel reformer to convert hydrocarbon fuels to hydrogen using high temperature steam.

6 Practical aspects of power generation

A by-product from all fossil fuel power generation is the emission of pollutants including the emission of CO_2 greenhouse gas. Historic and geographic data indicate that temperature of the earth has been increasing since the onset of the industrial revolution in the 1800s. The concentration of CO_2 is high compared to long-long- term historic levels and has been increasing very rapidly with the onset of industrial revolution, see Fig. 17. This correlates very well with the increased combustion of fossil fuels. The global temperature and CO_2 concentration correlate quite well as seen in Fig. 18. Change in global temperature as small as 1 K has a profound effect on weather patterns, distribution of flora and fauna, and such geographical phenomena as ocean currents and the sea level. Some of the CO_2 capture approaches for power include: (a) post capture (such as adsorption, absorption,

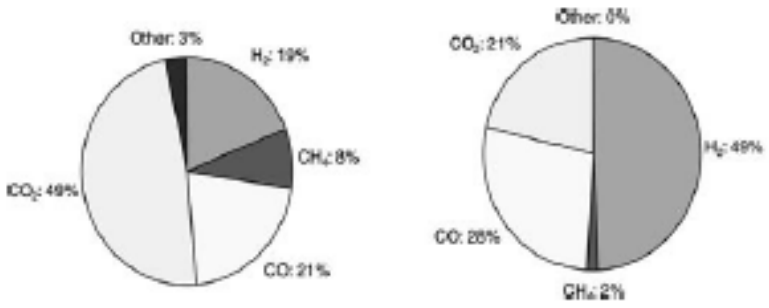

Figure 16: Chemical composition of the syngas produced by high temperature gasification of paper using steam at 700°C (left) and 1000°C (right).

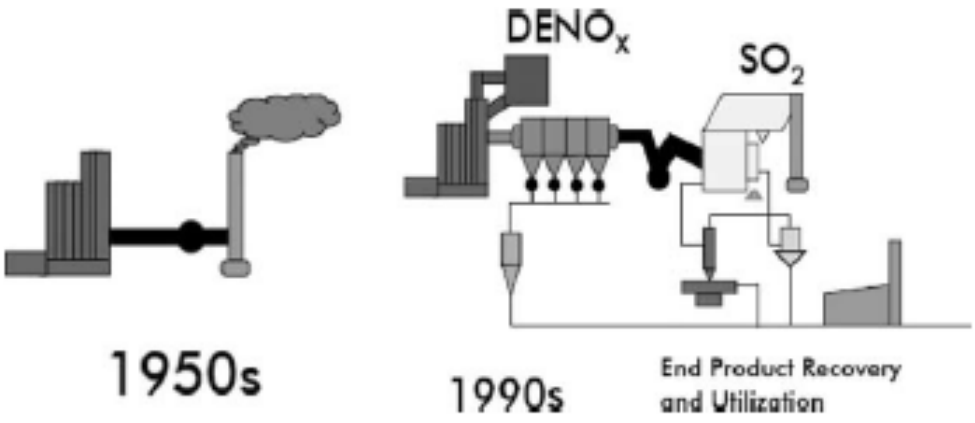

Figure 19: A schematic diagram of the power plant of the 1950s and 1990s.

natural gas is favorable for CO_2 mitigation. In case the fuel switching and other CO_2 mitigation options are not favorable, the CO_2 generated from a power plant can be sequestrated by capturing it from the tail end of the power plant and then sequestering it using either or some combination of sequestration approaches of: terrestrial ecosystems, geological storage in active oil beds, coal beds, depleted oil and gas wells, deep aquifers, mined caverns and salt domes.

In 2006, global CO_2 emission from fossil fuel use has shown an increase of about 2.6%. China topped the international CO_2 emission table in 2006 for the first time in history. Total CO_2 emission in China increased by 8.7% in 2006 compared to 1.4% in USA and almost unchanged in the EU-15 countries (the EU-15 had a decrease of 0.8% CO_2 emission in 2005). Even with this increase, the average Chinese emits 3.5 tons of CO_2 per year, whereas Britons emit nearly 10 tons and Americans 20 tons.

6.1 Pollutants emission

The emissions from a power plant depend upon the type of fuel used and the design and operational conditions of the power system. The older units in the 1950s had no pollution control device, while the 1990s unit had pollution control for particulate mater, NO_x, and SO_2. A schematic diagram of the 1950s and 1990s power plant is given in Fig. 19.

Fluidized bed uses crushed coal for power generation. Here the bed is kept low temperature (below 900°C) and the bed contains calcium-based sorbent material to capture SO_2 evolved during combustion. The NO_x emission is low since the combustion temperature in the bed is below the temperature at which thermal NO_x is formed. However, the emission of N_2O emission (a greenhouse gas that has more pronounced effect than CO_2 gas emission to the atmosphere) is a disadvantage since it is formed and propagates at low temperatures. Therefore, one must strike a balance to determine the favorable conditions for reducing N_2O emission and enhance sulfur capture.

7 Conclusions

Various methods of power generation, including some recent advances in power generation are presented. With the continued developments, very high efficiency thermodynamic efficiency can be achieved from fossil fuel combustion systems. Costs of coal and other solid fuels are more favorable than clean natural gas. However, with the recent developments in gasification and other

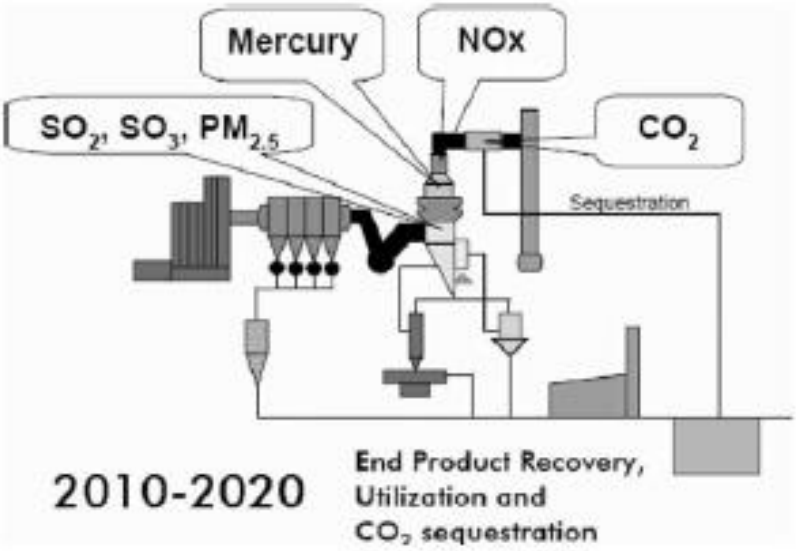

Figure 20: A schematic diagram of the future power plant with advanced pollution control including CO_2 capture and sequestration.

developments on integrated power systems, it is reasonable to achieve very high thermodynamic cycle efficiencies, close to 60%, with low pollution emission in the near future. Future large scale energy conversion systems are expected to have CO_2 capture technologies and sequestration so that one must seek innovative designs for advanced hybrid systems, which can potentially offer very high efficiency and low pollution emission.

CHAPTER 3

Virtual engineering and the design of power systems

D.S. McCorkle & K.M. Bryden
Department of Mechanical Engineering,
Iowa State University, Ames, IA, USA.

Abstract

The art and science of power system design is rapidly changing. Future power systems will have significantly lower emissions, operate at higher pressures and temperatures, utilize new fuels and new technologies, and be far more complex than current power plants. Power plant sensors and controls will be smaller and more capable, changing how power systems are operated and maintained. To achieve these goals, a new generation of power system design tools is needed. These tools will integrate all the models needed to describe and examine the performance of a power plant. This integration will be much more comprehensive than the current systems integration supported by process modeling software, in which simplified component descriptions are integrated into a complex system-level model of the power plant. Rather, these new engineering design tools will integrate micro-scale phenomena, component-level phenomena, and system-level demands to create an integrated hierarchy of models, which will simultaneously model all aspects of power system performance, operation, and maintenance. This integrated modeling environment will then be used to examine the impact of changes at the micro level on efficiency, emissions, and cost. These broadly integrated models will enable integrated optimization of power systems and will explicitly bring human judgment into the optimization and design of power systems during both design and operation. This chapter will examine how these virtual engineering design environments will be created and utilized to build a new generation of power plants. Examples of how virtual engineering is currently being used in the power industry will be given. In addition, the US Department of Energy's use of virtual engineering in the development of near-zero-emission power plants will be discussed.

1 Virtual engineering

Virtual engineering is an emerging technology that is growing in popularity. Virtual engineering seeks to create a virtual environment in which all aspects of engineering decision making can be addressed [1, 2]. The goal of virtual engineering is to enable a design team to alter the shape, size, or other characteristics of components within a power plant and immediately see the impact of the changes on systems throughout the plant. For example, an engineer seeking to modify a tangentially fired, pulverized coal furnace to co-fire coal and switchgrass could alter the burner configuration and immediately see the impact of the change on the performance of the furnace. In another example, an engineer could investigate the performance of a heat exchanger by altering the geometry, thickness, or spacing of any or all of the components and would immediately see the changes in heat transfer and fluid flow on both sides of the heat exchanger. Additionally, because the virtual engineering-based power plant is presented in a natural and accessible visual format, the design and changes can be readily shared with other plant stakeholders. This can provide a design platform that allows a number of concerns including those of construction, operations, maintenance, and engineering to be incorporated and tested before commitment to a physical plant. This will improve plant performance, reduce cost, and enable a wide range of new technologies to be readily incorporated into power plants.

The four key aspects of a virtual engineering environment are (1) the integration of models, data, and other engineering information to create a complete model of the system or component; (2) visualization of the resulting systems and information; (3) interactive analysis and design of the system, e.g. the ability to easily ask "what if" types of questions; and (4) high-level decision making tools.

- *Integration of models, data, and other engineering information* – All real systems are composed of a wide variety of models. Even a single component will need a number of models to describe the operation and performance. These models can range from simple integral models and algebraic expressions to detailed models of micro-scale phenomena. The first goal of virtual engineering is to couple these models together to create a single unified model that describes the behavior of a component. In addition, a power plant consists of a number of components. Each of these unified model sets describing a component's behavior needs to be assembled to create a complete plant. Currently, process simulation programs such as Aspen™ enable the user to link simplified models of components to create complex models of processing plants. The goal of virtual engineering is to take this one step further. First, a set of virtual components is created, each of which is composed of a suite of models. These virtual components are then linked to create a virtual system model that can understand how changes in one component impact the overall performance of the power plant. For example, a virtual pump may be composed of several models at varying levels of fidelity, including a computational fluid dynamics (CFD) model, a finite element analysis (FEA) model, a cavitation model, and a set of

pump curves. This virtual pump would then be coupled within the system to other virtual components, each of which is represented by an integrated set of models, to create a "complete" virtual system. The word "complete" does not imply that every detail is addressed by the virtual systems, though they could be, but rather that the virtual system can completely address the engineering questions that are being asked.

- *Visualization of the resulting systems and information* – Engineering experience and judgment are critical to the decision making process. Modeling results must be checked against experience to ensure that they are credible and usable. In addition, engineering judgment is needed to decide between various options with similar benefits and to include a variety of intangibles in the engineering process. While computer modeling can provide a variety of options and can help the engineer understand the consequence of various decisions, computational modeling cannot bring this needed engineering experience and judgment into the decision making process without human interaction. In the virtual engineering environment, the goal is to present the engineering system and information in a familiar, natural, and readily understandable interface that enables the engineer to quickly understand, explore, and design the system. Coupled with an appropriate expert (e.g. a design engineer, a plant engineer, or a construction manager), this can reduce design time and cost while resulting in better solutions.
- *Interactive analysis and engineering* – Today, nearly all aspects of power plant simulation require extensive offline setup, calculation, and iteration of a variety of separate models. The time required for each iteration for a single component can range from one day to several weeks. The results of the separate component analyses must then be integrated, often within the engineer's mind, to create an overall understanding of the system's response to various changes. This is a time consuming and inexact process. Tools are needed that enable the engineer to establish a dynamic thinking process to permit exploration of the 'what if'

solutions.

- *Interactive analysis and engineering* – Today, nearly all aspects of power plant simulation require extensive offline setup, calculation, and iteration of a variety of separate models. The time required for each iteration for a single component can range from one day to several weeks. The results of the separate component analyses must then be integrated, often within the engineer's mind, to create an overall understanding of the system's response to various changes. This is a time consuming and inexact process. Tools are needed that enable the engineer to establish a dynamic thinking process to permit exploration of the "what if" questions that are essential to engineering. In nearly all circumstances, an engineering answer now has a much greater value than an answer tomorrow, next week, or next month. Although many high-fidelity engineering analysis techniques have been developed, they are often not routinely used as a fundamental part of the engineering design, operations, control, and maintenance process because the time required to set up, compute, and understand the result, then repeat the process until an adequate answer is obtained, significantly exceeds the time available. This includes techniques such as CFD, FEA, and optimization of complex systems. Instead, these engineering tools are used to provide limited insight into the problem, to sharpen an answer, or to understand what went wrong after a bad design and how to improve the results next time. This is particularly true of CFD analysis. While faster, less expensive processors will provide faster solutions, we also need better algorithms that enable the engineer to understand the error in the analysis, automatically create needed reduced order models, and choose the right level of fidelity and accuracy to answer the question being asked.

- *High level engineering decision support tools* – Engineering is a process of making decisions for complex and uncertain systems. Therefore, tools that start with physics-based models and help the engineer understand the options and make the best decisions are essential to the virtual engineering process. The most commonly recognized decision support tools are optimization tools. Optimization tools require the user to provide a set of constraints in exchange for a set of best (or, in some cases, better) solutions that address a desired objective or set of objectives. Today, this process is generally hands-free in that the user specifies the needed conditions and preferences and then gets the results with human intervention, *a priori* interaction. Following the optimization process, the user specifies a new set of conditions based on the newly acquired information and repeats the process, *a posteriori* interaction. Once an optimized solution is found, it will often provide a starting place for further design or exploration. Because of this, tools are needed that support a paradigm of progressive interactions in which the engineering team works together in real time with the optimization process to direct the search for the needed design. Pro-

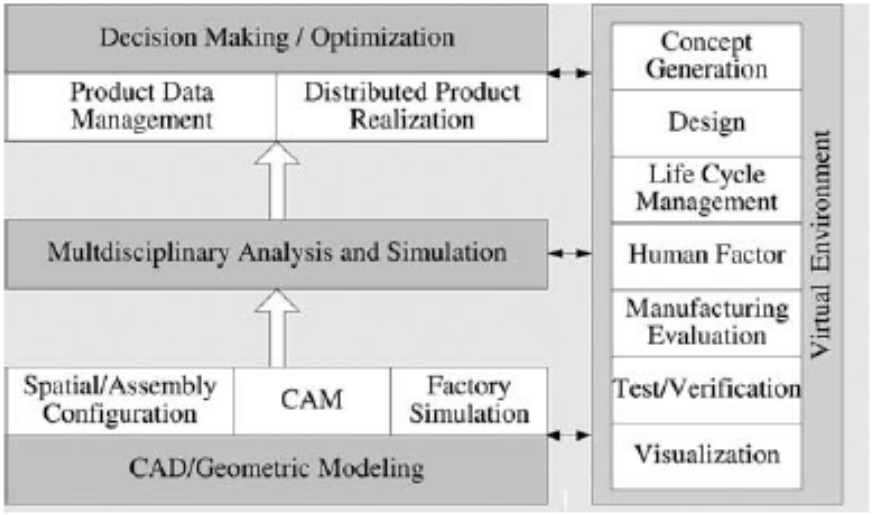

Figure 1: Framework of the virtual engineering system [4].

surface geometry to be altered interactively. Virtual cursors enable interaction with geometry surfaces, allow surface points to be displaced and material to be added or removed, and provide exact control of surface normals at specific points. The resulting surfaces are NURBS-based and can be exported to various CAD or analysis programs. Applications coupling virtual environments and engineering tools have been developed for assembly [6], hose routing [9], and design of three-dimensional mechanisms [7].

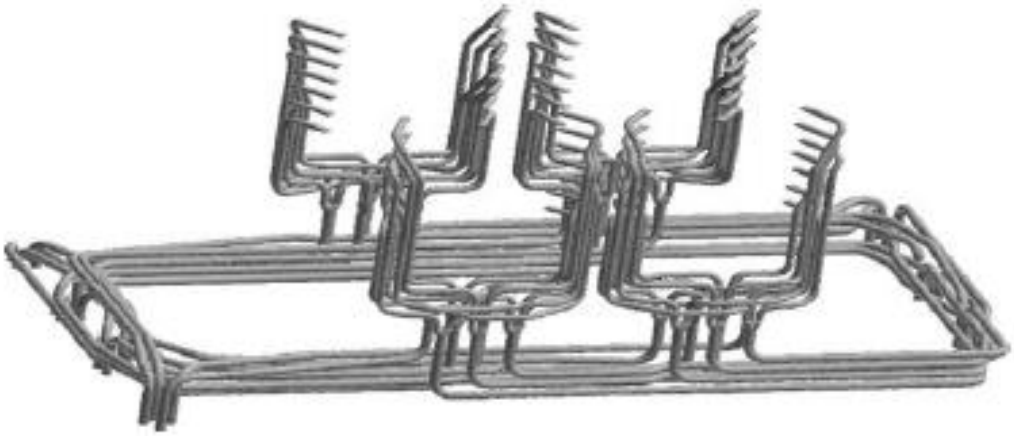

Figure 3: Coal piping being analyzed.

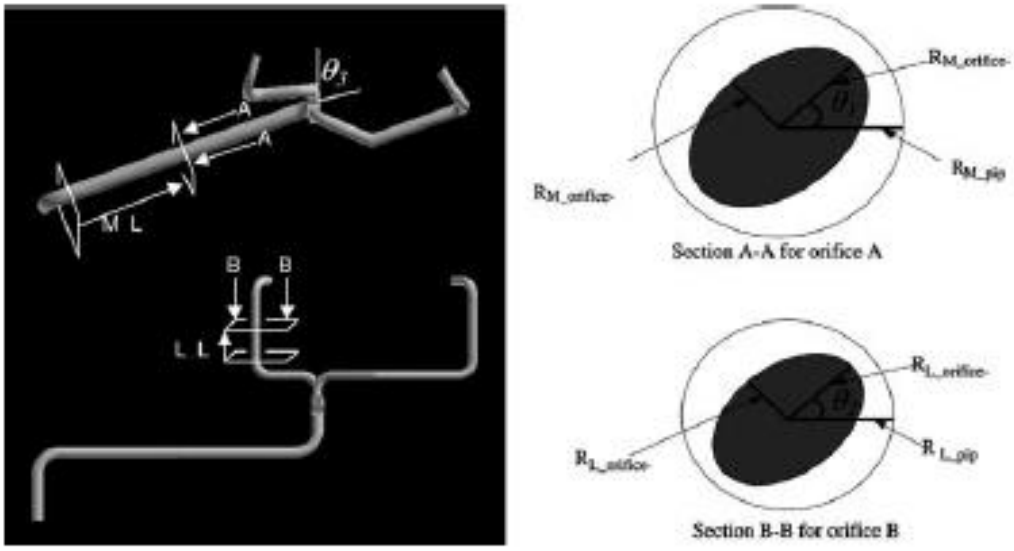

Figure 4: Sketch of design pipe geometry.

MAIN_ORIFICE_ANGLE	0	90
MAIN_ORIFICE_MAJOR_RADIUS	0.85	1.0
MAIN_ORIFICE_LOCATION	2.0	43.0
LEFT_ORIFICE_ANGLE	0	90
LEFT_ORIFICE_MAJOR_RADIUS	0.74	0.8
LEFT_ORIFICE_LOCATION	2.0	10.0
BIFURCATOR_ANGLE	-45.0	45.0

Figure 5: Constraints for the design variables.

1. *Reduce the number of calls to the CFD solver* – This requires that the optimization method be computed efficiently so that better designs can be found with fewer calls to the CFD solver. Currently, this is the primary focus of increasing the optimization's performance amongst the design community. A substantial amount of research has already been carried out on methods for dealing with this issue.
2. *Speed up the convergence rate when calculating the CFD model* – As in any design process, the faster the CFD code the better, because more design iterations performed within a given timescale increase the designer's ability to achieve the design target within real world time constraints. This method, which focuses on reducing the computational cost by speeding up the convergence rate of the CFD model, is commonly neglected by the design community, mainly because of the long history of separation between the design community and the CFD community.
3. *Introduce human experience into the optimization process to narrow the search space to a manageable size* – On the whole, the basis of the design process is trial and error, and the success of the final design depends largely on the designer's knowledge and intuition. By adding progressive human interaction to the design and optimization process, high-fidelity models like CFD can use the full extent of their capability when coupled with numerical optimization methods.

- *Define the design variables* – This is mainly done in the problem definition step.
- *Define the constraint file* – Seven inequality constraints are used in the optimization to obtain realistic configurations. Fig. 5 shows the complete constraint file for this model. In addition to the inequality constraints mentioned above, two side constraints are used to maintain the consistency of the two orifice openings with the baseline design. Therefore, only one radius of the elliptical orifice is the independent variable. It is worth mentioning that users can manually input this information through the graphical user interface (GUI) the system provides.
- *Define fitness evaluation functions* – The design of a coal transport system for a coal-fired power plant needs to address two main objectives. First, the piping system should deliver equal mass flow rates (gas and solid) at the main outlets (left and right). The objective function measuring the coal flow balance can be expressed as:

$$F(\vec{x}) = \sqrt{\frac{1}{2}\left((Q_L - \bar{Q})^2 + (Q_R - \bar{Q})^2\right)} \tag{1}$$

where $\vec{x}$ is the design variable vector and Q_L, Q_R, Q denote the coal mass flow rate associated with the left and right outlet and the average outflow rate respectively. Second, the particle distribution at the cross section immediately before the bifurcator should be as uniform as possible. This is an important factor in extending the distributor's life and meeting the requirement that the flow splitter split both the coal and air flow evenly. The object function measuring the quality of the particle distribution profile is determined by the standard deviation of the particle concentration in the cross section right before the bifurcator *MI*,

$$MI = \frac{1}{C_p}\left[\frac{1}{n-1}\sum_{k=1}^{n}\left(C_m(k) - C_p\right)^2\right]^{1/2} \tag{2}$$

where C_p is the mean particle concentration in the pipe's cross section, $C_m(k)$ is the local particle concentration measured at different locations on the surface, and n is the total number of cells on the surface. Because the correlation be-

3 Current development efforts

There are currently two development efforts focused on the broader issues of virtual engineering for power plants. These are:

- The Integrated Environmental Control Model (IECM) is being developed at Carnegie Mellon University and interactively calculates the performance, emissions, and cost of alternative power plant configurations of interest for preliminary design and scoping studies [18]. Plant options currently available in the IECM include a pulverized coal plant, a coal-based integrated gasification combined cycle plant, an oxyfuel combustion plant, and a natural gas-fired combined cycle plant. This demonstrates a broader virtual engineering tool that can be used during the initial development of a power plant concept. IECM has recently been coupled to a virtual environment and new detailed models of components can be imported and displayed within the virtual engineering environment.
- Advanced Process Engineering Co-Simulator (APECS) is currently under development at the National Energy Technology Laboratory. APECS links various solvers using the CAPE-Open standard for linking processing models as the integration method. APECS has been demonstrated for power plant design using the process simulation software Aspen™ and Fluent™ as the CFD package.

3.1 Integrated Environmental Control Model

IECM (Fig. 11) is a process simulator that can provide the key power plant operating parameters including performance, emissions, and cost during the policy level of the preliminary design of new power plants. IECM's strength is in linking high-level decisions on plant configuration with economic cost models and uncertainties in performance. With these aspects of plant operation and design explicitly characterized, the overall risks and payoffs, including the environmental payoff, of an advanced system design can be quickly determined.

3.2 Advanced Process Engineering Co-Simulator

New power plants are large capital investments that will be in operation for sixty or more years and require periodic costly maintenance. Small changes in operation can impact efficiency and significantly increase fuel cost. As a result, power companies and those who fund the construction of new power plants want to ensure success and have little interest in unproven and untried technologies even if they promise reduced emissions and improved efficiency. Because of this, new types of power plants have traditionally been built and designed in a series of lab scale experiments, prototypes, demonstration-scale and full-scale power plants using five to ten physical models. To reduce the cost and speed up the introduction of a new fleet of near-zero emission power plants, the US Department of Energy is working to create high-fidelity computer simulations to design and evaluate virtual power plants. Key to the development of these virtual power plants is the development of the APECS. APECS (Fig. 14) couples CFD, reduced order models, and custom engineering models with any process simulator supporting the CAPE-Open standard [19–21]. This significantly extends the capability of process

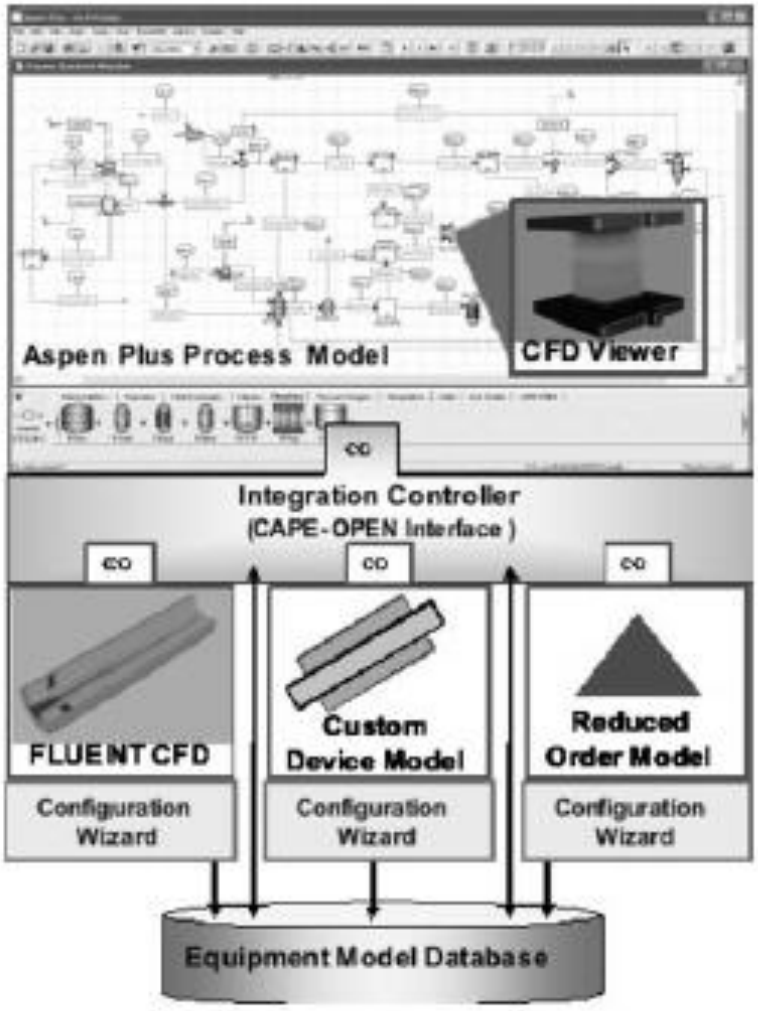

Figure 14: Software tools within APECS.

4 Building a virtual engineering application

Development of a virtual engineering environment from scratch is currently a significant challenge. A better way to approach the development of an application is to utilize VE-Suite [13, 22, 23]. VE-Suite, an object-oriented, open source software package developed for virtual engineering of complex engineering systems (e.g. power plants) design and analysis, is currently the only generalized virtual engineering software package. This section provides a brief overview of VE-Suite and the process of developing a virtual engineering application.

The architecture of VE-Suite is composed of three core engines driving the entire product design and analysis process: the computational engine (VE-CE), the graphical engine (VE-Xplorer), and the GUI (VE-Conductor) (Fig. 15). VE-CE

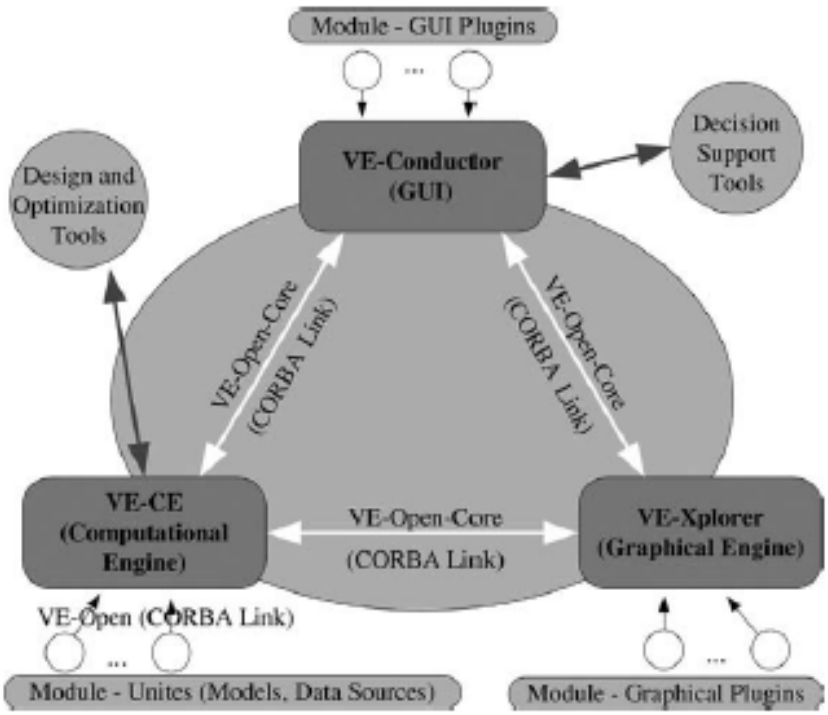

Figure 15: Architecture of VE-Suite.

handles the scheduling and synchronization of the data sources (model and information) being used within a product design and analysis process. VE-Xplorer displays all necessary three-dimensional data. VE-Conductor provides the user interface to control the software tools, engineering models, and graphical display. Similar to CAPE-Open [24], VE-Open [13] is a communication standard that supports the integration and communication between these core engines, as well as the integration with the specific modules developed by the user.

4.3.2 Computational unit

The computational unit for the coal pipe application wraps a Fluent™ computational model. This unit is designed to take the variables described above for the GUI plug-in and create and modify the Fluent™ numerical grid and rerun the model. In general, VE-CE computational units are capable of running a simulation containing a multitude of different types of models, each accepting and generating

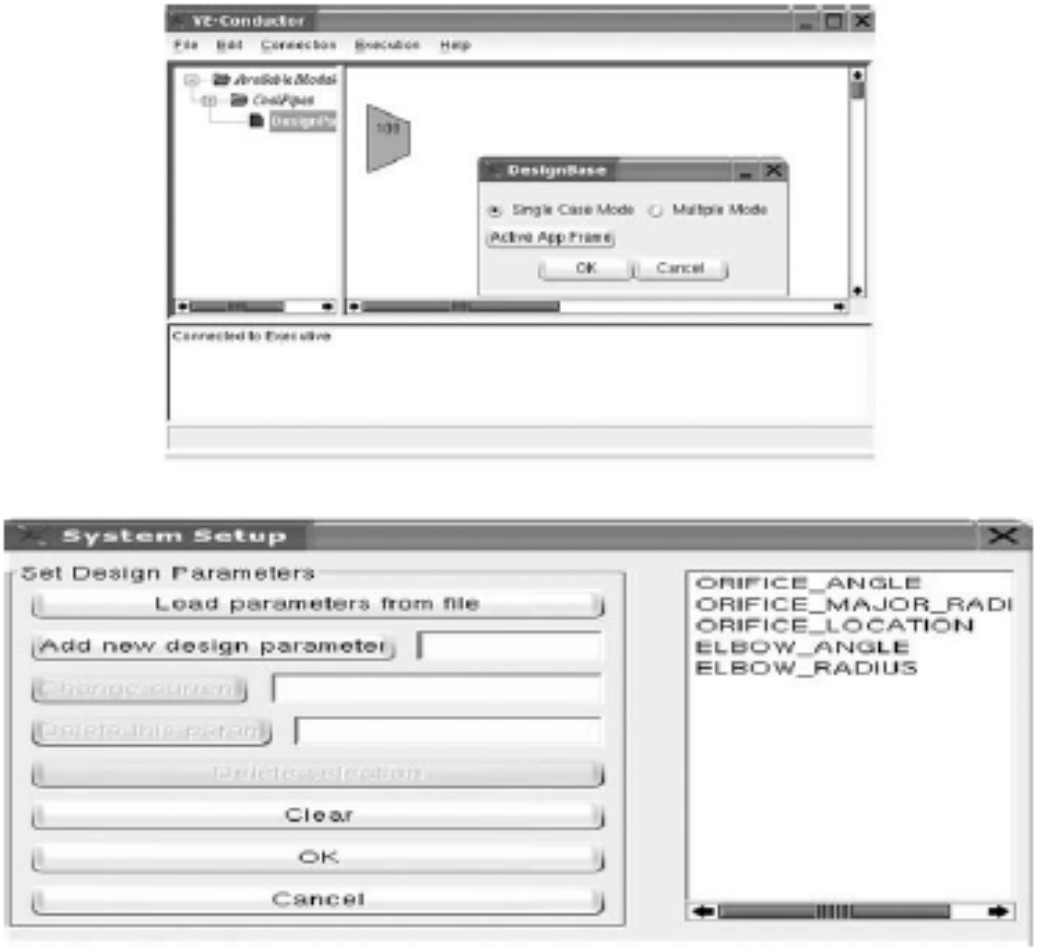

Figure 16: VE-Conductor plug-in for coal pipe design.

4.3.3 Graphical plug-in

A key aim of virtual engineering is to fully engage the human capacity for problem solving by creating a realistic experience for the user so that he or she can focus entirely on the engineering problem. The advantage is that previously indescribable complexities can be understood and the full range of engineering solutions can be explored. VE-Xplorer provides the core visualization functionality for the virtual engineering aspect of the framework. VE-Xplorer can load geometry files, three-dimensional simulation data, and experimental data of almost every format into a scene. To enable graphical display of the coal pipe data in VE-Xplorer, a graphical plug-in is created that is designed to retrieve and store all the designs

generated by the user. The graphical plug-in does not have the capability to graphically display the Fluent™ data but utilizes the capability of VE-Xplorer to handle this feature set. The graphical plug-in in this case adds the capability to catalogue and remotely retrieve the Fluent™ data from the computational unit described above. In addition, the graphical plug-in takes the user's input from VE-Conductor and changes the graphical CAD data so that the user can verify the design before sending the job to the computational unit to run a computationally expensive model.

5 Summary

Virtual engineering is an emerging technology that can provide a high-level integration of models to create a "game-like" engineering decision environment for power plant design. The strength of a virtual engineering environment is the explicit inclusion of multiple options and the integration of human experience and values with computational modeling to create a progressive interaction approach to engineering design. This integrated modeling environment will then be used to examine the impact of changes at the micro level on efficiency, emissions, and cost. These broadly integrated models will enable integrated optimization of power systems and will explicitly bring human judgment into the optimization and design of power systems during both design and operation.

CHAPTER 4

Steam power plants

E. Khalil
Department of Mechanical Power Engineering,
Cairo University, Cairo, Egypt.

Abstract

The efficient utilization of fossil energy in power generation together with low pollution in conventional thermal power plants is a topic that is gaining interest internationally. The energy availability and sustainability scenario is an area of growing interest and demand in many countries worldwide due to the greater desire to enhance standards of living, increase productivity and preserve a clean environment. Efficient energy use is favorable for better productivity, product quality, costs, and quality of human life but the use of energy adversely impacts our environment. The fundamental concepts of power generation had been refined to enhance the power generation efficiency through the use of modern techniques of waste heat recovery and co-generation. This chapter summarizes the basic power cycles in steam power plants and outlines the various methods of improvement. The main goal of efficient power generation is, among others, to rationalize the use of fossil fuels and enhance the combustion efficiencies. This is outlined in this chapter through a review of the various combustion modeling techniques for furnace flames under steady and time dependent configurations. The ability of numerical computations to predict the boiler furnace thermal behavior is an ultimate goal. The heat transfer to furnace walls through thermal radiation is reviewed briefly to demonstrate the present capabilities. Boiler furnace walls are subject to the major problems of fouling that result in deterioration of the performance and drastic reduction of the heat transfer characteristics. This work briefly highlights the fouling problem in power plant water walls and proposes a monitoring, inspection, and maintenance schedule. The information provides a quick guide on the commonly faced operation problems and methods to enhance energy conversion efficiency.

1 Introduction

Centralized power generation became possible when it was recognized that alternating current power lines can transport electricity at low costs across great distances by taking advantage of the ability to raise and lower the voltage using power transformers. Since 1881, electricity has been generated for the purpose of powering human technologies from various sources of energy. The first power plants were run on water power or coal, and today we rely mainly on coal, nuclear, natural gas, hydroelectric, and petroleum with a small amount from solar energy, tidal harnesses, wind generators, and geothermal sources. Rotating turbines attached to electrical generators produce most commercially available electricity. Turbines are driven by a fluid, which acts as an intermediate energy carrier. The fluids typically used are:

- *Steam in steam turbines* – Water is boiled by nuclear fission or the burning of fossil fuels (coal, natural gas, or petroleum). Some newer plants use the sun as the heat source: solar parabolic troughs and solar power towers concentrate sunlight to heat a heat transfer fluid, which is then used to produce steam. Another renewable source of heat used to drive a turbine is geothermal power. Either steam under pressure emerges from the ground and drives a turbine or hot water evaporates a low-boiling liquid to create vapor to drive a turbine.
- *Water in hydraulic turbines* – Turbine blades are acted upon by flowing water, produced by hydroelectric dams or tidal forces.
- *Wind* – Most wind turbines generate electricity from naturally occurring wind. Solar updraft towers use wind that is artificially produced inside the chimney by heating it with sunlight.
- *Hot gases in gas turbines* – Turbines are driven directly by gases produced by the combustion of natural gas or oil.

1. *Types of* service (base load or peak load).
2. *Location* (relative to water and fuel).
3. *Space available* (each power plant has a certain area/unit energy produced).
4. *Reliability:* Steam turbine life is extremely long. There are steam turbines that have been in service for over 50 years. Overhaul intervals are measured in years. When properly operated and maintained (including proper control of boiler water chemistry), steam turbines are extremely reliable. They require controlled thermal transients as the massive casing heats up slowly and differential expansion of the parts must be minimized.
5. *Environment:* Emissions associated with a steam turbine are dependent on the source of the steam. Steam turbines can be used with a boiler firing any one or a combination of a large variety of fuel sources, or they can be used with a gas turbine in a combined cycle configuration. Boiler emissions vary depending on fuel type and environmental conditions. Boiler emissions include nitrogen oxide (NO_x), sulfur oxides (SO_x), particulate matter (PM), carbon monoxide (CO), and carbon dioxide (CO_2). Recently, NO_x control has been the primary focus of emission control research and development in boilers. The following provides a description of the most prominent emission control approaches [2]. Combustion control techniques are less costly than post-combustion control methods and are often used on industrial boilers for NO_x control. Control of combustion temperature has been the principal focus of combustion process control in boilers. Combustion control requires tradeoffs – high temperatures favor complete burn-up of the fuel and low residual hydrocarbons and CO, but promote NO_x formation. Very lean combustion dilutes the combustion process and reduces combustion temperatures and NO_x formation. However, if the mixture is too lean, incomplete combustion occurs, increasing CO emissions [3].
6. *Cost* (capital cost and maintenance cost): There is broad consensus among scientists that we are not close to running out of fossil fuels. Despite this abundance, political considerations over the security of supplies, environmental concerns related to global warming and sustainability might move the world's energy consumption away from fossil fuels. A government-led move away from fossil fuels would most likely create economic pressure through carbon emissions trading and green taxation. Some countries are taking action as a result of the Kyoto Protocol, and further steps in this direction are proposed. For example, the European Commission has proposed that the energy policy of the European Union should set a binding target of increasing the level of renewable energy in the EU's overall mix from <7% today to 20% by 2020.

3 Steam power plants cycles

3.1 Basic cycle description

Rankine cycles describe the operation of steam heat engines commonly found in power generation plants as schematically shown here in Fig. 1. In such vapor

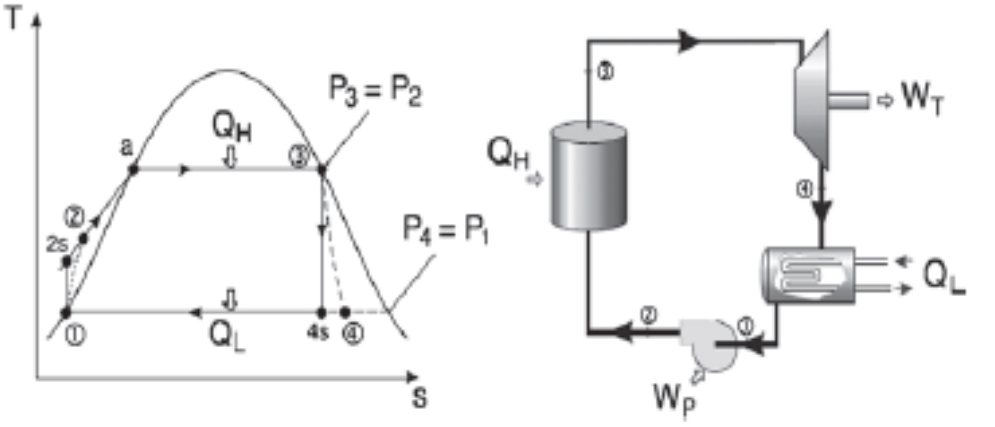

Figure 1: Simple Rankine cycle.

power plants, power is generated by alternately vaporizing and condensing a working fluid (in many cases water, although refrigerants such as ammonia may also be used) [1].

There are four processes in the Rankine cycle, each changing the state of the working fluid. These states are identified by number in Fig. 1.

- *Process 1-2$_s$:* First, the working fluid is pumped (ideally isentropically) from low to high pressure by a pump. Pumping requires a power input (for example mechanical or electrical).
- *Process 2$_s$-3:* The high pressure liquid enters a boiler where it is heated at constant pressure by an external heat source to become a saturated vapor. Common heat sources for power plant systems are coal, natural gas, or nuclear power.
- *Process 3-4$_s$:* The saturated vapor expands through a turbine to generate power output. Ideally, this expansion is isentropic. This decreases the temperature and pressure of the vapor.
- *Process 4$_s$-1:* The vapor then enters a condenser where it is cooled to become a saturated liquid. This liquid then re-enters the pump and the cycle repeats.

3.2 Actual Rankine cycle

In actual situations, both the water pumps and the steam Turbines do not operate isentropically and losses result in more power demand for pumping and less power actually generated by steam to blades [1]. The actual Rankine cycle is shown in Fig. 2.

Such losses are clearly shown in the following comparisons. That is,

$$h_3 - h_4 < h_3 - h_{4s} \quad \text{and} \quad h_2 - h_1 > h_{2s} - h_1$$

The performance of an actual turbine or pump is usually expressed in terms of isentropic efficiency. The isentropic efficiency of a turbine (η_T) is defined as the ratio of "work delivered by the actual turbine" to "work delivered by an isentropic turbine."

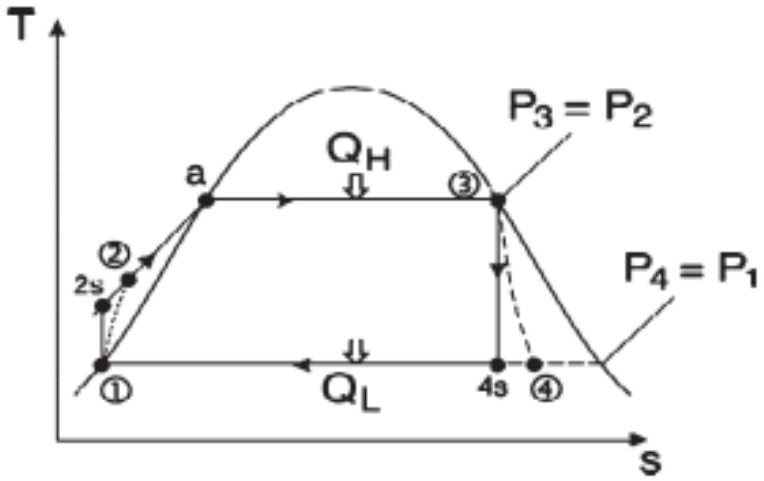

Figure 2: Practical Rankine cycle.

$$\eta_T = \frac{h_3 - h_4}{h_3 - h_{4s}} \tag{1}$$

3.3 Efficiency improvements in power plants

It is well known that the cycle efficiency is generally proportional to

$$\eta \propto 1 - \frac{T_L}{T_H} \tag{3}$$

The question that emerges is how to improve the cycle efficiency; naturally through lowering the heat sink temperature T_L and/or raising the heat source temperature T_H.

3.3.1 Lowering the condenser pressure

Setting the steam condenser pressure is generally restricted by the temperature of the available condenser water (lake, river, etc.) typically around 25°C or condenser saturation pressure of around $P_{sat} \cong 3.2$ kPa.

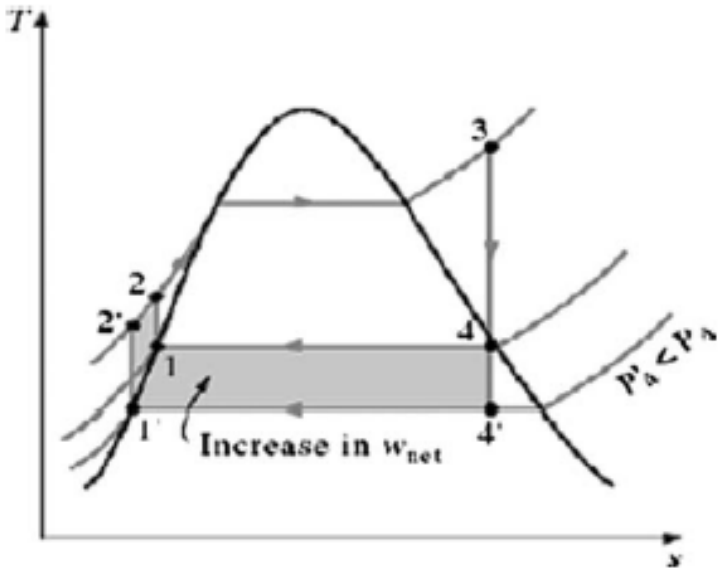

Figure 3: Lowering condenser temperature T_L through decreasing condenser operating pressure [1].

The pressure at the exit of the turbine can be less than atmospheric pressure with a condenser and the closed loop of the condenser permits the use of high water quality on the steam cycle side. However, lowering condenser pressure is not unlimited as it depends on the design condenser temperature and the limits of lower steam quality at turbine exit. In Fig. 3, the shaded area represents the gain in network of the system due to lowering the condenser pressure.

3.3.2 Superheating the steam to high temperatures

The average temperature at which heat is supplied in the boiler can be increased by superheating the steam. Dry saturated steam from the boiler is passed through a second bank of smaller bore tubes within the boiler until the steam reaches the required temperature. The value of T_H, the mean temperature at which heat is added, increases, while T_L remains constant. Therefore, the efficiency increases.

The quality of the turbine exhaust termed, x, increases, the value of steam dryness fraction at turbine exit should not be lower than about 0.9 to prevent water droplets effects on blading efficiency, as outlined in Fig. 4. With sufficient superheating, the turbine exhaust conditions may well fall in the superheated region.

3.3.3 Increasing the boiler pressure

Increasing the operating pressure of the boiler automatically raises the temperature at which boiling takes place. This consequently raises the average temperature

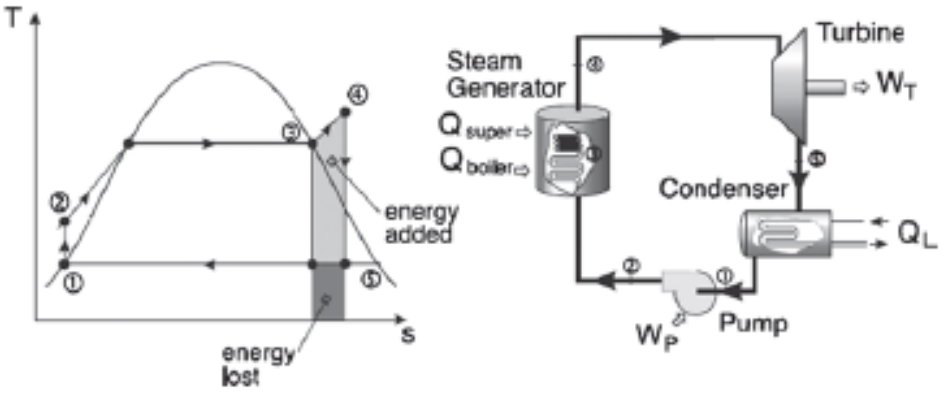

Figure 4: Increase T_H by adding superheat.

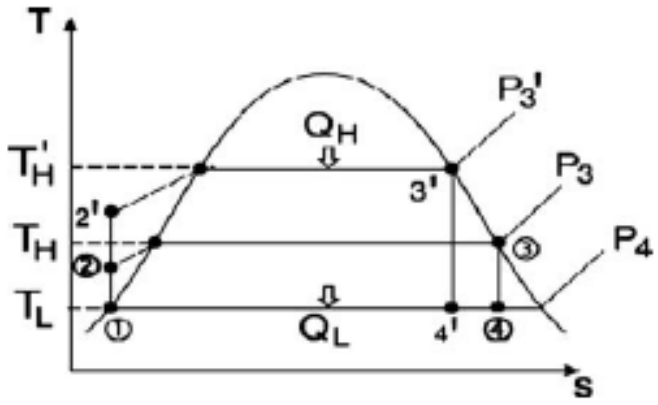

Figure 5: Effect of increasing the boiler pressure.

3.3.4 Rankine cycle with reheat

1. The moisture content at the exhaust of the turbine should be no greater than 10% – this can result in physical erosion of the turbine blades.

2. As higher boiler pressures are required for high efficiency, this leads to a higher moisture content ratio in the low pressure turbine expansion [1].
3. To improve the turbine exhaust steam conditions, the steam can be reheated between two turbine expansion stages or steps as indicated in Fig. 6. The following points emerge:

   - The temperature of the steam entering the turbine is limited by metallurgical constraints.
   - Modern boilers can handle up to 30 MPa and a maximum temperature of $t_{max} \approx 650°C$.
   - Materials, such as ceramic blades, can handle temperatures up to 750°C.

Advantages of using Rankine cycle with reheat: This arrangement provides high steam quality or even slightly superheated vapor at turbine exit. Therefore, for a given T_H the Rankine cycle, efficiency increases without reducing the steam quality at turbine exit.

Rankine cycle with regeneration: To increase the cycle efficiency, to near the Carnot cycle efficiency, added heat Q_H should be at as high temperature T_H as it possibly can. Also, heat should be rejected, Q_L, at the lowest possible T_L. In such configuration, the Rankine cycle is provided with *feed water heaters (FWHs)* to heat the high-pressure sub-cooled water at the exit of the pump to the saturation temperature. As shown in Fig. 7, most of the heat addition (Q_H) is performed at high temperature.

Feed water heaters: There are two different types of FWHs commonly used in power plants: *open FWH*, where the two streams of high temperature steam and low temperature water mix in an open heater at constant pressure; *closed FWH*, where a heat exchanger is used to transfer heat between the two streams but the two streams do *not* mix. The two streams can be naturally maintained at different pressures.

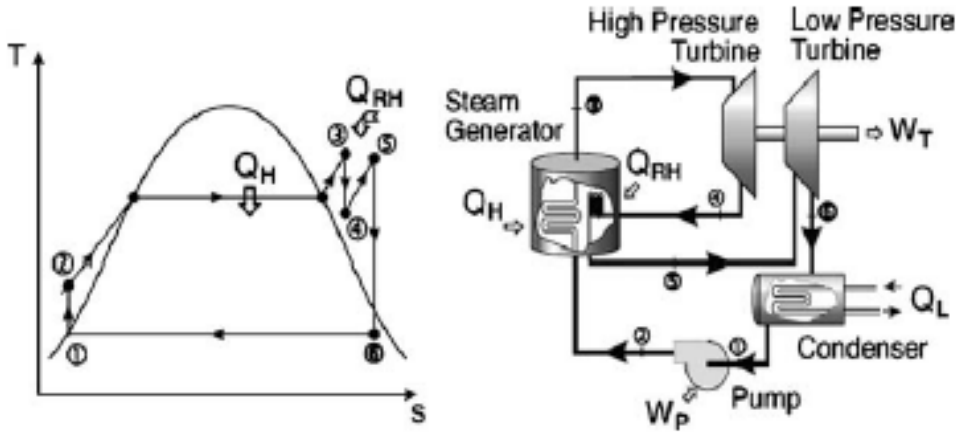

Figure 6: Rankine cycle with reheat.

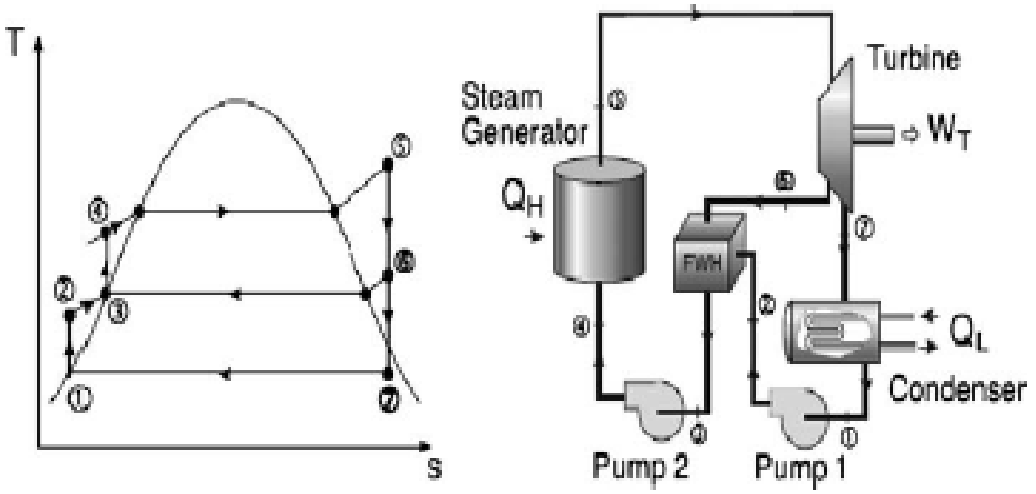

Figure 7: Rankine cycle with regeneration [1].

1. *Open FWH:* In this arrangement, the working fluid passes isentropically through the turbine stages and pumps. Steam enters the first stage turbine at state 1 and expands to state 2 – where a fraction of the total flow is bled off into an open FWH at P_2. The rest of the steam expands into the second stage turbine at state point 3. – This portion of the fluid is condensed and pumped as a saturated liquid to the FWH at P_2. A single mixed stream exits the FWH at state point 6. The mass flow rates through each of the components are typically calculated by performing a mass balance over the turbine. A heat balance is also performed to calculate the various enthalpies at various states.
2. *Closed FWH:* Such configuration can be practically realized in two alternatives typically:

   - Pump the condensate back to the high-pressure line (Fig. 8a).
   - A steam trap is inserted in the condensed steam line that allows only liquid to pass (Fig. 8b).

The incoming feed water does not mix with the extracted steam; both streams flow separately through the heater, hence the two streams can have different pressures.

Advantages of using heat regeneration:

1. It improves the cycle efficiency.
2. It provides a convenient means of deaerating the feed water (removing the air that leaks in at the condenser) to prevent corrosion in the boiler.
3. It also helps to control the large volume flow rate of the steam at the final stages of the turbine.

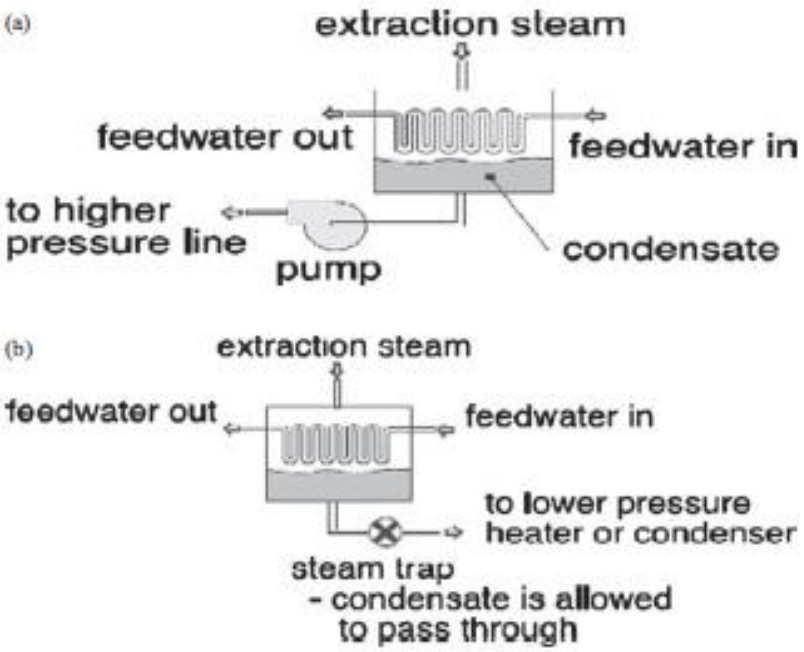

Figure 8: (a) Forward type feed water heaters; (b) cascaded type feed water heaters.

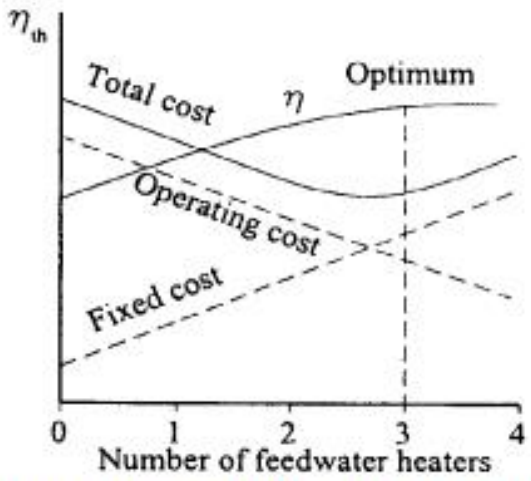

Figure 9: Effect of number of FWHs on the thermal efficiency.

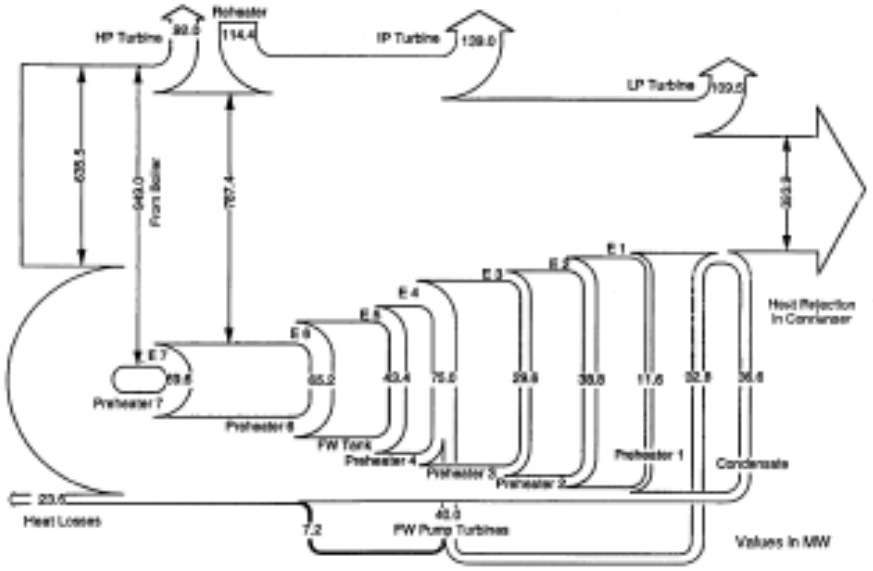

Figure 10: Power flow diagram for a 330 MW steam turbine unit.

The output power is indicated as the sum of the high-, intermediate- and low-pressure stages. Heat rejected in the condenser was shown to be 393.9 MW [5].

Table 1 lists the performance of a 330 MW steam turbine working in a Steam Power Plant in Cairo, Egypt. The performance indices are those of July 2007. The average thermal efficiency was 37.582%. Improvements can well be implemented by co generation and reducing losses [5].

4 Boiler furnace combustion

In furnaces and combustors, it is most essential to represent adequately the characteristics of heat transfer and energy balance in a mathematical model of the flow and reaction processes. This is done to enable determination of the actual heat flux distribution to the furnace walls and to predict the local gas temperature distribution. In real furnaces and combustors, two modes of heat transfer exist, namely radiation and convection. A fundamental calculation of heat transfer requires the simultaneous solution of fluid flow, chemical reaction, and energy transfer. The inter-dependence and interaction of these processes make the problem extremely complex; the general approach adopted is to develop simplified models that deal with the turbulence and the reaction characteristics. Radiative and convective heat transfer is discussed here in terms of available models, their assumptions, formation and validation in furnaces and combustion chambers.

4.1 Turbulent combustion

4.1.2 Mathematical formulation

Three time averaged velocity components in X, Y, and Z coordinate directions were obtained by solving the governing equations using a "SIMPLE numerical algorithm" (semi-implicit method for pressure linked equation). The turbulence characteristics were represented by a modified and appropriately extended two-equation $k-\varepsilon$ model [7, 8] to account for normal and shear stresses and near-wall functions. Fluid properties such as densities, viscosity and thermal conductivity were obtained from references [9–13]. The present work uses the computer program 3DHVAC [7, 8]. The program solves the differential equations governing the transport of mass, three momentum components, energy, relative humidity, and the air age in 3D configurations. The different governing partial differential equations are typically expressed in a general form as:

$$\text{Div}\,(\rho V\Phi - \Gamma_{\Phi,\text{eff}} \cdot \text{grad}\,\Phi) = S_{\Phi} \tag{4}$$

where ρ is the air density (kg/m^3), Φ is the dependent variable, V is the velocity vector, $\Gamma_{\Phi,\text{eff}}$ is the effective diffusion coefficient, S_{Φ} is the source term of Φ.

The effective diffusion coefficients and source terms for the various differential equations are listed in Table 2.

The solution of the governing equations can be realized through the specifications of appropriate boundary conditions. The values of velocity, temperature, kinetic energy, and its dissipation rate should be specified at all boundaries.

Table 3 highlights the boundary conditions.

Table 2: Coefficients and constants of the partial differential equations.

	Φ	$\Gamma_{\Phi,\text{eff}}$	S_{Φ}
Continuity	1	0	0
X-momentum	U	μ_{eff}	$-\partial P/\partial x + S_{\text{U}}$
Y-momentum	V	μ_{eff}	$-\partial P/\partial y + S_{\text{V}}$
Z-momentum	W	μ_{eff}	$-\partial P/\partial z + S_{\text{W}} + \rho g\beta\Delta t$
H-equation	H	μ'_{eff}	S_{H}
k-equation	K	μ'_{eff}	$G - \rho\varepsilon$
ε-equation	ε	μ'_{eff}	$C_1\varepsilon G/k - C_2\rho\varepsilon^2/k$

Table 3: Boundary conditions.

Walls	A non-slip condition at all solid walls is applied to the velocities. The logarithmic law of the wall (wall function) was used here, for the near wall boundary layer.
Supply outlets	At inlets, the air velocity was assumed to have a uniform distribution; inlet values of the temperature were assumed to be of a constant value and uniform distribution. The kinetic energy of turbulence and its dissipation rate are commonly estimated as follows: $$k_{in} = 3(0.5(I_{in}U_{in})^2), \varepsilon_{ini} = C_\mu(k_{in})^{1.5}/l_e,$$ where I_{in} is the intensity of disturbance at air inlet and l_e is the dissipation length at air inlet.
Initial values	All velocity components were set as zeros initially, and temperatures were assumed to be equal to the steady state value of the comfort condition. The kinetic energy and its dissipation are estimated as follows: $$k_{initial} = 11 \times 10^{-5}, \varepsilon_{initial} = C_\mu(k_{initial})^{1.5}/cd,$$ where c is a constant and d is the distance to nearest sidewall.

4.2 Combustion models

A total of 11 combustion models have been used together with equations for U, V, W, k, and ε. They are summarized on the following panels and their relative merits identified. All models require the solution of equations, of the general form (4).

Here $\Phi = H$ and f, where

$$H = M_{fu}H_{fu} + \sum M_i C_{p_a} T_a + \tfrac{1}{2}(U^2 + V^2 + W^2) \tag{5}$$

and

$$f = f_1/f_2$$

$$f_1 = [M_{fu} - (M_{ox}/i)] - [M_{fu} - (M_{ox}/i)]_{\text{air stream}}$$

$$f_2 = [M_{fu} - (M_{ox}/i)]_{\text{fuel stream}} - [M_{fu} - (M_{ox}/i)]_{\text{air stream}}$$

where i is the stoichiometric ratio; M_{fu} is the fuel mass fraction; M_{ox} is the oxidant mass fraction; U, V, W are the mean velocity components in the X, Y, and Z coordinate directions; C_{pa} is the specific heat at constant pressure of the species; T_a is the mean temperature of species.

4.2.1 Fast chemical reactions models

4.2.1.1 Combustion model 1

1. Fuel and oxidant do not coexist at same place at any time, reaction rate is infinitely fast, equilibrium is attained [1, 2].

2. An equation for mixture fraction (f) that has no source term is solved.
3. There are no fluctuations for (f).

$$C_pT = H - M_{fu}H_{fu} + f(H_{fu} + C_pT_{\text{fuel stream}}) + (1-f)(C_pT_{\text{air stream}})$$

with $C_0 = \sum G_a C_{0a} / \sum G_a$ and $C_{0a} = a_0 + a_1T + a_2T^2 + a_3T^3$

4.2.1.2 Combustion model 2

1. The effect of concentration fluctuations is considered here in terms of (g) which is the concentration fluctuations expressed as g = square of (f') fluctuations.
2. The modeled form of the scalar transport equation has a source term expressed in terms of generation term of concentration fluctuations and its dissipation rate.
3. Two delta functions at $f = 0$ and $f = 1$ were assumed.

$$C_pT = H - M_{fu}H_{fu} + f(H_{fu} + C_pT_{\text{fuel stream}}) + (1-f)(C_pT_{\text{air stream}})$$

unless $f_+ > 0$, where $f = \alpha f_+ + (1-\alpha)f_-$, $T = \alpha T_+ + (1-\alpha)T_-$ (α is a fraction less than unity), and

$$T'^2 = \alpha\,(T_+ - T)^2 + (1-\alpha)\,(T - T_-)^2 \tag{6}$$

Computing time = 1.25 × that for model 1.

4.2.1.3 Combustion model 3

1. The modeled form of the scalar transport equation has a source term expressed in terms of generation term of concentration fluctuations and its dissipation rate.
2. A clipped Gaussian probability distribution of mixture fraction (f) is incorporated instead of the two delta functions at $f = 0$ and $f = 1$.
3. The model requires the solution of transport equations for f and g as well as those of the mass, momentum and energy.

Equation (7) is expressed as:

$$T = AT_{\text{air stream}} + BT_{\text{fuel stream}} + \frac{1}{\sigma\sqrt{2R}}\int_0^L \left[\frac{H - M_{fu}H_{fu}}{C_p\mu}\exp\left[-\frac{1}{2}\left(\frac{f-\mu}{\sigma}\right)^2\right]\right]df$$
$$M_{fu} = \int_{01}^{1} M_{fu}(f)P(f)\,df \tag{7}$$

Equation (7) above gives the fuel mass fraction and similar equations for other scalar properties

Computing time = 1.4 × that for model 1.

4.2.2 Finite chemical reaction rate models

4.2.2.1 Combustion model 4

1. In this situation, fuel and oxidant are mixed prior to combustion in a single step; finite rate is assumed.
2. The modeled form of the scalar transport equation has a source term expressed in an Arrhenius form for the reaction rate.

3. This model requires the solution of transport equations for fuel mass fraction (M_{fu}). The effect of turbulence on reaction rates may be introduced as: m_{ox}^2, m_{fu}^2, $m_{ox}m_{fu}$, etc. [14–16].

$$R_{fu} = A\rho^2 M_{ox} M_{fu} \exp(-E/RT) \quad \text{Arrhenius} \tag{8}$$

or

$$R_{fu} = C_R g_{fu}^{1/2} \rho\varepsilon / k \quad \text{Eddy break up} \tag{9}$$

where R_{fu} is the rate of fuel consumption, A is the pre-exponential constant, E is the activation energy, R is the universal gas constant, g is the square of concentration fluctuations, C_R is a constant.

The source term in the g equation is taken be $(\partial M_{fu}/\partial x_i)^2$ and not $(\partial f/\partial x_i)^2$.

Computing time = 1.7 × that for model 1.

4.2.2.2 Combustion model 5

1. In this situation, fuel and oxidant are mixed prior to combustion in a multi-steps; Finite rate is assumed.
2. The modeled form of the scalar transport equation has a source term expressed in an Arrhenius form for the reaction rate for each intermediate reaction step.
3. This model requires the solution of transport equations for fuel mass fraction (M_{fu}). The effect of turbulence on reaction rates may be introduced as: m_a^2, m_b^2, m_c^2, $m_a m_b$, etc.

$$\begin{aligned}
CH_4 + OH &\rightarrow CH_3 + H_2O \\
CH_4 + H &\rightarrow CH_3 + H_2 \\
CH_2 + O_2 &\rightarrow CH_2O + OH \\
CH_2O + O &\rightarrow CHO + OH \\
CHO + OH &\rightarrow CO + H_2O \\
CO + OH &\rightarrow CO_2 + H \\
H + O_2 &\rightarrow O + OH \\
O + H_2O &\rightarrow OH + OH
\end{aligned}$$

Computing time = 3 × that for model 1.

4.2.2.2 Combustion model 5

1. In this situation, fuel and oxidant are mixed prior to combustion in a multi-steps; Finite rate is assumed.
2. The modeled form of the scalar transport equation has a source term expressed in an Arrhenius form for the reaction rate for each intermediate reaction step.
3. This model requires the solution of transport equations for fuel mass fraction (M_{fu}). The effect of turbulence on reaction rates may be introduced as: m_a^2, m_b^2, m_c^2, $m_a m_b$, etc.

$$\begin{gathered}
CH_4 + OH \rightarrow CH_3 + H_2O \\
CH_4 + H \rightarrow CH_3 + H_2 \\
CH_2 + O_2 \rightarrow CH_2O + OH \\
CH_2O + O \rightarrow CHO + OH \\
CHO + OH \rightarrow CO + H_2O \\
CO + OH \rightarrow CO_2 + H \\
H + O_2 \rightarrow O + OH \\
O + H_2O \rightarrow OH + OH
\end{gathered}$$

Computing time = 3 × that for model 1.

4.2.2.3 Combustion model 6

1. Model 6 incorporates the effect of turbulence on the finite chemical reaction rates.
2. This is carried out by the solution of an extra transport equation for the correlation $m_{ox} m_{fu}$.
3. The Damkohler number defined as $N_D = t_s/t_k$.
4. t_s is defined as the stretching time scale of flame eddies.
5. t_k is defined as the chemical kinetics time scale.

$$\begin{aligned}
R_{fu} &= A\rho^2 M_{ox} M_{fu} \exp(-E/RT) + R'_{fu} \\
R'_{fu} &= A\rho^2 m_{ox} m_{fu} \exp(-E/RT)
\end{aligned} \tag{10}$$

This obviates the need for an Eddy break up term.

Computing time = 1.9 × that for model 1.

4.2.2.4 Combustion model 7

1. Model 7 incorporates the effects of turbulence and temperature on the finite chemical reaction rates.
2. This is carried out by the solution of an extra transport equation for the correlation $m_{ox} T' m_{fu} T'$.
3. Correlations relating temperature and concentration fluctuations are solved in the general form of the transport equations.
4. The effect of density fluctuation correlations is also considered [14–16].

$$\begin{aligned}
R'_{fu} = A\rho^2 m_{ox} m_{fu} \exp(-E/RT)[(m_{ox} m_{fu})/(M_{ox} M_{fu}) \\
+ a_1(T'^2)/(T^2) + a_2(.....) + ...]
\end{aligned} \tag{11}$$

4.2.2.6 Grid distribution and timing A staggered grid system is employed for the velocities to avoid the decoupling effects between the velocity and the pressure that are frequently observed with the non-staggered grid (Fig. 11).

A hyperbolic grid distribution is employed, with the grid points, for instance in the Z direction given by the functions as suggested by Henkes [18]. All the computations at the production level were run on a PC and required an average

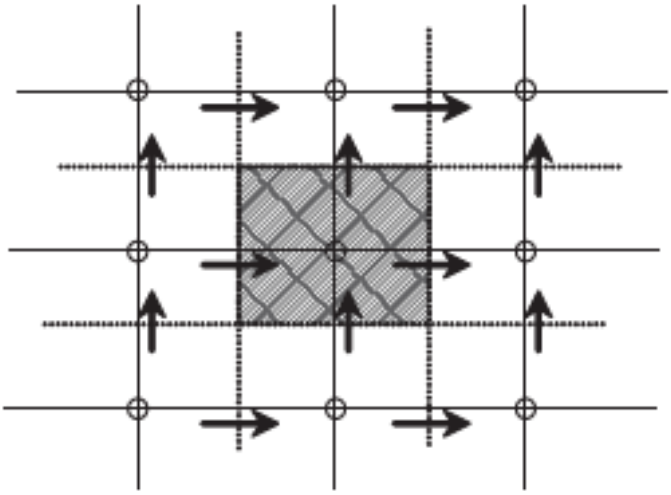

Figure 11: Grid arrangement.

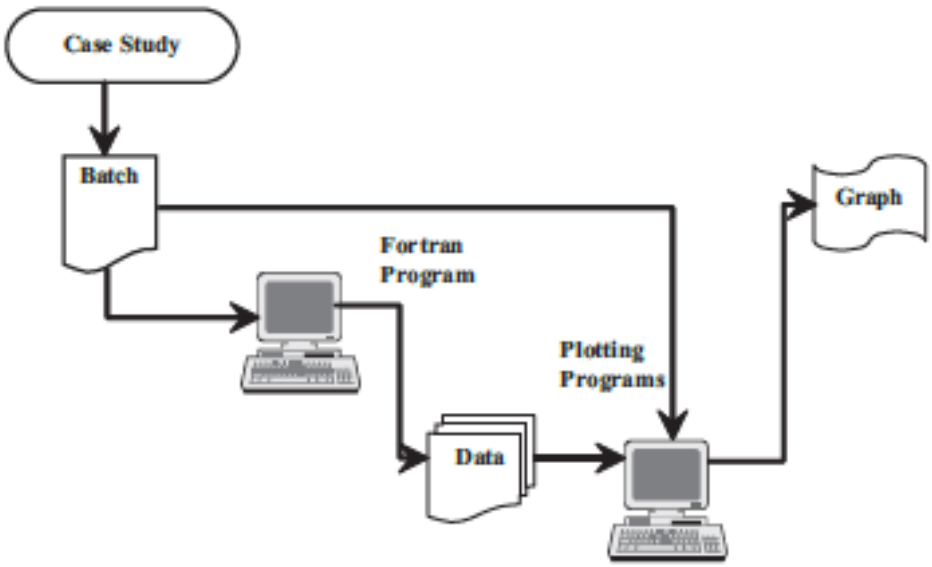

Figure 12: Program flow chart.

4.3 Boiler furnace computations

The computational technique is used to calculate the flow pattern and temperatures in real boiler furnaces as reported by Kameel and Khalil [19, 20]. Figures 13–17

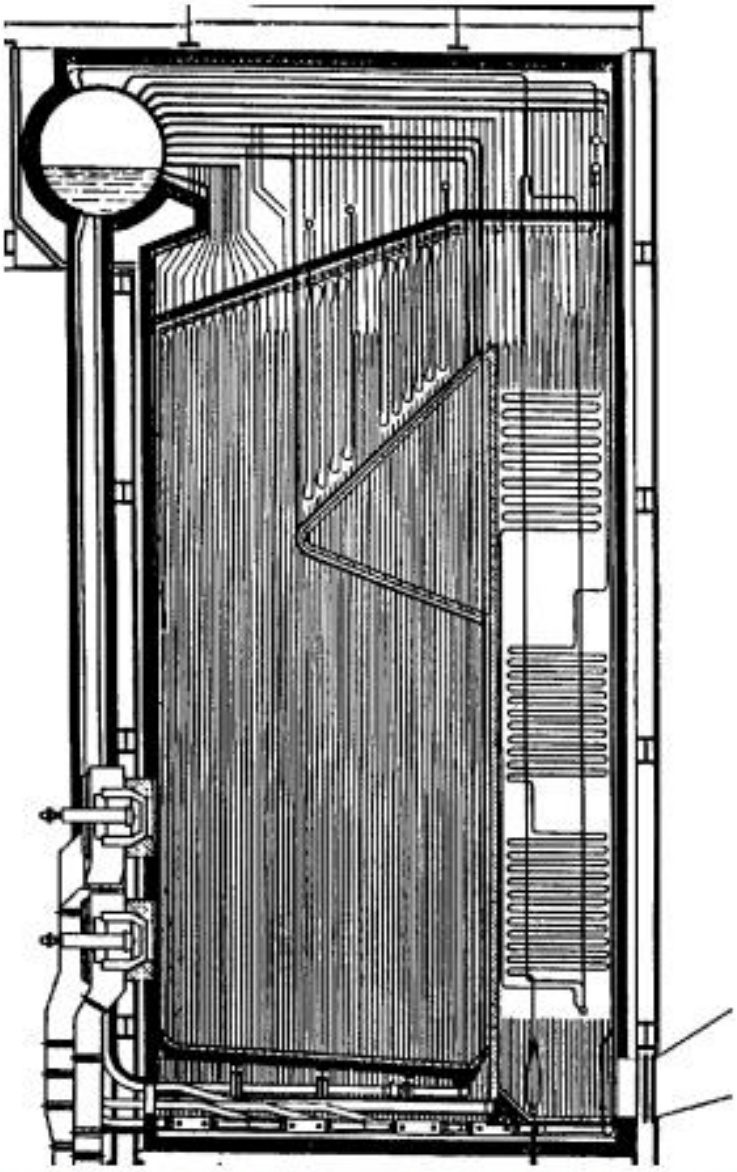

Figure 13: Power plant boiler house configuration (courtesy of Stienmuller).

demonstrate the capabilities of the numerical methods to predict various furnace performance parameters.

4.3.1 Examples of engineering simulations

The furnace of the 80 ton/hour steam at 64 bars is shown in Fig. 13 and the corresponding calculations are shown in Figs. 14 and 15. These include temperatures and flow velocities at start up and during running.

The predicted velocity vectors and thermal contours clearly identified the flames locations and characteristics. Mixing and interaction between the different burners and flames are clearly shown at start up. In Fig. 15 the corresponding predictions outline the emergence of the various flame envelopes and the extent of the flames.

The unsteady flame behavior at start up is shown in Figs. 16 and 17 in terms of the heat release and fuel consumption. The time-dependent fuel mass fraction depletion along the flame centerline is shown in Fig. 16 for different volumes of rich fuel mass fractions at fuel mass fractions >0.1 and 0.15. The predictions identified flame squashing and stretching phenomena [19, 20]. Detailed predictions of the flame shape and the temperature distributions evolvement with time are indicated in Fig. 18 for a vertical cylindrical furnace burning Natural gas. The Furnace details are those listed by Kameel and Khalil [19, 20]. The furnace diameter was 0.3 m and of a length of 0.9 m. In the present non-swirl combusting flow, the Arrhenius model yields very good representative model. Such model is so sensitive to the boundary conditions especially near or at the flame regions. In high temperature regions, the switching between the Arrhenius model and the eddy-break-up model was frequently observed, which consequently influences the transient prediction and the steady sate results. When combustion model 4 is

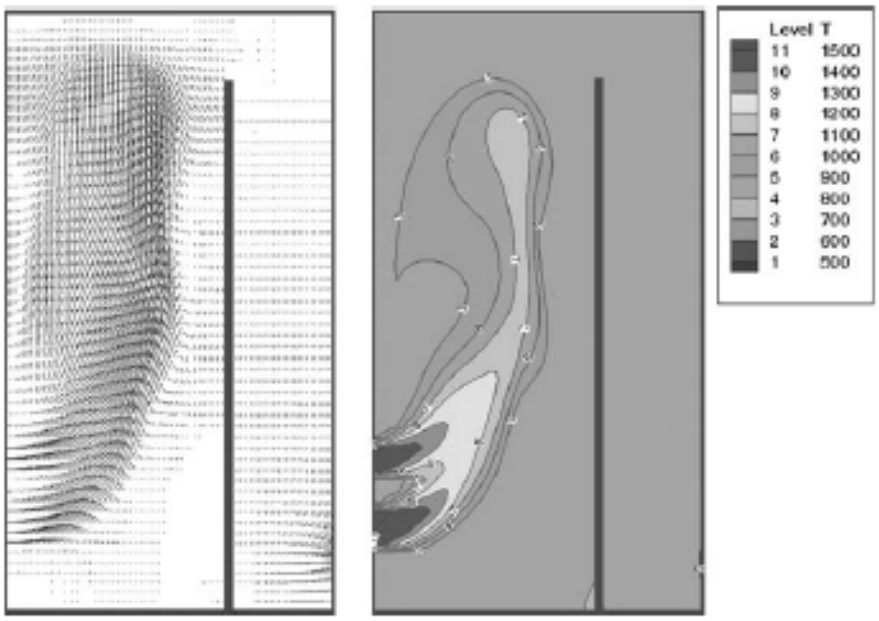

Figure 14: Velocity vectors and temperature contours at boiler start-up.

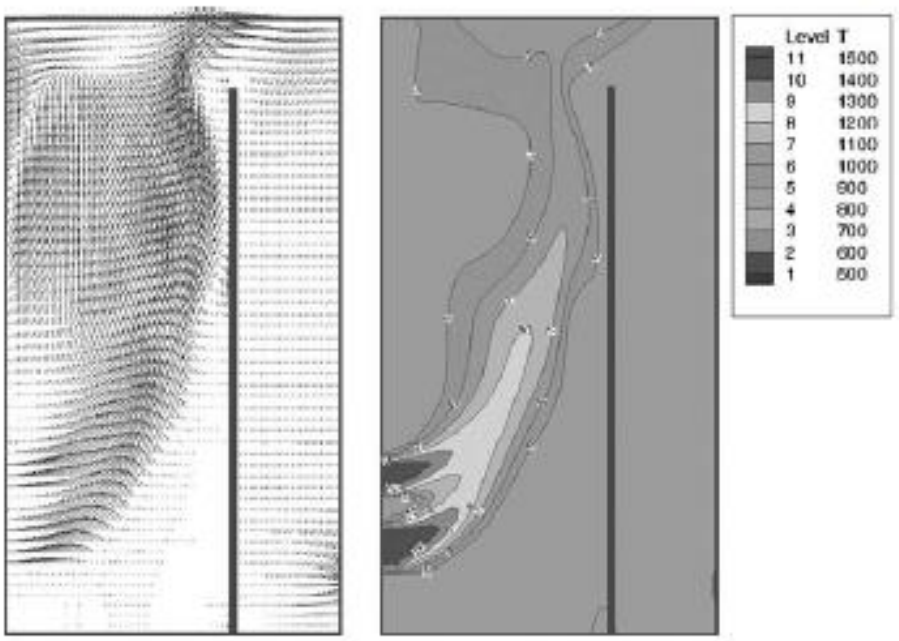

Figure 15: Velocity vectors and temperature contours after boiler running up.

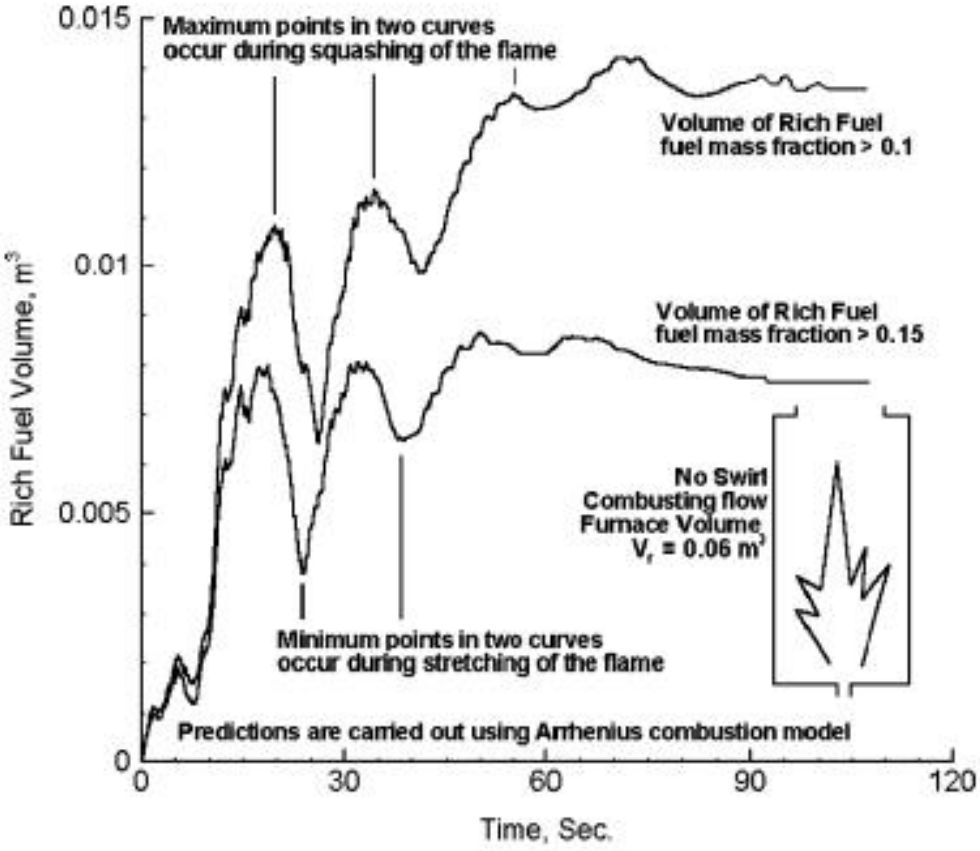

Figure 16: Predicted fuel depletion along furnace centerline at no swirl.

5 Heat transfer calculations in boiler furnaces

In furnaces and combustors, it is most essential to represent adequately the characteristics of heat transfer and energy balance in a mathematical model of the flow and reaction processes. This is done to enable determination of the actual heat flux distribution to the furnace walls and to predict the local gas temperature distribution. In real furnaces and combustors, two modes of heat transfer exist, namely radiation and convection. A fundamental calculation of heat transfer requires the simultaneous solution of fluid flow, chemical reaction, and energy transfer.

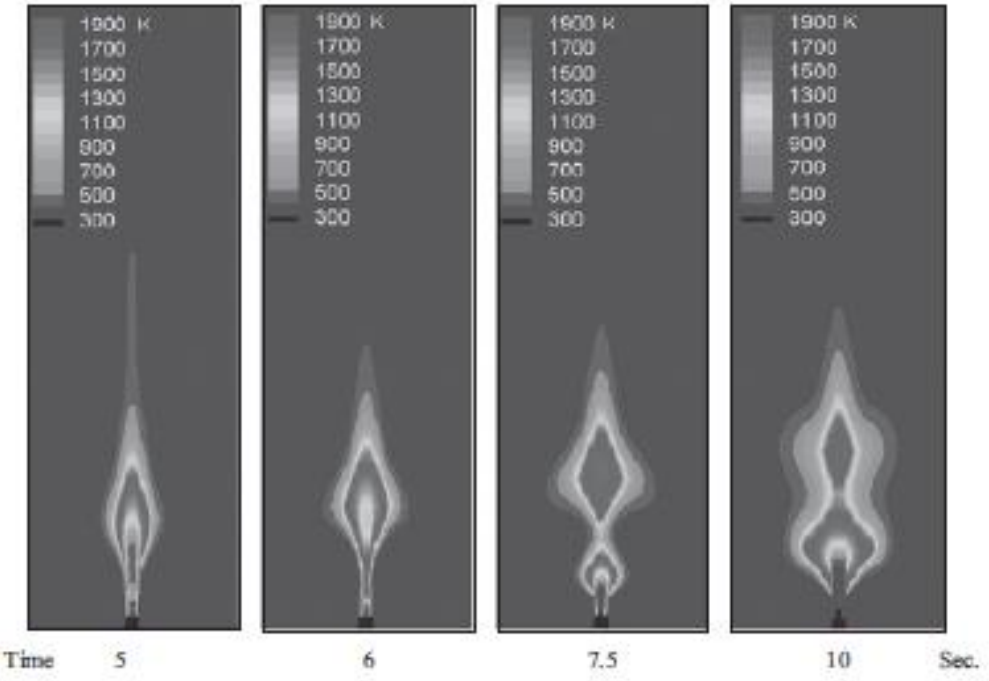

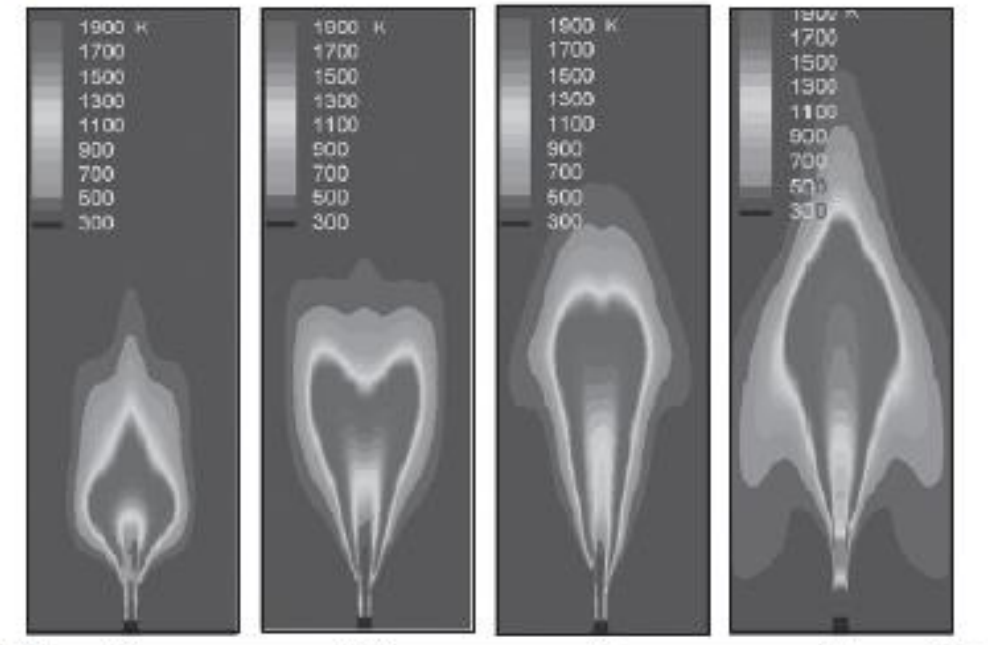

5.1 Equation of radiant energy transfer

The basis on which all the methods of solving the radiation problems stand is the equation of radiant energy transfer. It is driven by writing a balance equation

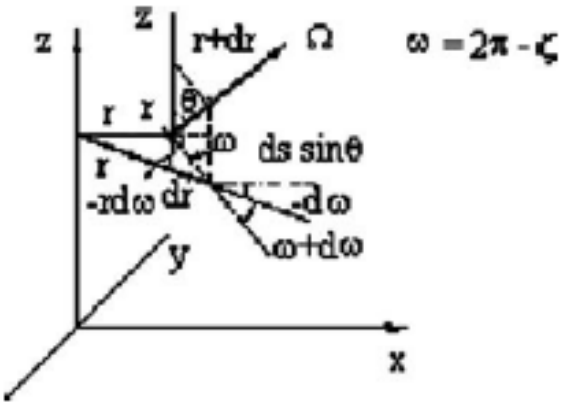

Figure 20: Radiation intensity distribution.

for monochromatic radiant energy, passing in specified direction, through a small volume, in an emitting-absorbing-scattering medium. For steady-state conditions, and for coherent isotropic scattering, this equation is expressed as following,

$$(\Omega \cdot \nabla) I_{\lambda}(r, \Omega) = \mu_0 \frac{\partial I}{\partial r} - \frac{\eta_0 \partial I}{r \partial \xi} + \xi_0 \frac{\partial I}{\partial x} + \frac{\eta_0}{r} \frac{\partial I}{\partial \theta} \tag{13}$$

and $I = I(r, \theta, x, \zeta)$, ζ is an angular variable that equals 2π-ω. μ_0, η_0, ζ_0 are the directional cosines, and are defined as shown in Fig. 20; $\mu_0 = \sin\theta \cos\zeta$; $\eta_0 = \sin\theta \sin\zeta$; $\zeta_0 = \cos\theta$.

5.2 Representation of real furnace gas

In natural gas and oil fired boiler furnaces, only three species contribute significantly, in the infrared region, to radiation [1, 21]. These species are

- carbon dioxide,
- water vapor, and
- hot soot particles within the flame.

The gases radiate in several bands, while the soot emits continuously over a wide range of the wavelength.

$$\varepsilon(T, L) = \frac{1}{\sigma T^4} \int_0^\infty E_\lambda(t)[1 - \exp(-K_{a,\lambda} L)] d\lambda \tag{14}$$

where L is the radiation path length, $E\lambda(T)$ is the Blanck spectral distribution of emissive power, σ is the Stefan–Boltzmann constant.

For real gas situations, the following grey gas emittance-path length relation does not hold:

$$\varepsilon_{\text{grey}} = 1 - \exp(-\text{KL}) \tag{15}$$

A modified expression was deduced by Khalil and Truelove [21], by representing the real gases by a mixture of grey gases. The partial pressures of carbon dioxide and water vapor are introduced into the expression for the emittance of gas mixture ε_g as a function of absorption coefficient, optical path length, partial pressures of water vapor and carbon dioxide, soot concentration and density.

5.3 Radiation models

Various types of mathematical models that were proposed to adequately represent the radiation heat source in the energy equations are found in the literature. The more conveniently applied models are those listed here:

- zone method,
- spherical harmonic model,
- discrete ordinate model, and
- flux models.

5.3 Radiation models

Various types of mathematical models that were proposed to adequately represent the radiation heat source in the energy equations are found in the literature. The more conveniently applied models are those listed here:

- zone method,
- spherical harmonic model,
- discrete ordinate model, and
- flux models.

The basic concept is to solve the radiation intensity equation with adequate physical and boundary conditions with full introduction of water vapor, carbon dioxide and soot radiating proportions. On one hand, the Spherical harmonics approach solves the radiation equation with retaining of adequate terms of harmonics terms. On the other hand, the basic concept of the Discrete Ordinate model Proposed by Khalil and Truelove [21] is very simple, the angular integral in the radiant energy transfer equation are approximated using a numerical quadrature scheme, as shown in Fig. 21.

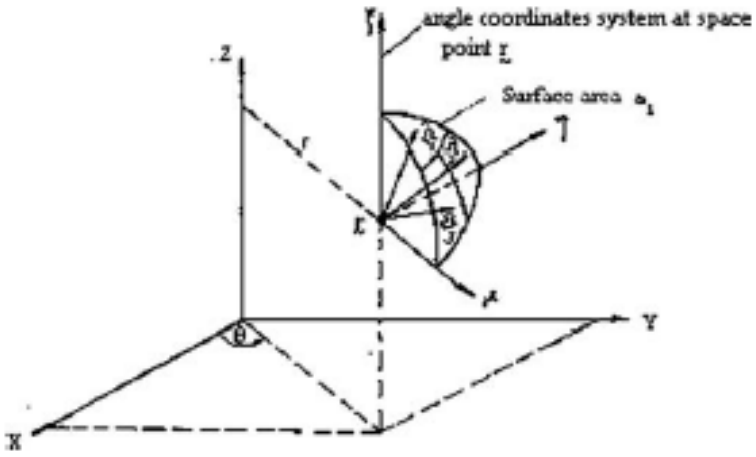

Figure 21: Angular quadrature weights a_i as elements of area on the surface of the unit sphere in angle space. One octant is shown here for clarity.

The radiation source term S_H in the energy equation is time-averaged as

$$S_H = K\sum_{i=1}^{N} a_i I_i - 4K\sigma\overline{T}^4 \tag{16}$$

where $i = 1, \ldots, N$ and $I_i = I(r, \zeta, x, \Omega_i)$.

A sample of the predicted wall heat flux in the furnace of Pai *et al.* [22], at the

6 Power plant water problems

6.1 Introduction

Despite the great technical achievements in the design and manufacture of heat exchangers in the past two decades, the problem of fouling on heat exchanger surfaces still remains one of the major unresolved problems in thermal sciences. In the Egyptian Central Workshop of Cairo Production Electricity Company, many types of power plants' heat exchangers are manufactured for the replacement of failing items. Most of the heat exchangers may not achieve the predicted validity period due, in part, to following non-standard operating procedures: fouling is one bad outcome of such wrong procedures. Table 4 illustrates some of the basic cost components of heat exchangers' manufacturing or re-tubing in only one year; however, not all the Egyptian power plants' heat exchangers are manufactured in the Central Workshop. [23]:

Table 4: Cost of manufacturing and re-tubing of Egyptian power plant heat exchangers in one year (1$ = 5.7 LE[Egyptian Pounds]).

No.	Heat exchanger type	Power plant	Cost (LE)
1	Air pre-heater (baskets)	Damanhour	5292169
2	Low pressure heater (water–steam)	Abu Kair	2200000
3	Air pre-heater (baskets)	Assiut	1833862
4	High pressure heater (water–steam)	Damanhour	708400
5	Air cooler for gas unit	Al Soiof	253000
6	Hydrogen coolers	Damanhour	163482
7	Boiler super heater coils	Assiut	7860
Total cost			10458773

6.2 What is fouling?

Fouling is generally defined as *the accumulation of undesired deposits of materials on the surfaces of processing equipment*. It has been recognized as a nearly universal problem in heat exchangers design and operation. It affects the operation of equipment in two ways:

- The fouling layer has a low thermal conductivity. This increases the resistance to heat transfer and reduces the effectiveness of heat exchangers – increasing temperature.
- As deposition occurs, the cross-sectional area is reduced, which causes an increase in pressure drop across the apparatus.

6.2 What is fouling?

Fouling is generally defined as *the accumulation of undesired deposits of materials on the surfaces of processing equipment*. It has been recognized as a nearly universal problem in heat exchangers design and operation. It affects the operation of equipment in two ways:

- The fouling layer has a low thermal conductivity. This increases the resistance to heat transfer and reduces the effectiveness of heat exchangers – increasing temperature.
- As deposition occurs, the cross-sectional area is reduced, which causes an increase in pressure drop across the apparatus.

Measurement of the fouling resistance is typically performed by measuring the total thermal resistance ($1/UA$) for the clean and fouled conditions. The fouling resistance (R_f) is obtained by subtraction of the $1/UA$ values for the fouled and clean conditions, respectively, giving:

$$R_f/A = 1/(UA)_f - 1/(UA)_c \tag{17}$$

where A is the surface area on which the R_f is based. For tube side fouling, the UA values for the clean and fouled conditions are defined by eqns. (18) and (19), respectively:

$$1/(UA)_c = 1/h_i A_i + t_w/k_w A_w + 1/h_o A_o \tag{18}$$

$$1/(UA)_f = (1/h_i + R_f)(1/A_i) + t_w/k_w A_w + 1/h_o A_o \tag{19}$$

The inside (h_i) and outside (h_o) heat transfer coefficients must be equal in the dirty and clean tube conditions. Otherwise, the measured fouling resistance R_f will be erroneous.

6.3 Types of fouling

Fouling research has resulted in the definition of six different types of fouling that may occur with liquid or gases:

- *Precipitation fouling (scaling)* is the most common form of fouling and is associated with inverse solubility salts. Examples of such salts are $CaCO_3$, $CaSO_4$, $Ca_3(PO_4)_2$, $CaSiO_3$, $Ca(OH)_2$, $Mg(OH)_2$, $MgSiO_3$, Na_2SO_4, $LiSO_4$, and Li_2CO_3. The characteristic which is termed inverse solubility is that, unlike most inorganic materials, the solubility decreases with temperature. The most important of these compounds is calcium carbonate, $CaCO_3$. Calcium carbonate exists in several forms, but one of the more important is limestone. Running primarily through openings in limestone rock, it becomes saturated with calcium carbonate. Water pumped from the ground and passed through a water heater becomes

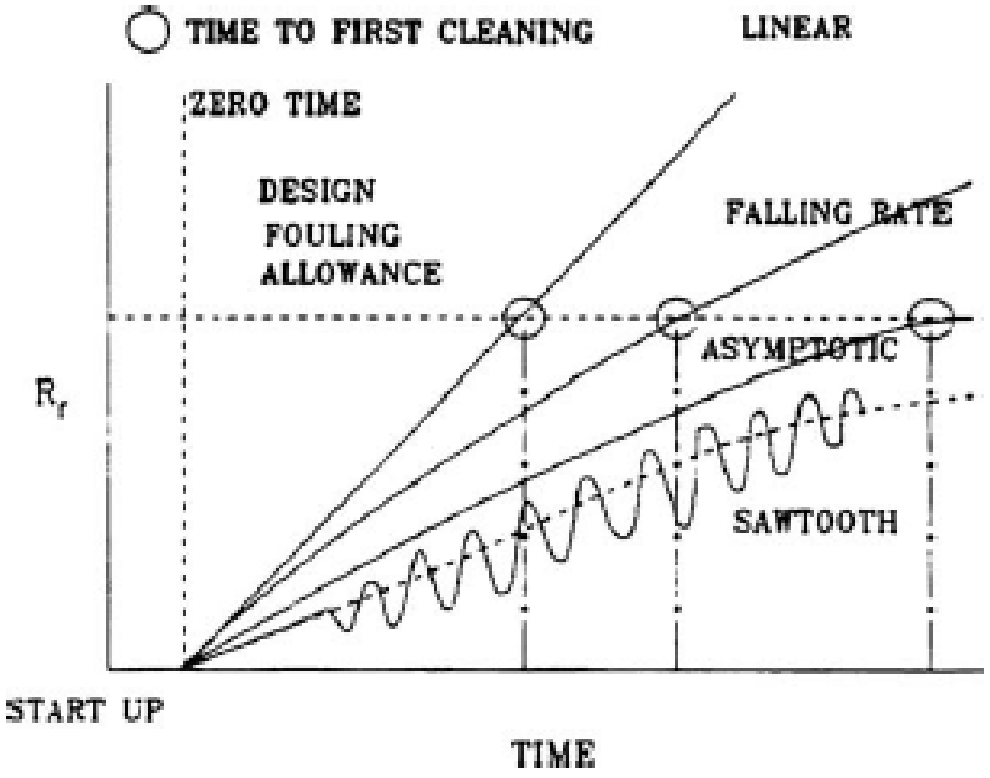

Figure 25: Variation of apparent differential fouling with time for industrial cooling waters.

8. Extrapolate the plot as a linear falling rate or asymptotic rate to the point of intersection with the design fouling allowance.
9. Plan to clean at the time shown by the intersection point.
10. Continue to monitor to refine the extrapolation.
11. After cleaning, repeat the process to establish a cycle.
12. Alternatively, plot the rate of pressure-drop build-up.

Enhancement of nuclear power plant safety by condensation-driven passive heat removal systems

K. Vierow
Department of Nuclear Engineering,
Texas A&M University, USA.

Abstract

In response to increasingly higher demands on nuclear power plant safety systems, the nuclear community is responding by developing "passive" safety systems that are inherently safe. Passive systems are those that do not rely on power supplies, moving parts or human intervention. Condensation heat transfer is a primary driving force for many of these systems. These passive condensation heat transfer systems are reliable and inherently safe because they rely on basic physical forces such as gravity and small pressure differences to transport energy and maintain the plant within design specifications. In recent years, due to advancements in our understanding of the phenomena and in analysis capabilities, designs for essential heat removal systems such as the containment long-term cooling systems have come to rely extensively on passive condensation heat exchangers. The development of innovative systems for future reactors promises to further increase the safety, reliability and economic competitiveness of nuclear power. While significant advancements have been made, challenges remain particularly with regard to accurate, detailed analytical evaluations of system performance. This chapter discusses the numerous ways in which passive condensation heat transfer enhances nuclear power plant safety in current and future nuclear power plants. The discussion focuses on U.S.-design light water reactors and U.S. reactor safety codes although there are many commonalities to reactors of other designs. The physical phenomena are described and the state-of-the art in analysis methods are presented. Challenges for improved analysis are summarized.

1 Passive systems with condensation heat transfer

1.1 Definition

Adoption of passive systems for heat removal during design basis and hypothetical accident scenarios is one of the strategies for achieving simplification and improving safety and reliability of future nuclear reactors. Passive systems are those that do not require any external input such as AC power sources or operator action to function. Compared with active systems, the passive designs are much simpler because they do not depend on the availability of large power supplies and they do not rely on safety-grade containment cooling systems, both of which add cost and complexity. Yadigaroglu [1] and Juhn *et al.* [2] provide reviews of the various passive designs.

The driving forces for these systems are relatively small forces such as natural circulation for cooling and gravity for condensate return. In particular, the heat transfer processes are driven by small pressure and temperature differences. Thus, to achieve the needed cooling rates, heat transfer with phase change is necessary. In one of the first passive concepts, General Electric designed the Simplified Boiling Water Reactor (SBWR) Passive Containment Cooling Systems (PCCS) with vertical heat exchangers that condense containment steam and transfer the heat to a pool outside the containment [3, 4]. The design has evolved [5] and become the basis for passive systems of several current plant designs in the U.S., Europe and Japan.

Another leading design takes advantage of the large heat transfer area on containment walls to condense steam on the inner surface and remove heat through the outer surface by natural circulation of air [6].

There is a strong move towards passive safety systems because the equipment is driven by failsafe forces or mechanisms such as gravity and natural circulation. Adoption of passive systems with efficient heat removal mechanisms will promote future installation of additional nuclear power plants that will increase both reliability and security to our energy supply.

1.2 Goals and requirements

Key goals of these condensation-driven passive heat removal systems include:

1. enhanced safety systems,
2. improved reliability, and
3. greater economic competitiveness via simplification.

2 Roles of passive condenser systems in nuclear power plants

The passive condensation heat transfer systems are divided into three classifications herein.

1. In-vessel decay heat removal during normal shutdown or refueling.
2. In-vessel decay removal under hypothetical accident conditions.
3. Containment heat removal under hypothetical accident conditions.

"In-vessel" refers to occurrence inside the reactor pressure vessel. "Containment" refers to occurrence in the containment atmosphere surrounding the reactor pressure vessel. Decay heat is the energy released by decay of radioactive fission products following reactor shutdown.

Current safety systems in U.S. Pressurized Water Reactors (PWR) and Boiling Water Reactors (BWR) and their possible passive condenser heat exchanger replacements are described below.

2.1 In-vessel decay heat removal during normal shutdown or refueling

The Residual Heat Removal (RHR) system, an active system, maintains the core in a safe condition during normal shutdown and refueling by pumping cooling water through the reactor core and removing core decay heat. Under hypothetical conditions, the RHR may be lost and alternative active cooling sources may not be available. The loss of RHR situation could lead to core boil-off, fuel rod heatup, and eventually core damage and has therefore been widely studied [11].

Steam condensation in the steam generator U-tubes can become one of the major heat removal mechanisms. As a passive mechanism, steam generated by coolant boil-off would enter the steam generator tube primary side via the hot leg, along with any noncondensable gases ingested during preparation for maintenance and/or refueling. Reflux condensation is the mode of phase change heat transfer occurring when a condensing gas and the liquid condensate flow in opposite directions. In the situation under investigation, steam flows vertically upward in steam generator U-tubes and water forms a condensate film that returns downward to the tube inlet plenum.

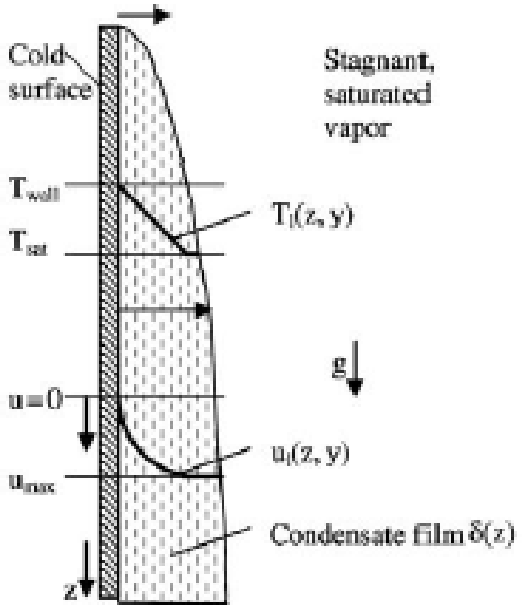

Figure 1: Film condensation along a vertical flat plate.

operation, the water level is above the core, but below the hot leg elevation. Various primary system closures such as the reactor vessel head may not be secured and air or nitrogen can be drawn into the system. Under hypothetical conditions, the RHR may be lost and alternative active cooling sources are not available.

Nitrogen injection from the accumulator into the reactor Coolant System (RCS) following a LOCA also corresponds to midloop operation with noncondensable gases present. If the accumulator valve were to fail following water injection, nitrogen would enter the RCS and degrade the heat transfer performance of the steam generator. Although the possibility of such a scenario occurring is highly unlikely, the consequences must be known.

Assuming loss of AC power, the possible alternative cooling sources are:

1. gravity drain from the Reactor Water Storage Tank,
2. core boil-off and steam venting, and
3. reflux condensation heat transfer in the steam generators.

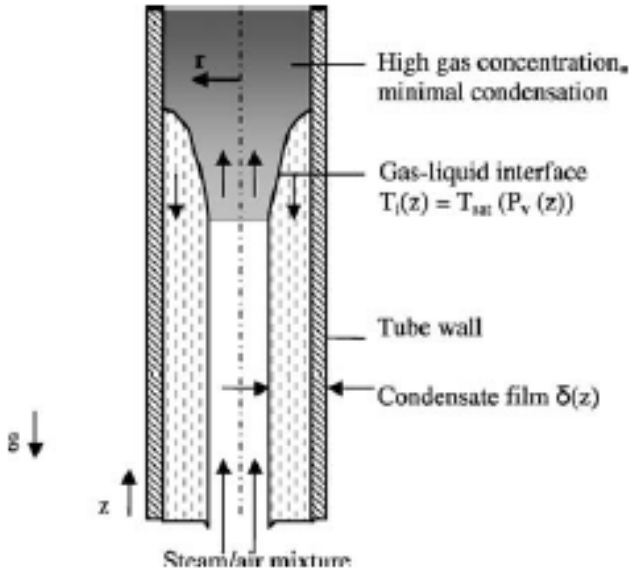

Figure 2: Reflux condensation.

Reflux condensation does not occur on the downflow side of PWR U-tubes because the steam/gas mixture and the condensate liquid are flowing in the same direction.

3.3 Condensation in vertical tubes with steam/noncondensable gas inflow from the tube top end

3.3.1 Condensation in IC tubes under normal shutdown and isolation conditions

The ICS consists of multiple loops, each with an isolation condenser unit that condenses steam on the primary side and transfers heat through the tube wall to the secondary side water pool. Condensed steam drains from the tubes back to the reactor pressure vessel to maintain core cooling. Each ICS loop has noncondensable gas vent lines from the top and bottom headers that can purge noncondensable gas from the unit and assure good heat transfer performance. The ICS is expected to have an inflow of essential pure steam under most operating conditions. During a severe accident, hydrogen from a core coolant interaction may enter the tubes. Noncondensable gases from the containment can enter the ICS units after the reactor pressure vessel depressurization.

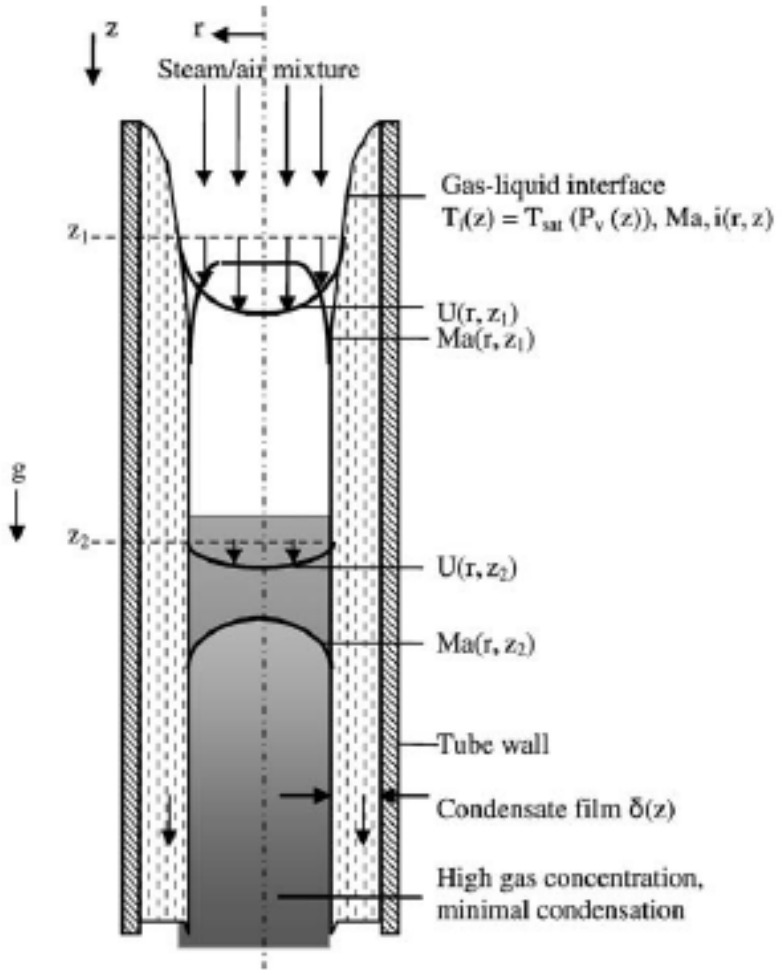

Figure 3: Film condensation in a vertical tube with downward flow.

interfacial shear and increasing condensate film turbulence. With the gas and liquid film both flowing downward, turbulence thins the film and reduces film resistance to heat transfer. Additionally, the increased interfacial shear promotes turbulence and mixing in the gas core. The resistance of the noncondensable gas boundary layer to condensation heat transfer is reduced. A second distinction concerns the axial variation of the cross-section average temperature and species concentration for the internal flow case. In contrast to the stagnant atmosphere case, the temperature decreases with distance along the condenser tube and the noncondensable gas concentration increases. Axial variations of the conditions driving heat and mass transfer arise, but they do not occur in the stagnant gas, vertical flat plate situation.

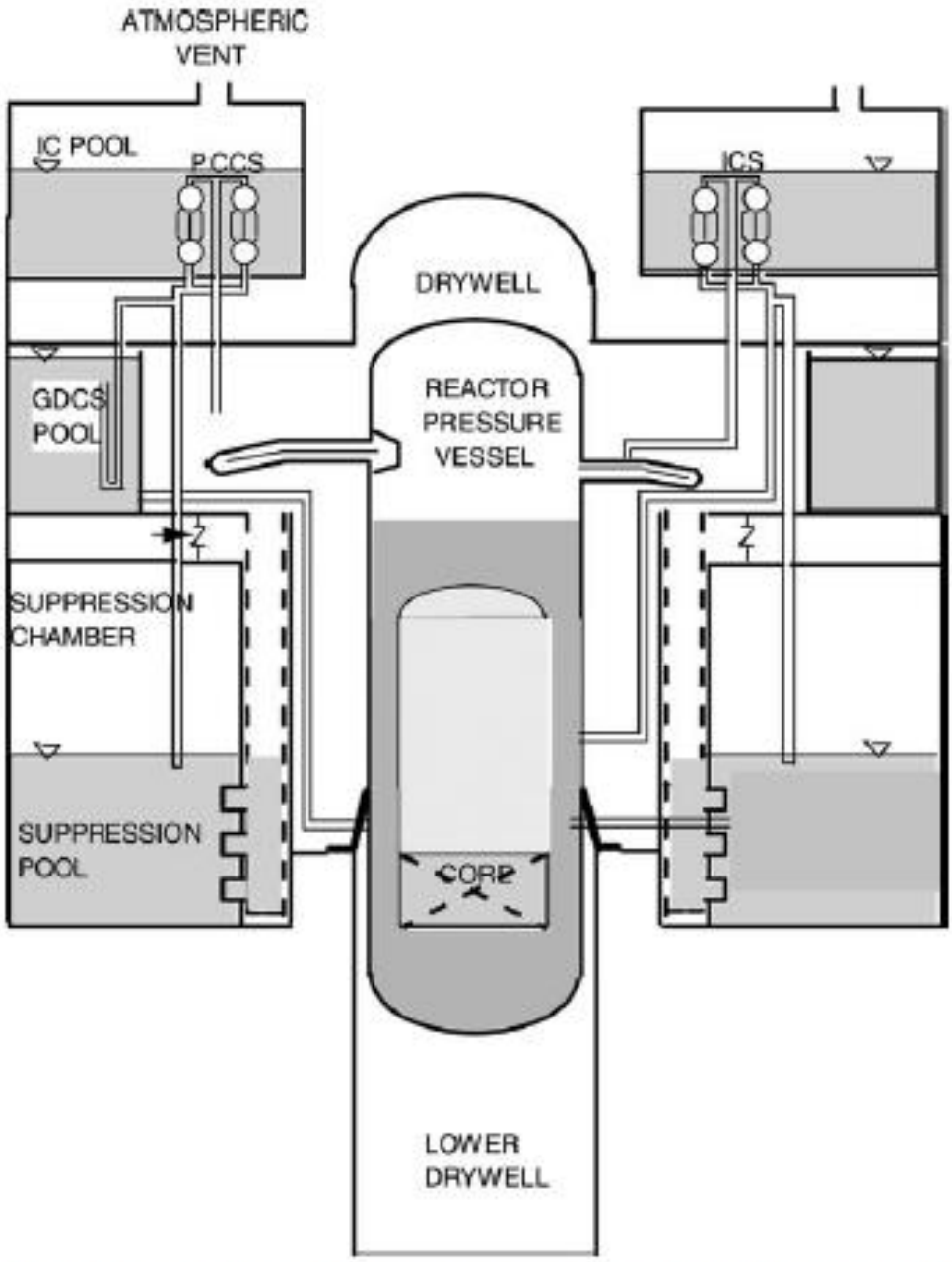

Figure 4: Economic Simplified Boiling Water Reactor Isolation Condenser System and Passive Containment Cooling System.

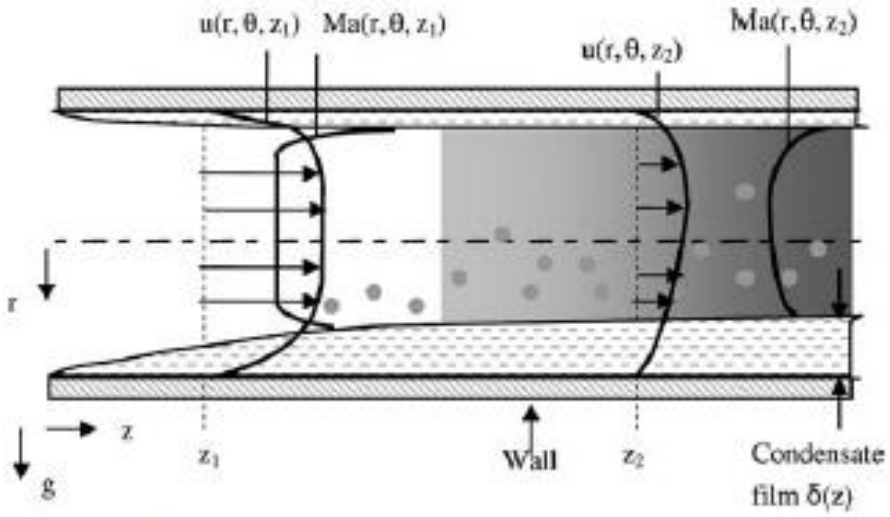

Figure 5: Film condensation in a horizontal tube.

Read Page 169 to 178 Condensation

5 Analysis challenges

Remaining challenges for analysis of passive systems driven by condensation heat transfer arise from incomplete understanding of phenomena, uncertainty in boundary conditions and numerical issues. These issues impact analysis at the fundamental heat transfer level and at the reactor system level.

Major challenges include:

1. Better understanding of condensate film behavior in reflux and horizontal condensers, including both film sublayers and the film surface interactions. Boundary layer analysis may be a useful tool for this purpose.
2. Peripheral characteristics of condensate film behavior in horizontal and inclined tubes. Additional experimental study with film visualizations would be beneficial.
3. Mixing in large volumes to predict noncondensable gas concentrations at condenser tube inlets.
4. Accurate calculations over a long duration.
5. Accounting for the tighter coupling of the primary loop pressure with the containment pressure in passive plants than in active plants.

CHAPTER 6

Modern CFD application on aerothermal engineering aspects of natural draft cooling towers

D. Bohn[1] & K. Kusterer[2]
[1]*Institute of Steam and Gas Turbines, RWTH Aachen University, Aachen, Germany.*
[2]*B&B-AGEMA GmbH, Aachen, Germany.*

Abstract

Natural draft cooling towers are a very efficient way to provide the cold end of thermal power plants with a steam turbine cycle. The cooling tower shape, details of construction and arrangement and type of cooling fill have a significant influence on the cooling tower efficiency, in particular, on the cold water temperature that can be reached. Furthermore, influences of cross wind situations on the performance of the cooling tower are of high interest. Modern computational tools for three-dimensional flow simulations (CFD) can be coupled by local heat and mass transfer calculation schemes with the cooling water film calculation and thus allow a comprehensive numerical investigation of the aerodynamic and thermodynamic behaviour of natural draft cooling towers under specific operating conditions. After validating the numerical approach, the numerical method has been used for determination of the influences of fill types, of the inner rim structure at the tower outlet and of an additional flue gas discharge on the cooling tower performance. Furthermore, numerical calculations of several cross wind operating conditions have been performed. The numerical simulations show clearly that the equipment of the cooling tower with a modern fill-type achieve higher efficiencies. Cross wind situations lead to a significant reduction in the cooling tower efficiency and thus to higher cold water temperatures. A major result of the simulations is that under unfavourable circumstances, a periodic cold air ingestion at the tower outlet might appear that leads to unstable operating conditions with reduced efficiencies. The inner rim structure at the tower outlet has a stabilizing effect in cross wind situations.

1 Introduction

Cooling towers provide the cold end for steam turbine cycles mainly used in thermal power plants for producing electricity. The objective of the cooling tower and condenser operation is to condense steam exiting from the low-pressure turbines at a pressure, which should be as low as possible to maximize the power output from the plant. The condenser pressure is thermodynamically linked to the cooling water temperature offered by the cooling tower. The closer it is to ambient temperature, the better it is for the cycle performance.

High efficiencies are typically achieved with wet cooling towers. In this design, cooling water heated in the condenser is cooled by convection and evaporation in contact with ambient air. The contact time and area between air and water are increased by spraying the water over a fill (a grid of bars or plates) and by passing air through the fill. The water to be cooled then trickles from the top through the cooling fills. The water is cooled in two ways when the cooling air is passing by. A small amount of water evaporates so that evaporative heat is extracted from the cooling water flow. Furthermore, heat is transferred from the water to the cooling air by convection.

Most efficient designs, although comparatively expensive, are based on buoyancy driven air flow. Natural draft cooling towers exist in two flow arrangements, a counterflow and a crossflow arrangement (see Fig. 1). In mechanical draft cooling towers, a fan provides the necessary air amount to the fill. Due to higher air velocities the heat transfer is enhanced and, thus, mechanical draft cooling towers are much smaller in size than natural draft cooling towers, but the necessary fan power reduces the overall power output of the plant. Modern natural draft cooling towers can be as high as 200 m or even more with base diameters of approximately 150 m. Figure 2 shows a typical natural draft cooling tower with a modern design including an additional flue gas discharge in the centre of the tower.

Natural draft cooling towers are very sensitive to special operation conditions, e.g. additional flue gas discharge and environmental conditions, e.g. cross wind effects. The incoming air in case of a cross wind situation is unevenly distributed to the fill and the buoyancy driven air flow in the tower might be affected by cold

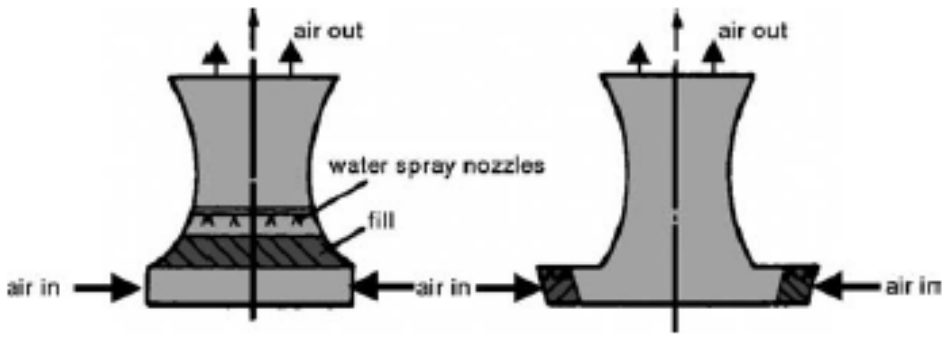

Figure 1: Natural draft cooling towers with counterflow (left) and crossflow (right) arrangement.

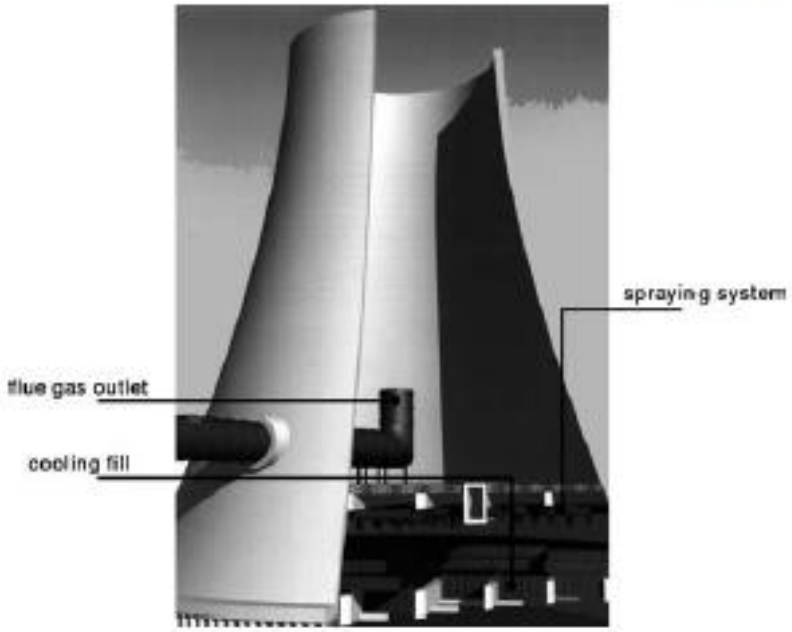

Figure 2: Modern natural draft cooling tower (counterflow arrangement).

2 Numerical modelling

2.1 Implementation of a heat transfer and mass transfer model

The water-side and air-side flow in a wet cooling tower is a two-phase flow with complex heat transfer and mass transfer conditions between both fluids. Thus, the complete numerical simulation of all relevant conservation equations for the three-dimensional flow in cooling towers is still beyond the economical application for industrial use with respect to time and cost efforts. Therefore, a simplification is introduced by handling the wet air as a one-phase mixture of fluids consisting of the two components (1) dry air and (2) water steam. This is necessary to take into account the change in density due to the local wetness. In the following section, this one-phase model fluid is mentioned as "air" or "air-side."

The energy balance and mass balance between the cooling water film and the air can be established. Transferred heat and mass flow values are implemented as additional source terms to the governing equations for the calculations on the cooling film side and wet air flow. As the flow of the cooling water cannot be taken into account additionally to the air flow directly in the finite volume cells of the computational grid, information on inlet and outlet temperatures and the local mass flow for the cooling water flow have to be stored separately for every cell and have to be exchanged with the neighbouring cells in the flow direction of the water.

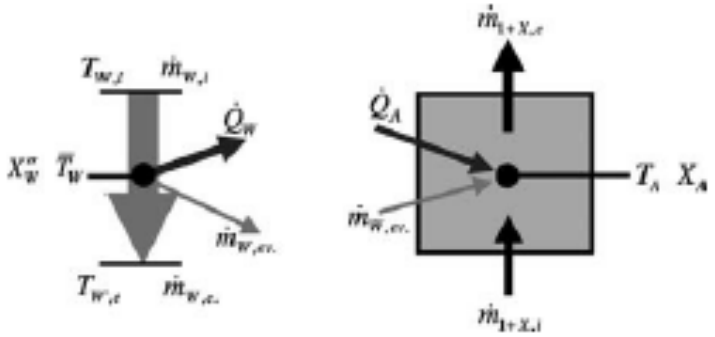

Figure 3: Physical parameters for heat and mass balances at a cooling water element (left) and a finite volume cell of the air-side (right).

saturated. Altogether, the local heat flux transferred from the cooling water element can be calculated as follows:

$$\dot{Q}_{\mathrm{W}} = \alpha \cdot A \cdot \left(\overline{T}_{\mathrm{W}} - T_{\mathrm{A}}\right) + \beta_x \cdot A \cdot \left(X''_{\mathrm{W}} - X_{\mathrm{A}}\right) \cdot \Delta h_{\mathrm{ev}} \tag{1}$$

In case the air in the finite volume cell is saturated with water as well as the air in contact to the cooling water film, but a temperature gradient between the cooling water film and the air-side is established, the diffusion process continues further despite the saturated air condition due to the gradient of the water content. This leads to a re-condensation of water on the air-side. The re-condensed water and small droplets taken away by mechanical forces are the reason for the visible plume at the cooling tower exit. The re-condensation of steam on the air-side is not part of the used numerical models up to now.

The outlet temperature of the cooling water for the cooling water element can be calculated based on the first law of thermodynamic as following:

$$T_{\mathrm{W,e}} = \frac{\left(\dot{m}_{\mathrm{w,i}} \cdot c_{\mathrm{W}} \cdot T_{\mathrm{W,i}} - \dot{Q}_{\mathrm{W}} - \dot{m}_{\mathrm{W,ev}} \cdot c_{\mathrm{W}} \cdot \overline{T}_{\mathrm{W}}\right)}{\dot{m}_{\mathrm{W,e}} \cdot c_{\mathrm{W}}} \tag{2}$$

The heat flux into the air-side finite volume cell is mainly determined by the convectively transferred heat:

$$\dot{Q}_{\mathrm{A}} = \alpha \cdot A \cdot \left(\overline{T}_{\mathrm{W}} - T_{\mathrm{A}}\right) + \dot{m}_{\mathrm{W,ev}} \cdot h''_{\mathrm{S}} \tag{3}$$

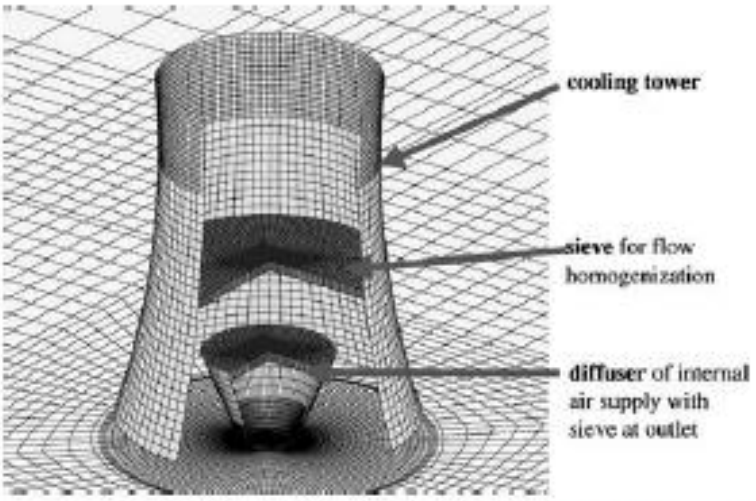

Figure 5: Numerical model and grid of single cooling tower.

the other one placed in front of the tower waist have been taken into account by a pressure loss model based on pressure loss coefficients.

A fully turbulent flow has been reached in the experiments by additional turbulators on the surface of the cooling tower. Thus, the standard-k, ε-model with an additional wall roughness parameter has been used in the numerical simulations. Furthermore, calculations with the original geometry size have been performed. In that case, the flow has a very high Re number and a turbulent boundary layer is established. Therefore, the calculations can be performed with a hydraulic even surface, means without an additional roughness parameter.

For the cross wind simulation, a velocity profile has to be prescribed at the inlet boundary, which should be an approximation of the atmospheric boundary layer. This is reached by a velocity distribution in dependency of the atmospheric height z in the following exponential law [8]:

$$\frac{c(z)}{c_{\infty}} = \left(\frac{z}{z_{\infty}}\right)^{0.25} \tag{9}$$

3.1.2 Results for cooling tower arrangement

The numerical grid is shown in Fig. 7. The arrangement of the cooling towers has been exposed to a cross wind with an offset angle of 15° to the centre connection line of the cooling towers. Thus, an asymmetric velocity and pressure distribution can be expected. This can be seen in the calculated pressure fields in Fig. 8a and b. Whereas Fig. 8a shows the experimental case with a rough

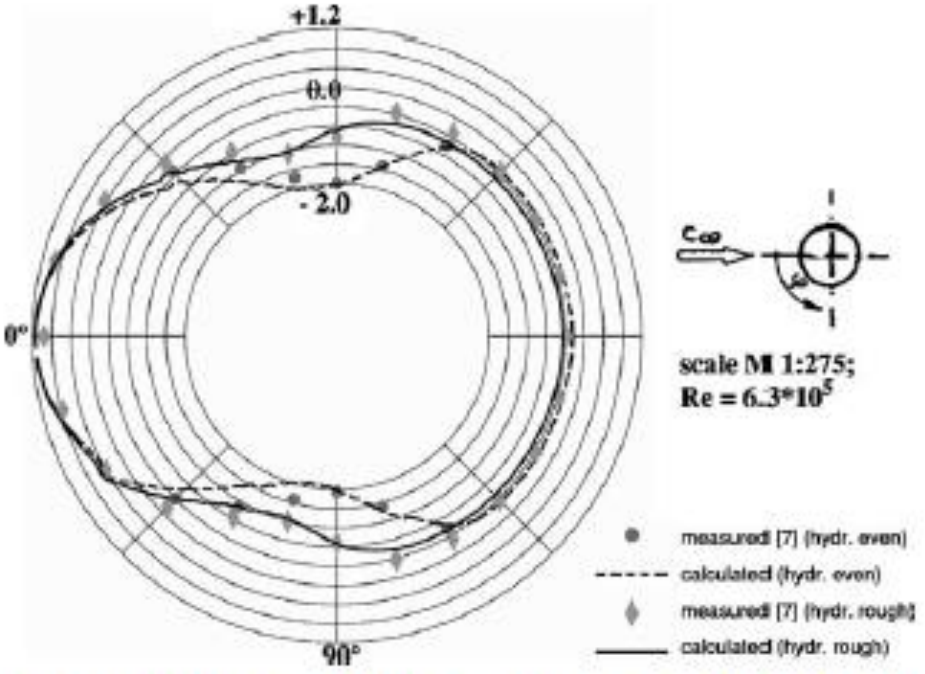

Figure 6: Distribution of c_p-values on the cooling tower surface (single tower) at a height of $0.79H_{tot}$.

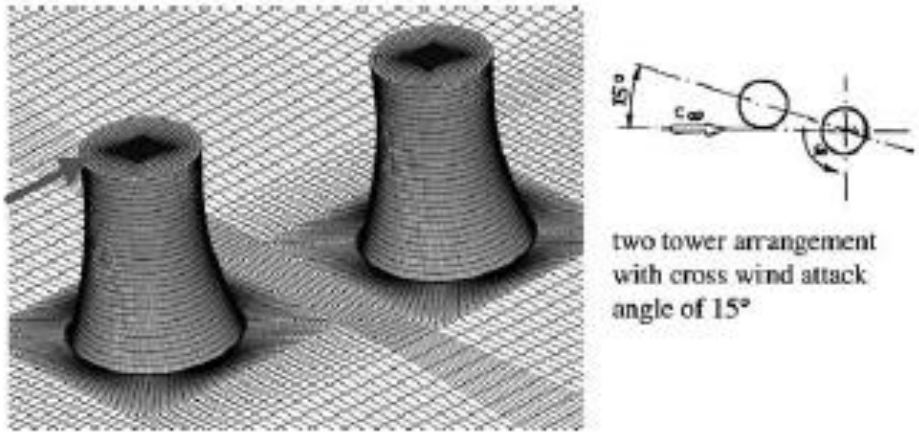

Figure 7: Numerical model and grid of two-tower arrangement.

4 Influences on the cooling tower performance

Based on the validation calculation of the cooling tower as shown in Section 3.2, the influence of several design features on the cooling tower performance is investigated by application of the numerical method.

4.1 Different fill types

With respect to the calculations for validation (reference case), the fill type has been fibrated concrete. It has been replaced by a modern plastic fill type as shown in Fig. 14 for an example. Such modern fill types are characterized by an improved heat transfer, low pressure losses and a high life-span.

The correlations of the evaporation number k_V are needed for the new fill type. The following correlation in dependency of the local mass flow ratio λ can be given:

$$k_{V,fill} = 1.92 \cdot \lambda^{0.633} \tag{14}$$

For the spraying zone and droplet/moisture area, the following correlations have been used:

$$k_{V,spray} = 0.15 \cdot \lambda^{0.633} \tag{15}$$

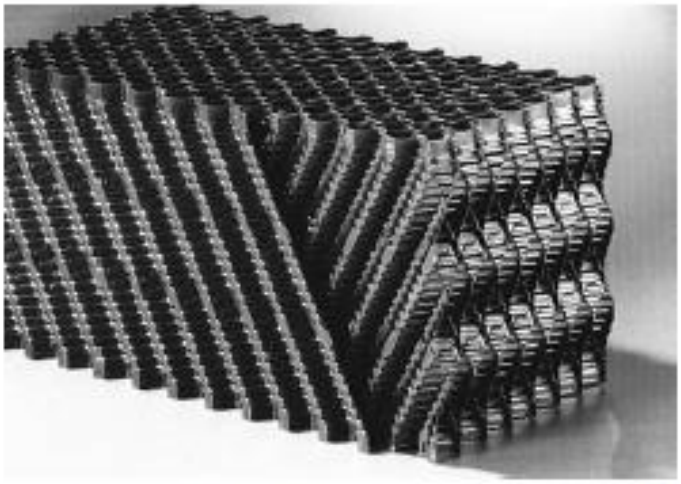

Figure 14: Typical plastic fill element for cooling tower application.

$$k_{V,drop} = 0.03 \cdot \lambda^{0.633} \tag{16}$$

Table 2: Comparison of the operating conditions.

	Plastic fill type	Fibrated concrete fill type
Environmental temperature	282.65 K	282.65 K
Humidity	77.17%	77.17%
Environmental air pressure	1.013 bar	1.013 bar
Water inlet temperature	306.05 K	307.35 K
Inlet water mass flow	17500 kg/s	16250 kg/s

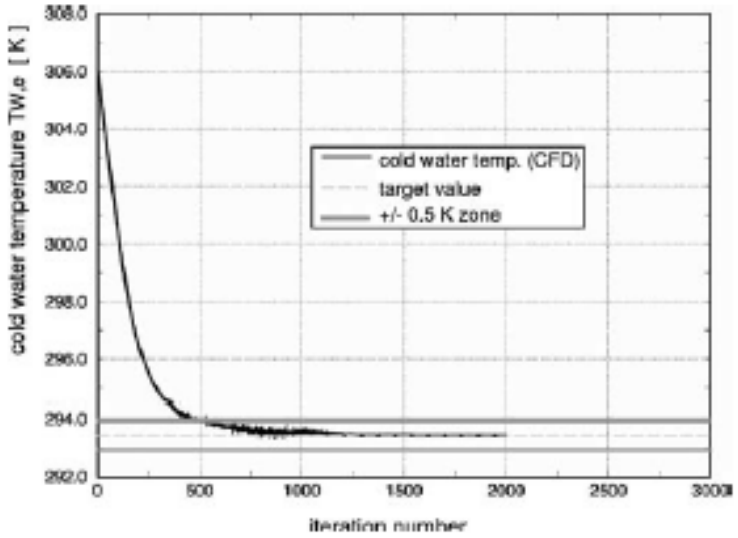

Figure 15: Cold water temperature calculation.

Table 3: Integral results on transferred heat and mass flow.

	Calculation		Design point
Cold water temperature	293.455 K		293.450 K
Total heat (transferred from water)	914.35 MW		915.0 MW
Convective heat	252.63 MW	27.63%	
Evaporation heat	661.72 MW	72.37%	
Total transferred heat in spraying area	55.60 MW	6.08%	
Total transferred heat in fill region	699.51 MW	76.50%	
Total transferred heat in droplet region	159.24 MW	17.42%	
Evaporated water mass flow	267.90 kg/s	1.53%	
Dry air mass flow	14137 kg/s		13230 kg/s
Averaged cooling tower outlet temperature	300.28 K		

4.2 Geometry of the cooling tower rim

Further numerical simulations with the plastic fill type focus on another detail of the construction of the cooling tower that is the structure of the cooling tower rim. In the previous simulations, the cooling tower rim has been modelled in a simple way, but with respect to the statics of the cooling tower, it is necessary to add a special rim structure. Such structures stabilize the cooling tower and can be located at the outer or inner side of the cooling tower rim. Figure 17 shows a stabilizing structure at the inner rim side.

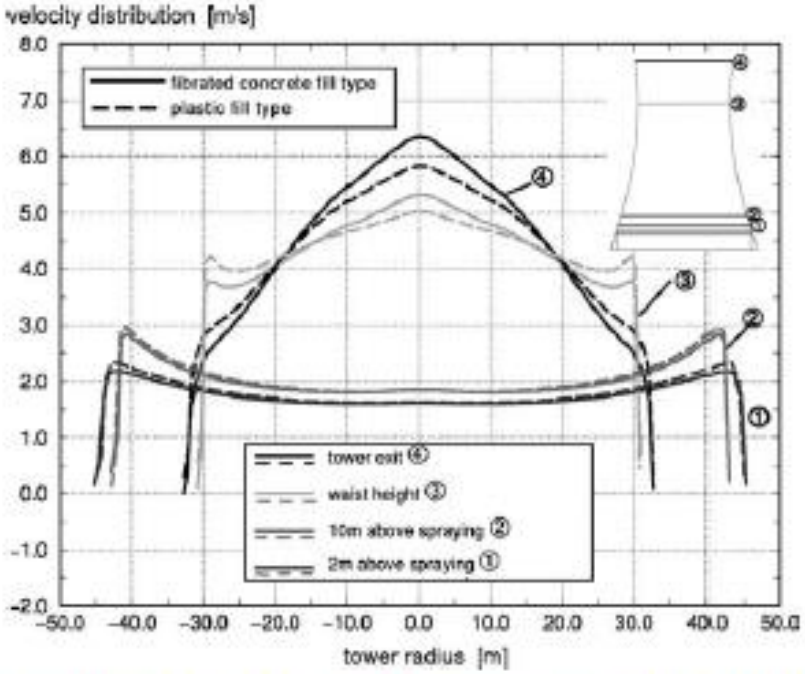

Figure 16: Velocity distribution in the cooling tower for different fill types.

Figure 17: Stabilizing structure at the inner rim side.

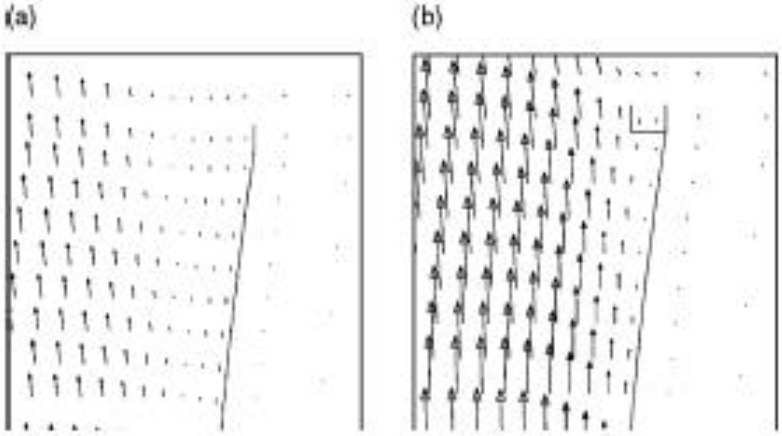

Figure 18: Flow vector at tower exit (tower rim): open gap (a) without and (b) with inner rim structure.

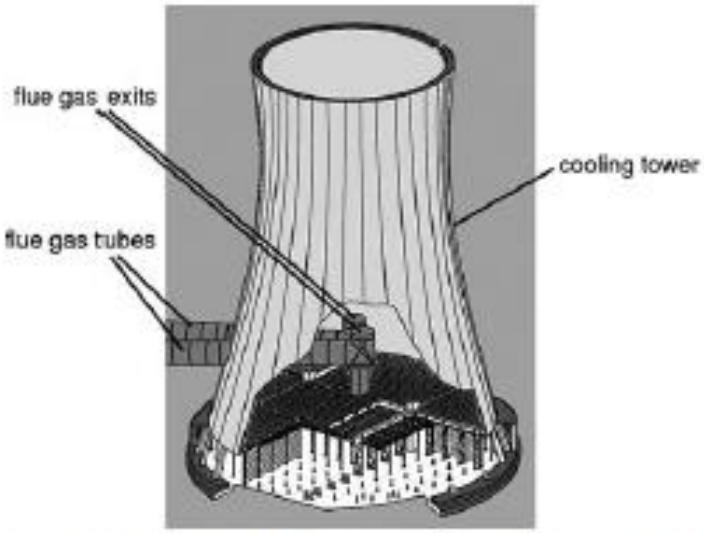

Figure 19: Natural draft cooling tower with additional flue gas operation.

(Fig. 18b). In that case, the velocity vectors show not only increased velocities at the exit but also that the recirculating flow area has vanished.

4.3 Additional flue gas discharge operation

Additional flue gas discharge operation for cooling towers has been established in recent years. In that case, the additional construction of a high chimney for the flue gas is not necessary. Thus, the costs for the construction of the power plant are reduced. Another advantage might be seen in the optical appearance of the power plant. Figure 19 shows a drawing for a typical construction of a cooling tower with additional flue gas discharge operation.

5 Cross wind effects on the cooling tower performance

A final set of numerical simulations for the cooling tower application deals with the impact of different cross wind situation, i.e. different wind velocities. It is

(a)

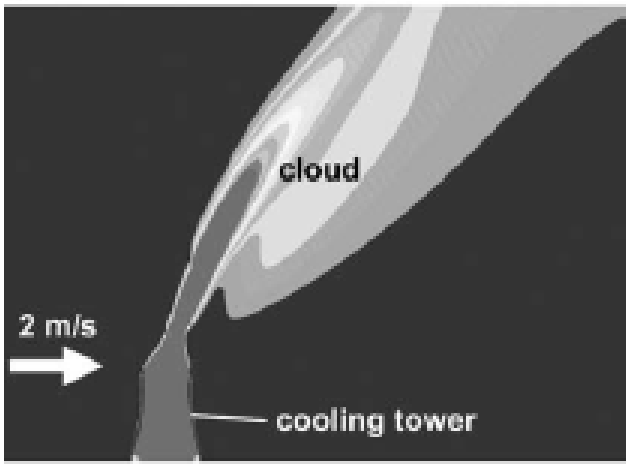

(b)

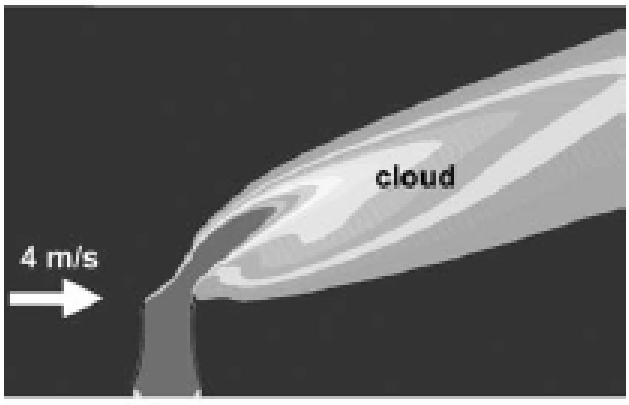

(c)

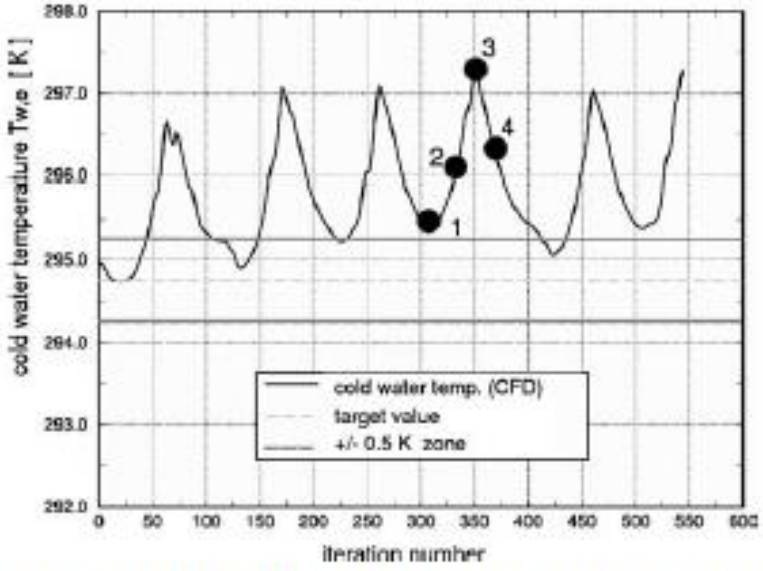

Figure 23: Cold water temperature calculation, cross wind velocity 2 m/s, cooling tower *without* inner rim structure.

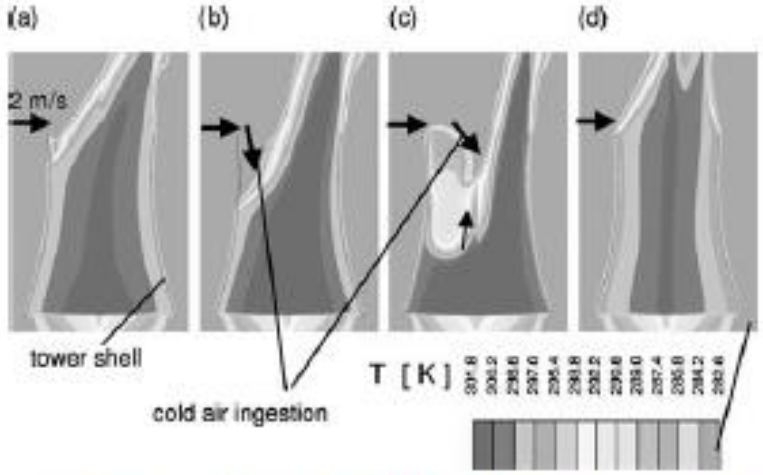

Figure 24: Temperature distribution at indicated iteration steps, cross wind ve-

Innovative gas turbine cooling techniques

R.S. Bunker
GE Global Research Center, USA.

Abstract

Advanced heat transfer and cooling techniques form one of the major pillars supporting the continuing development of high efficiency, high power output gas turbine engines. Conventional gas turbine thermal management technology is composed of five main elements including internal convective cooling, external surface film cooling, materials selection, thermal-mechanical design at the component and system levels, and selection and/or pre-treatment of the coolant fluid. The present summary will examine specific cooling technologies representing cutting edge, innovative methods expected to further enhance the aero-thermal-mechanical performance of turbine engines. The techniques discussed will include forced convective cooling with unconventional turbulators and concavity surface arrays, swirl-cooling chambers, latticework cooling networks, augmentations of impingement heat transfer, synergistic approaches using mesh networks, and film cooling.

1 Introduction

The technology of cooling gas turbine components, primarily via internal convective flows of single-phase gases and external surface film cooling with air, has developed over the years into very complex geometries involving many differing surfaces, architectures, and fluid-surface interactions. The fundamental aim of this technology area is to obtain the highest overall cooling effectiveness with the lowest possible penalty on the thermodynamic cycle performance. As a thermodynamic Brayton cycle, the efficiency of the gas turbine engine can be raised substantially by increasing the firing temperature of the turbine. Modern gas turbine systems are fired at temperatures far in excess of the material melting temperature limits. This is made possible by the aggressive cooling of the hot gas path components using a portion of the compressor discharge air, as depicted in Fig. 1. The use of 15–25%

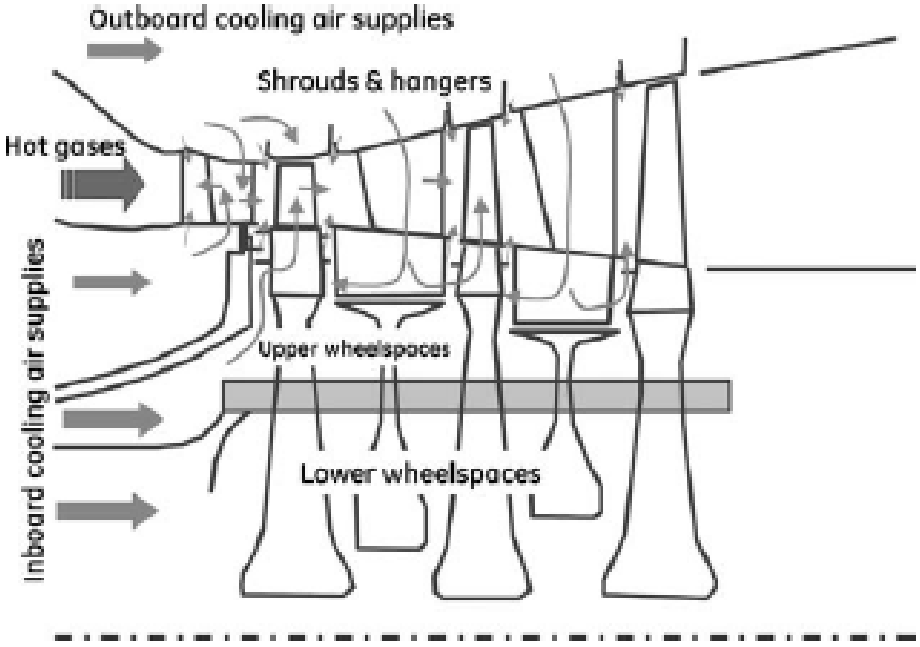

Figure 1: Schematic of turbine with cooling flows.

of this compressed air to cool the high-pressure portions of the turbine presents a severe penalty on the thermodynamic efficiency unless the firing temperature is sufficiently high for the gains to outweigh the losses. In all properly operating cooled turbine systems, the efficiency gain is significant enough to justify the added complexity and cost of the cooling technologies employed. Actively or passively cooled regions in power generating gas turbines include the stationary vanes or nozzles and the rotating blades or buckets of the high-pressure stages, the shrouds bounding the rotating blades, and the combustor liners and flame holding segments (fuel nozzles, splash plates). All such engines additionally cool the interfaces and secondary flow regions around the immediate hot gas path. A more detailed schematic of the cooling for an aircraft engine combustor and turbine first stage, which may be thought of also as an aero-derivative power turbine, is shown in Fig. 2.

Cooling technology, as applied to gas turbine components is composed of five main elements, (1) internal convective cooling, (2) external surface film cooling, (3) materials selection, (4) thermal-mechanical design, and (5) selection and/or conditioning of the coolant fluid. Cooled turbine components are merely highly specialized and complex heat exchangers that release the cold side fluid in a controlled fashion to maximize work extraction. The enhancement of internal convective flow surfaces for the augmentation of heat transfer was initially improved some 25–30 years ago through the introduction of rib-roughenerers or turbulators, and also pin-banks or pin-fins. Figure 3 shows an example schematic of a blade cooling circuit that utilizes many turbulated passages, a pin bank in the trailing edge, and impingement in the leading edge (coolant is released via film holes, tip holes, and trailing edge). These surface enhancement methods continue to play a large role in today's turbine cooling designs. Film cooling is the practice of bleeding

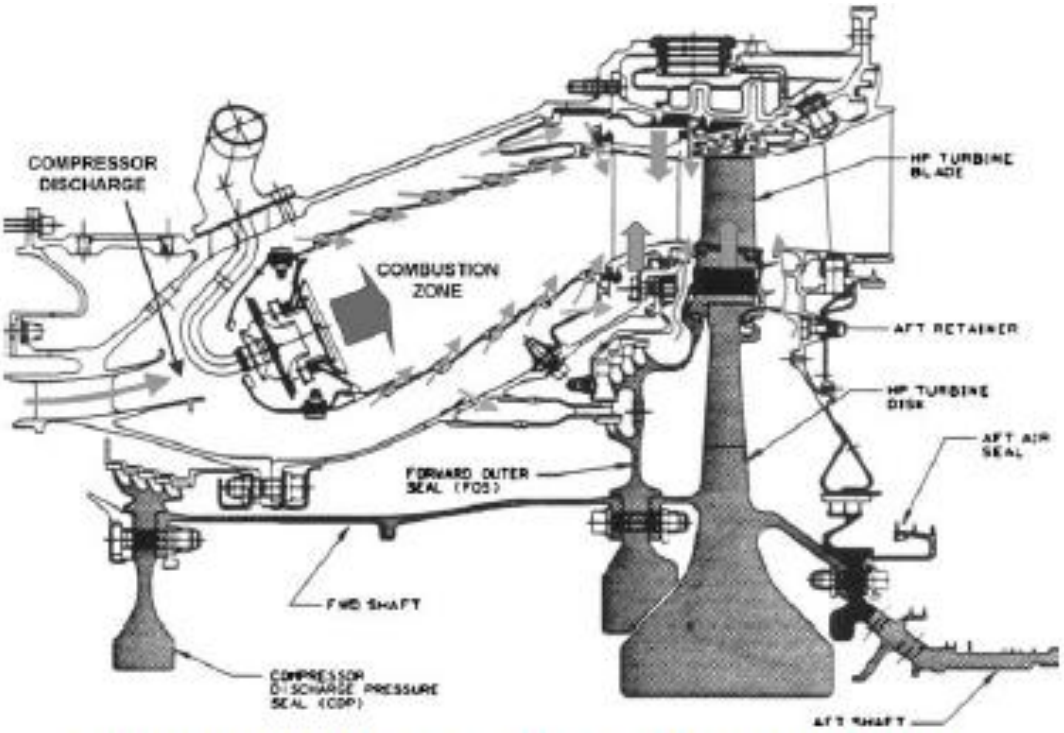

Figure 2: Cooling flows for a combustor and high-pressure turbine.

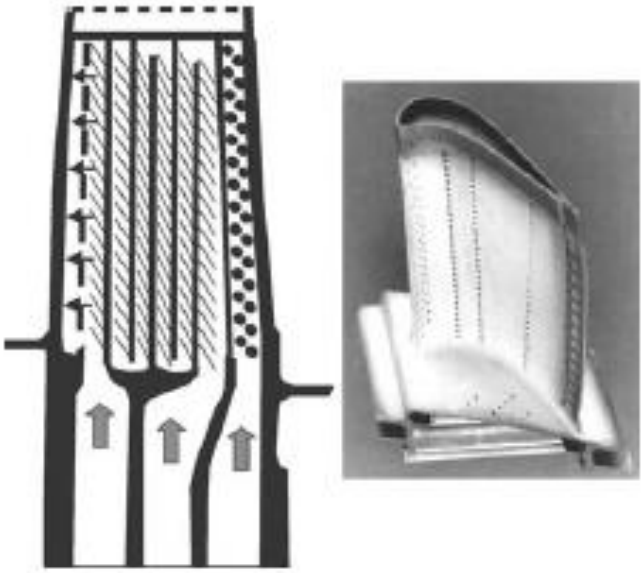

Figure 3: Schematic of a blade cooling circuit.

internal cooling flows onto the exterior skin of the components to provide a heat flux reducing cooling layer, as shown by the many holes placed over the airfoil in Fig. 3. Film cooling is intimately tied to the internal cooling technique used in that the local internal flow details will influence the flow characteristics of the film jets injected on the surface.

2 Turbulated channel cooling

One of the most common means for enhancing heat transfer coefficients within internal cooling passages, and especially the serpentine passages of many turbine blade designs, is the use of turbulators, also known as rib rougheners. Turbulators in the form of trip strips placed transverse to the bulk flow direction were one of the first improvements made to the cooling of blades, and hence many investigations have been made into the heat transfer and friction characteristics. Basic transverse turbulator research, which resulted in widely used data and correlations, was performed by Webb *et al.* [1], Burggraf [2], and Han *et al.* [3, 4]. With the advancements in materials and manufacturing technologies of the last decade, a drastically larger realm of surface enhancement techniques has become cost effective for use in the cooling of turbine airfoils. Turbulators may now be of varying shapes, orientations, segmentations, and sizes, essentially providing a continuous spectrum of possible geometries for achieving flow-surface interactions that serve to enhance local and global heat transfer coefficients. The bulk of researchers concentrated on turbulators of relative height e/D <0.2, but greater than that relative roughness typically associated with uniform surface roughness. The general findings of all such research has been that surface averaged heat transfer coefficients within stationary, turbulated passages may be enhanced by factors from 1.8 to 2.8, while the friction factors or required pumping power are increased by factors of 3–10. Many parameters have been investigated in turbulated passages (angle to the bulk flow, P/e, e/D, shaping, taper, etc.), and many more in serpentine circuits, but the range of effects has remained much the same over the years.

Read other cooling methods Page 217 to 239

CHAPTER 8

Hot gas path heat transfer characteristics/ active cooling of turbine components

T. Simon[1] & J. Piggush[2]
[1]*Department of Mechanical Engineering, University of Minnesota, USA.*
[2]*Pratt and Whitney, Inc., USA.*

Abstract

Gas turbines play an important role in the lives of all of us. They are instrumental in providing electricity or fuel to our homes and in transportation via aircraft and ships. Despite over 50 years of operation and their current ubiquity, gas turbines continue to evolve, becoming more fuel efficient, reliable, and durable. With present emphasis on further improvement in efficiency and operation with alternative fuels, significant engineering challenges remain. The gas turbine did not come about by virtue of a single, momentous breakthrough, but rather by numerous small advances on many fronts, including heat transfer, aerodynamics, materials, dynamics, lubrication, and fuels. The efforts of tens of thousands of engineers have produced the present, extensive body of knowledge that provides our basis for further development. Given the complexity of the engine, it is quite easy to become overwhelmed when trying to become acquainted with the technology on which it is based. This chapter is offered to help in one aspect of gas turbine technology, the gas path heat transfer within the turbine. It aims first to describe the physics of engine heat transfer by developing from simple ideas an introduction to the complex heat transfer phenomena within. This effort attempts to address how the engineer applies heat transfer tools available in the literature to support designs, which will advance engine life and enhance efficiency. If successful, the newcomer will establish a foothold in the technology and the more experienced engineer will be reminded of some basic concepts.

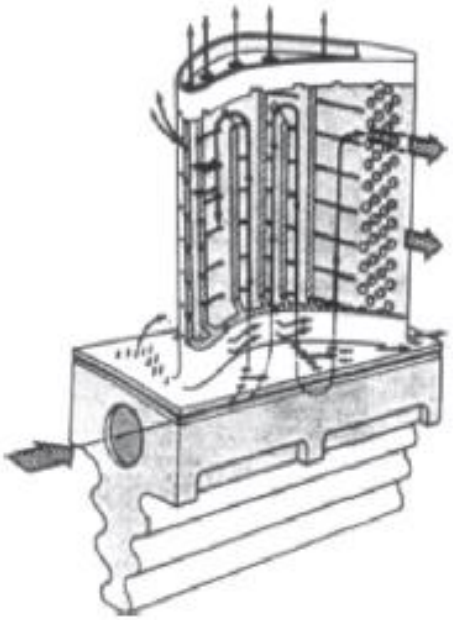

Figure 1: Coolant flows: internal channels in airfoil and endwall, impingement jets, trailing edge and tip region flows, film cooling flows (from NASA Glenn).

2 Hot gas path heat transfer characteristics

The flow entering the turbine gas path has come from the combustor, as shown in Fig. 2. Within the combustor, fuel (either a liquid similar to kerosene or diesel fuel or a gas, such as methane, syngas or high hydrogen and syngas (HSG) processed from coal) and air combine in a highly exothermic reaction that leads to high-temperature products of combustion at the high combustor pressure. A modern combustor called a dry, low-NO_x combustor operates lean and without water injection. A second type called a catalytic combustor has a selective catalytic reduction in the exhaust stream. In the low-NO_x combustor, excess air is used to maintain the combustor exit temperature at a suitable limit, consistent with the engine design and turbine durability limits. Combustor designs often have a strong swirl in the combustion zone to enhance mixing and shorten the reaction zone. About 30% of the airflow enters the primary combustion zone either through a swirl section, or through holes in primary zone of the combustion chamber. The remainder of

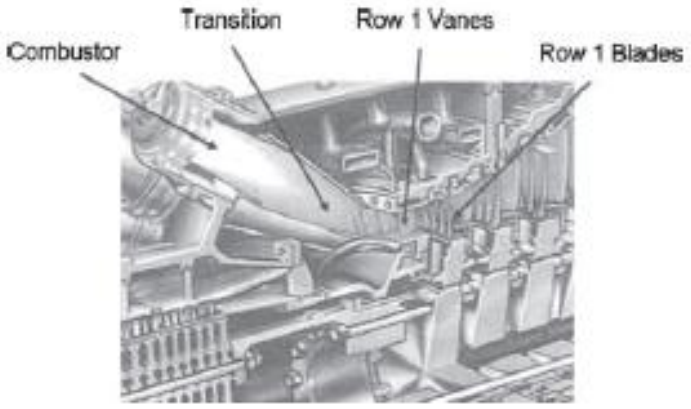

Figure 2: Hot gas path of a Siemens SGT6-5000F Gas Turbine (from Brummel *et al.* [3]).

the air, about 70% of the total airflow, is supplied through holes in the combustor liner as dilution air to mix and cool the flow and to protect the liner from reaching excessive temperature levels. In the case of a catalytic combustor, a catalytic reactor section is put downstream of the fuel/air mixing section of a pre-burner. This reactor consists of rather fine channels coated with a catalyst, such as palladium oxide. The catalytic reaction takes place at temperature levels that are below the turbine inlet temperature so a downstream combustor is needed to raise the gas temperature to the turbine inlet temperature. This combustor is similar to the dry low-NO_x combustor.

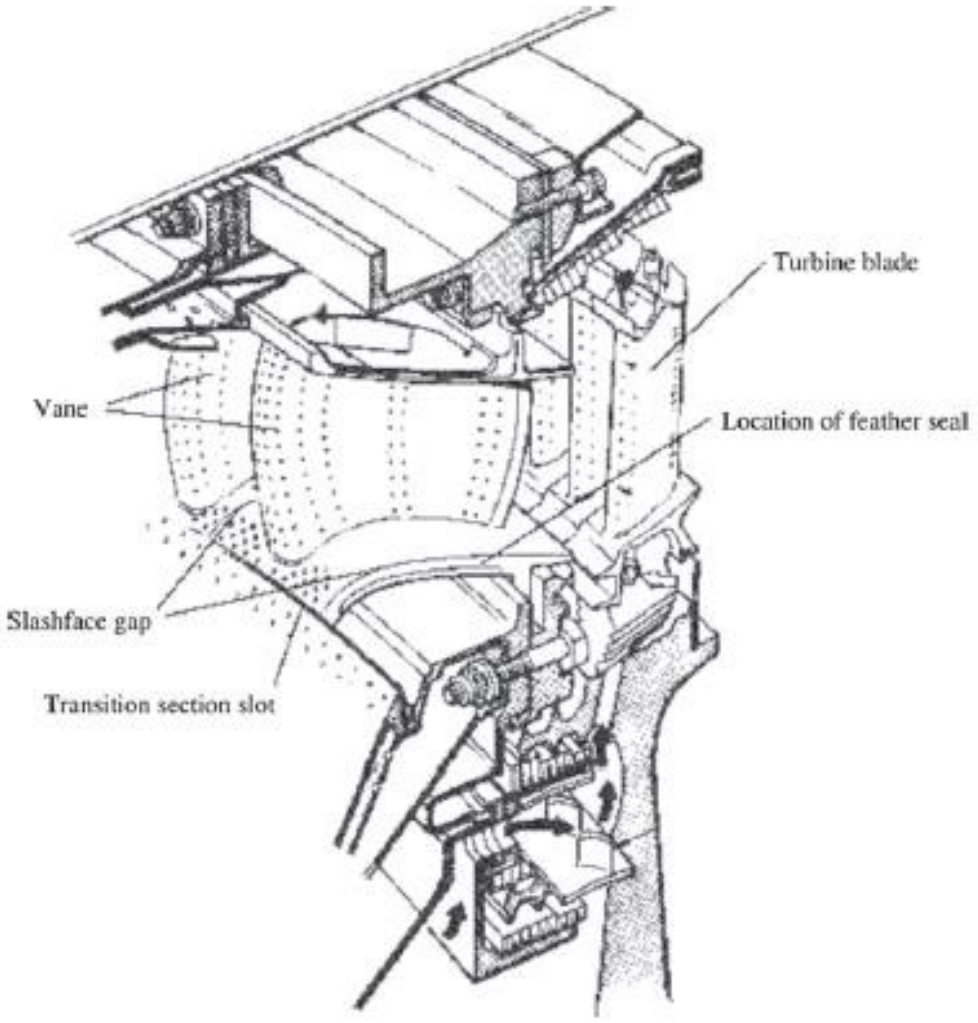

Figure 3: First stage vane and rotor section showing the transition section to vane slot as well as the slashface or gutter gap (from Cumpsty [4]).

3 Active cooling of the gas turbine components in the gas path

As discussed in the Section 1, stage temperature profiles of gas turbine engines often exceed the temperature capability of the turbine materials. To correct the problem, designers incorporate passages and heat transfer augmentation features on the internals of airfoil castings. When relatively cool fluid drawn from the compressor is

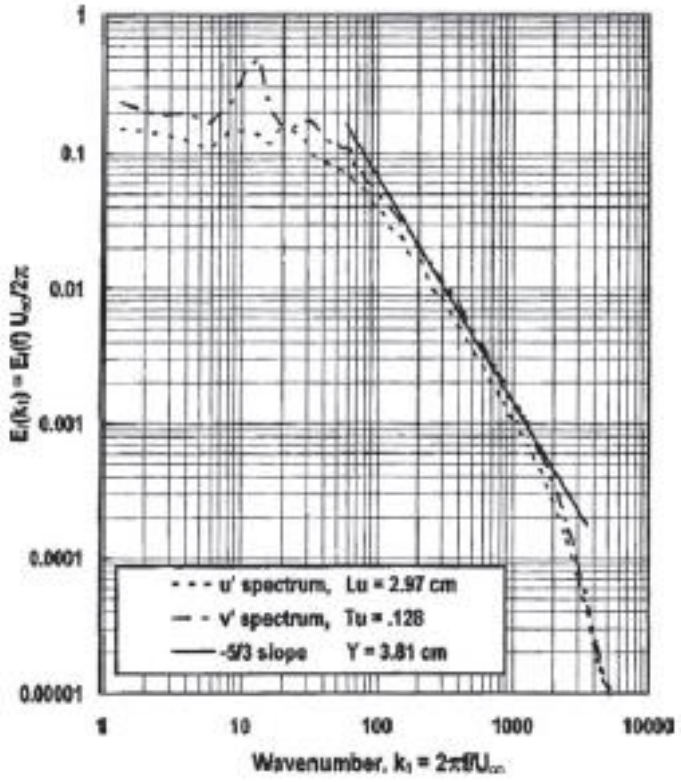

Figure 7: One-dimensional spectra of u' and v' for the combustor with a short spool showing the inertial subrange isotropy (from Ames [14]).

passed through the internal passages, the metal temperature of the airfoil can be maintained below the limits defined by material capability. The design of these internal passages has evolved over many years leading to configurations that are complex and highly effective. Some of the most popular schemes are highlighted in the following portion of the chapter.

3.1 Impingement cooling

Impingement cooling can be a very effective way to cool internal surfaces of a turbine airfoil. Properly designed impingement cooling schemes tend to have high heat transfer coefficients but also large pressure drops. As impingement cooling systems require some rather unique geometries; a feed plenum, hole plate, and an impingement target and plenum, the use of impingement cooling systems is typically confined to the first stage vane (where the high heat loads and relatively low cooling supply pressure to passage dump pressure ratio precludes the use of long-channel cooling circuits) and the leading edge and trailing edge regions of other airfoils. There are several mechanisms associated with the impinging jet that improve heat transfer. These will be discussed in the following sections.

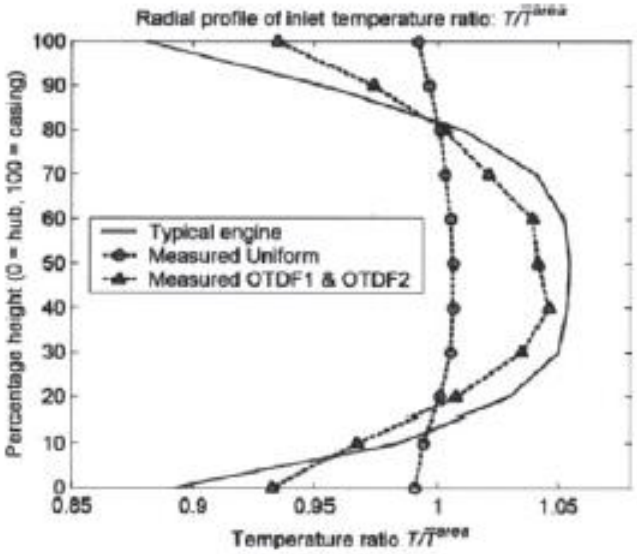

Figure 8: Circumferentially averaged temperature distributions at the turbine vane inlet. Shown is a measured profile in a real engine (typical engine), a measured profile in a simulator in which distortions due to discrete fuel and dilution air injection and endwall cooling flows are active (OTDF1 and OTDF2), and a profile measured in the simulator when the inlet temperature distortion mechanisms are not active (measured uniform).

3.1.1 Single jets

The structure of the impinging jet is of interest. A schematic of a representative geometry is shown in Fig. 9. In the simplest case, the jet flow originates in a plenum where the coolant fluid has little or no momentum. The fluid passes through a hole or slot into a lower pressure zone, driven by the pressure difference between the two plenums. As the fluid passes through the hole, it may be thought of as a slug flow with a negligibly thin boundary layer around the edge of the jet and a very flat velocity distribution across the jet core (as shown in Fig. 9). The thin boundary layers can be attributed to the rapid spatial acceleration of the flow approaching the hole exit plane. The jet has relatively high momentum as it passes into the low-pressure zone. The flow on the periphery of the jet shears on the low momentum fluid external to it, eventually leading to a breakdown of the shear layer into a train of large turbulent eddies. This causes the jet to widen and entrain external flow. The velocity profile of the jet becomes non-uniform, as shown in Fig. 9. If the jet length to diameter ratio is sufficient, the shear layer between the jet and the surrounding flow consumes the core of the jet, which leads to high levels of turbulence in the vicinity of the center of the jet. The large eddies in the shear layer also establish circulation in the low-pressure plenum, mixing that fluid. Finally, the jet impinges upon the target surface. Due to the high momentum of the jet perpendicular to the wall, the boundary layer at the impingement point is

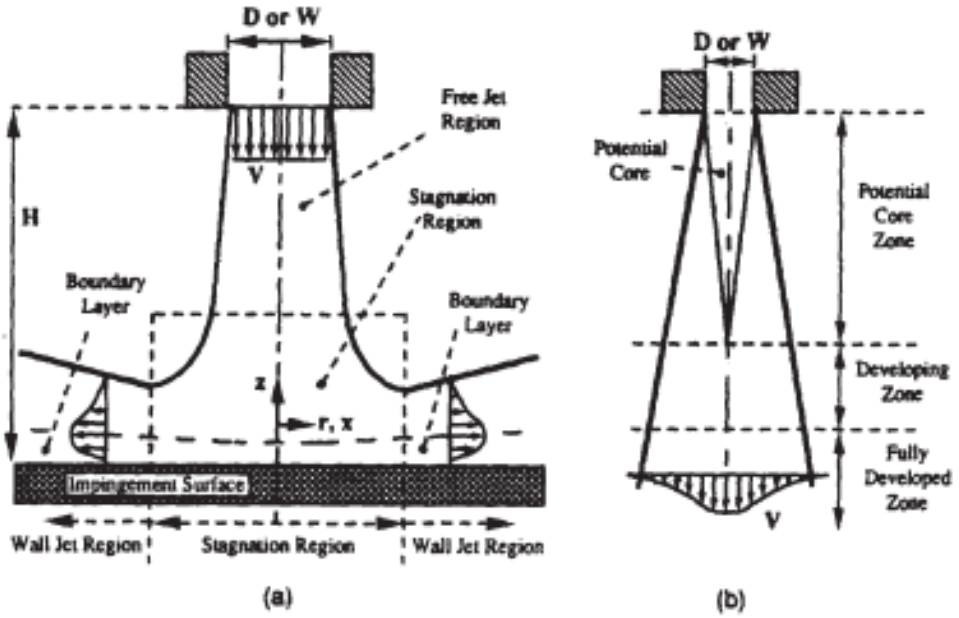

Figure 9: Different regions of an impingement jet (from Viskanta [16]).

3.1.2 Impingement arrays

The single jet is of academic importance and helps introduce the reader to the general physics of the flow field. In turbine applications, impingement jets are typically arranged in two- or three-dimensional arrays. Both arrangements tend to be strongly influenced by the effect of cross flow, which develops as the spent jet air exits the stagnation zone on the target surface. Cross flow interaction with the jet causes the development of several important flow structures in addition to the jet shear layer vortex structure discussed above. The interaction of the jet fluid and the endwall boundary layer creates a counter-rotating vortex pair. The flow structure and mechanism causing the vortex pair is similar to a cylinder in cross flow and its interaction with the endwall boundary layer. The cross flow perceives the jet as an obstacle and passes around it, and a horseshoe vortex is formed. Finally, behind the jet, there exists a wake zone characterized by the presence of what Kelso *et al.* [18] term the upright vortex and also the presence of wall vortices. The vortices are shown in Fig. 10. For a more extensive treatment of the interaction of the jet and cross flow, the reader is referred to the thorough work of Kelso *et al.* [18] and also Lee *et al.* [19]

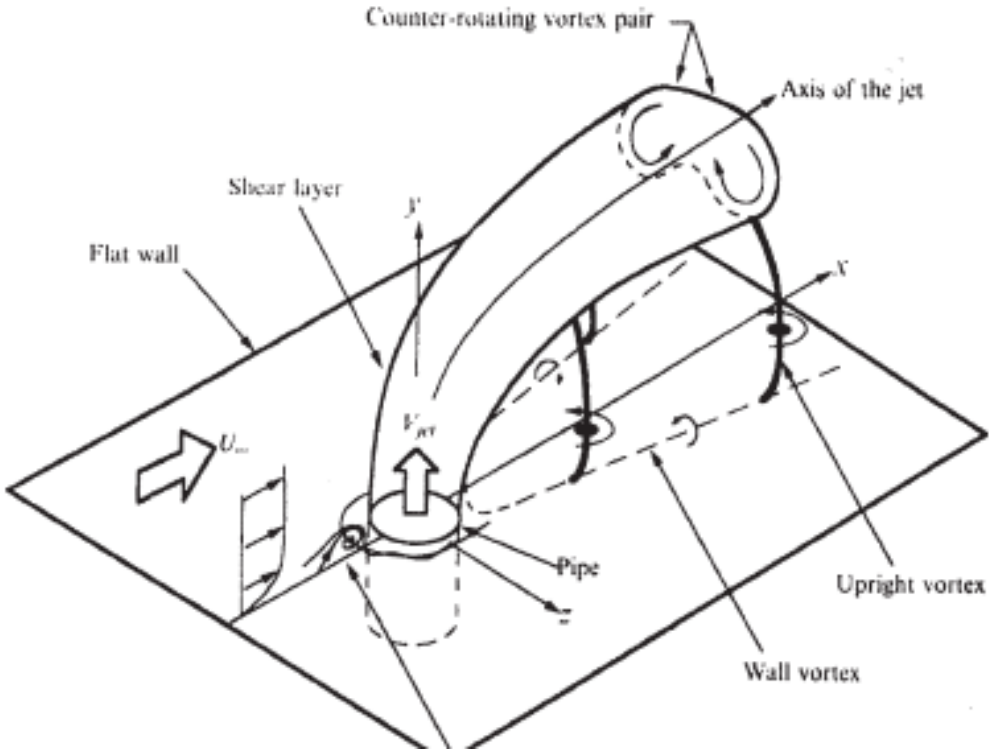

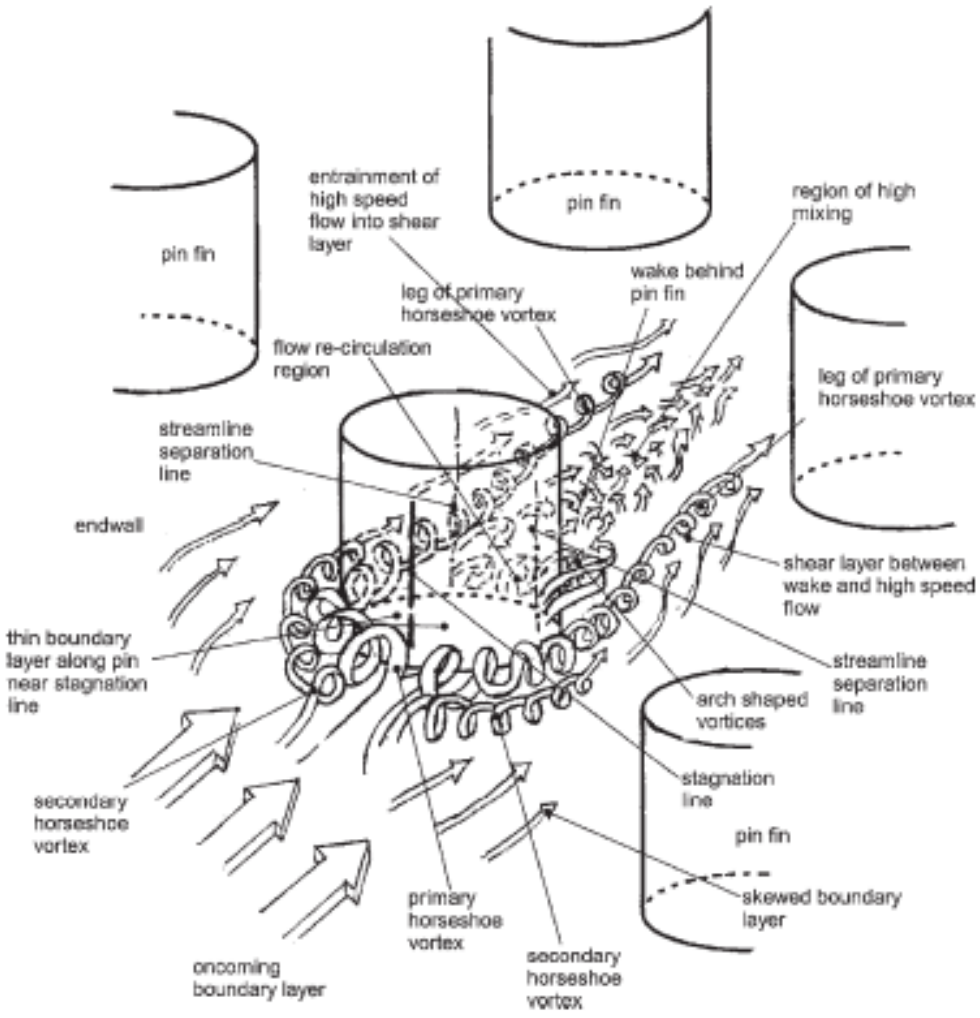

Figure 16: Flow field around pin fins within an array. The oncoming boundary layer gives rise to the primary and secondary horseshoe vortices. The pin creates a wake region with strong mixing (from Ligrani *et al*. [32])

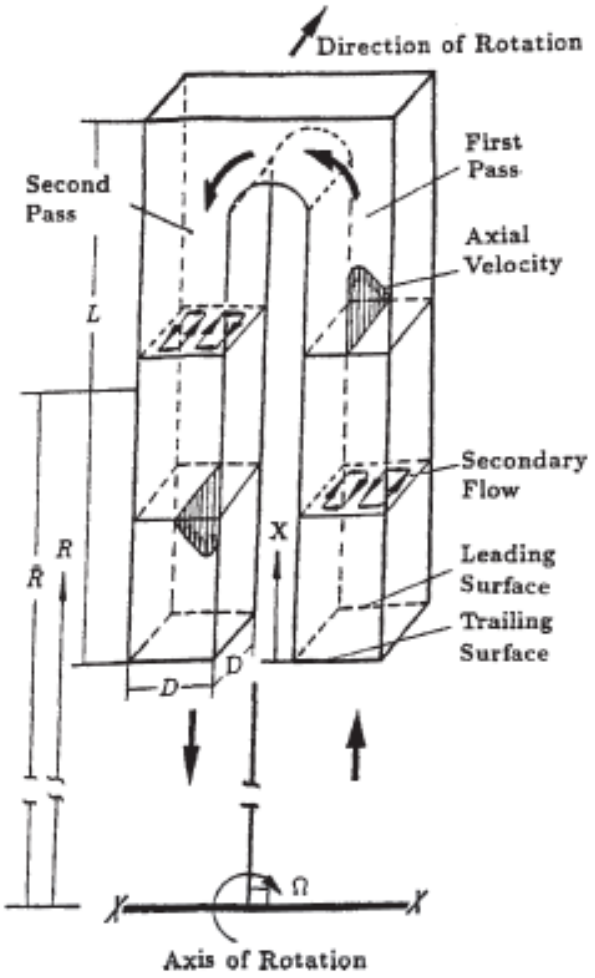

Figure 20: Depiction of the streamwise and secondary flow fields in a rotating channel.

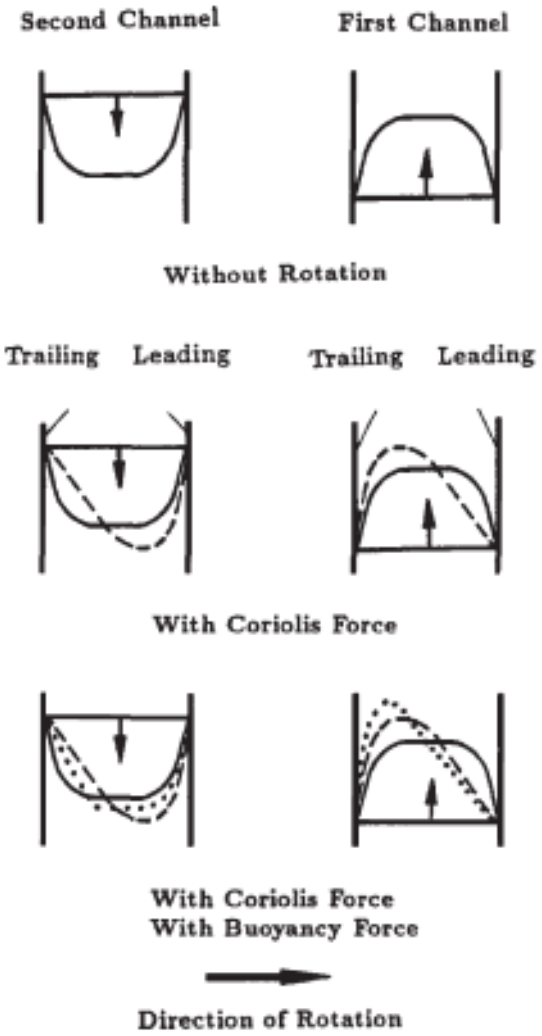

Figure 22: Effects of inertia, Coriolis, and rotational buoyancy. Note that, given the clockwise direction of rotation, the direction of the vector is out of the page (taken from Han *et al*. [1]). Solid lines, without rotation; dashed lines, with Coriolis force only; dotted line, with buoyancy and Coriolis forces.

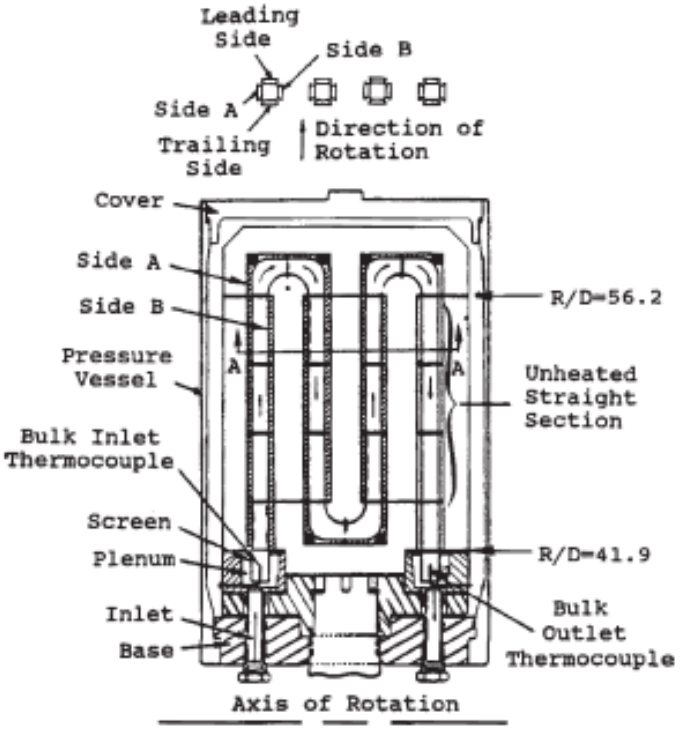

Figure 23: Serpentine coolant passage model used by Wagner *et al.* [40].

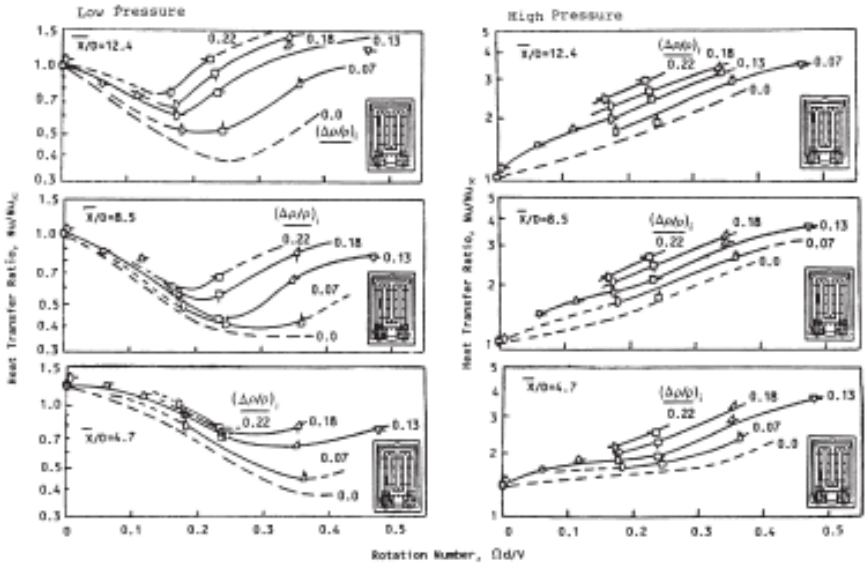

Figure 24: Effect of rotation number and density ratio on heat transfer ratio on the leading surface (low pressure) and trailing surface (high pressure) of a

Read other cooling methods in Chapter 8

CHAPTER 9

Design and optimization of Turbo compressors

C. Xu & R.S. Amano
Department of Mechanical Engineering,
University of Wisconsin-Milwaukee, USA.

Abstract

A compressor has been refereed to raise static enthalpy and pressure. A successful compressor design greatly benefits the performance of the whole power system. Lean design methodologies have been used for industrial power system design. The compressor designs require benefit to both OEM and customers, i.e. lowest cost for both OEM and end users and high efficiency in all operating range of the compressor. The compressor design and optimization are critical for the new compressor development and compressor upgrade. The design experience and design considerations are also critical for a successful compressor design. The design experience can accelerate compressor lean design process. An optimization process is discussed to design compressor blades in turbo machinery. The compressor design process is not only an aerodynamic optimization, but structure analyses also need to be combined in the optimization. This chapter discusses an aerodynamic and structure integration optimization process. The design method consists of an airfoil shape optimization and a three-dimensional gradient-based optimization coupled with Navier–Stokes solvers. A model airfoil of a transonic compressor is designed by using this approach, with an efficiency improvement. Airfoil sections were stacked up to a three-dimensional rotor blade of a compressor. The efficiency is improved over a wide range of mass flow. The results indicate that the optimization process can provide improved design and can be integrated into a compressor design procedure. Initial design considerations of turbo compressor are commonly performed with experience base, although computer technology and numerical methods have made a significant progress. Three-dimensional computational fluid dynamics codes are still not major design tools for compressors. Major design systems for industrial compressor design are largely based on one-dimensional mean line and two-dimensional through flow tools. The experience of designers is one of the key factors to drive design success. The discussions and information

on compressor design considerations in open literature are also reviewed. This chapter consists of three parts: Part I provides an overview of the turbo compressors and basic design procedures. Part II discusses a blade optimization process. An axial compressor blade design was used as an example to illustrate the optimal design. Part III provides some design experience of centrifugal compressors.

1 Part I: Compressors and their design

1.1 Introduction

Compressors are devices to pressurize working gases. One of the basic applications for the compressors is to increase the gas pressure and deliver gas to the downstream of the compressor. For example, compressors can provide higher-pressure gas for combustion, high-pressure gas to drive gas tools, transport process gas through pipelines, or compressor gas for heat recovery or gas conditioning circles.

Compressors can be separated into two basic types: The positive displacement and continuous flow compressors. The reciprocating and rotary compressors are two major positive displacement compressors. Ejectors and turbo compressors are the two main continuous compressors. Axial and centrifugal compressors are the two basic types of turbo compressors. The main purpose of this part is to describe an industrial turbo compressor design process.

Gas turbine and compressor manufactures are competing to produce more efficient and wide operating range machines. Correspondingly, many research works and developments were carried out to meet the manufacturers' needs [1–8]. Compressor blade design is one of the critical processes to ensure the overall compressor have good performance. For all the turbo compressors, there are two major parts: rotating blade and stationary blade. The basic functions of compressor moving blades are added the work to gas and turn the gas to the required angles to have diffusion in the flow path to increase the static pressure and discharge to next component. For the stationary blades, the basic function is to turn the gas to the required angles to have a right diffusion level for the gas. The design goal for modern compressor blades are to achieve the desired flow turning with minimum losses and can tolerance high incident within the constraint of geometric orientation of the blade row requirements defined by overall compressor design.

Both rotating and stationary blades involve the airfoil and blade designs. The basic compressor blade performance was mainly determined by five key factors: shape of the blades, airfoil or blade section stagger angle, solidity, inlet and discharge flow angle, airfoil or blade section loading. Unlike turbine blades through which flows are accelerated, the adverse pressure gradient due to the flow diffusion in compressor blades. The adverse pressure is an unfavorable force on the boundary layer development. It is very difficult to achieve a thin boundary layer. The boundary layer separation often happens inside the compressors. Therefore, the main challenge for compressor blade design is to generate a blade shape to meet the flow angle requirements and reasonable loading distributions.

Efficiency had been a major criterion in the design of compressor and turbine components for many years. The search for maximum efficiency is traditionally made by successive modifications of the geometries and verification by wind tunnel tests and flow calculations. Such a process can be time consuming and outcome strongly depended on the designs' experiences. This approach is difficult to have advanced design such as shock-free transonic blades and blades with optimized dihedral.

Many design methods were proposed in both research stage and industrial applications [1–9]. The blade design methods can be categorized into two basic methods. One is direct design and another is inverse design method. For direct design method, blade was design first based on the designer experience and then a Navier–Stokes equation code or a fast inviscid code was used to evaluate the airfoil performance. The process of design and performance calculations are completed until a satisfy airfoil was built. The designed airfoils are then stack-upped to produce a three-dimensional blade. Normally, some three dimensional optimization processes are used to continue optimizing the design [1–9]. In inverse design method [5], normally Euler equations with modified boundary conditions were used for an iterative procedure to search the desired design.

With the rapid progress in computational fluid dynamics (CFD) and computer technologies, compressor design has been developed from purely empirical methods to apply more CFD simulation into design process. The CFD method allows the aerodynamic designer to have detailed flow information and to optimize the blades. However, at the beginning stage of the design, the experience data are very helpful to accelerate the design and provide the basic information, to engineers in other discipline. In this chapter, we will start with basic introduction of the compressor, and then talk about design process and optimization, and finally the design experience the author will be discussed.

1.2 Types of turbo compressors

Turbo compressors can be categorized into two types: compressors and turbines. Compressors absorb power to increase the fluid pressure or head, and turbines produce power by expanding fluid to a lower pressure or head. Compressors have a wide application in order to provide the high-pressure gas for combustion in jet engines, to transfer process fluid in pipelines, to provide high-pressure gas to driving tools, etc. The compressor system is one of the important parts of a power system. Both centrifugal compressors and axial compressors are continuous flow compressors.

Compressors are categorized into three types according to the nature of the flow path through the passages of the rotors. When the fluid through flow path is wholly or mainly parallel to the axis of rotation, these types of compressors called axial compressors as shown in Fig. 1a. Centrifugal compressors having through flow paths are wholly or mainly in a plane perpendicular to the rotational axial as shown in Fig. 1b. When the through flow in the compressors has a significant amount of velocities in both radial and axial directions, we call this type of compressors as

mixed flow compressors as shown in Fig. 1.c. Sometimes, mixed flow compressors are also reference as centrifugal compressors.

The axial compressor was first patented by Sir Charles Parsons in 1884 [10]. His compressor concept just simply reversing an axial turbine for use as a compressor; however, the efficiency of compressors from reversing turbines was less than 40%. The difficulties associated with the development of axial compressors stemmed from the fundamentally different nature of the flow process compared with that in axial-flow turbine. It was not until 1926 that any further improvement on axial compressor efficiency was undertake when A.A. Griffith [11] outlined the basic principles of airfoil theory of compressor and turbine design.

Axial flow compressors are the most common types of compressor for aircraft engines and big industrial gas turbine. The gas in an axial compressor flows in an axial direction through a series of rotating rotor blades and stationary stator vanes. The flow path of an axial compressor decreases in cross-section area in the direction of flow, reducing the volume of the gas as compression progresses from stage to stage of compressor blades.

In axial compressors as shown in Fig. 2, the gas being delivered to the face of compressor by the gas inlet duct, the incoming gas passes through the inlet guide vanes (IGVs). Gas entering the first set of rotating blades and flowing in axial direction, is deflected in the direction of rotation. The gas speed is slowed down and turns as it is passed onto a set of stator vanes, following which it is again picked up by another set of rotating blades, and so on, through the compressor. The pressure of the gas increases each time it passes through a set of rotors and stators. The increase in the stage pressure almost inevitably leads to some aerodynamic constraints. The main constraint is increased Mach number, possibly giving rise to shock induced boundary layer separation or increased losses due to poor diffusion of the flow. The maximum stage pressure achieved was about 2.1 based on the recent development.

The aerodynamic principles are applied to the compressor design to increase axial compressor efficiency. The axial compressor blades are treated as lifting surfaces like aircraft wings or propeller blades. The cascade effect is a primary consideration

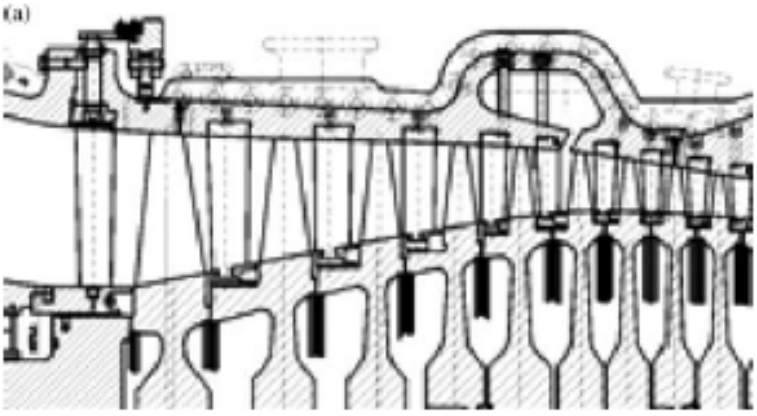

Figure 1: Types of compressors: (a) axial, (b) centrifugal, and (c) mixed flow compressors.

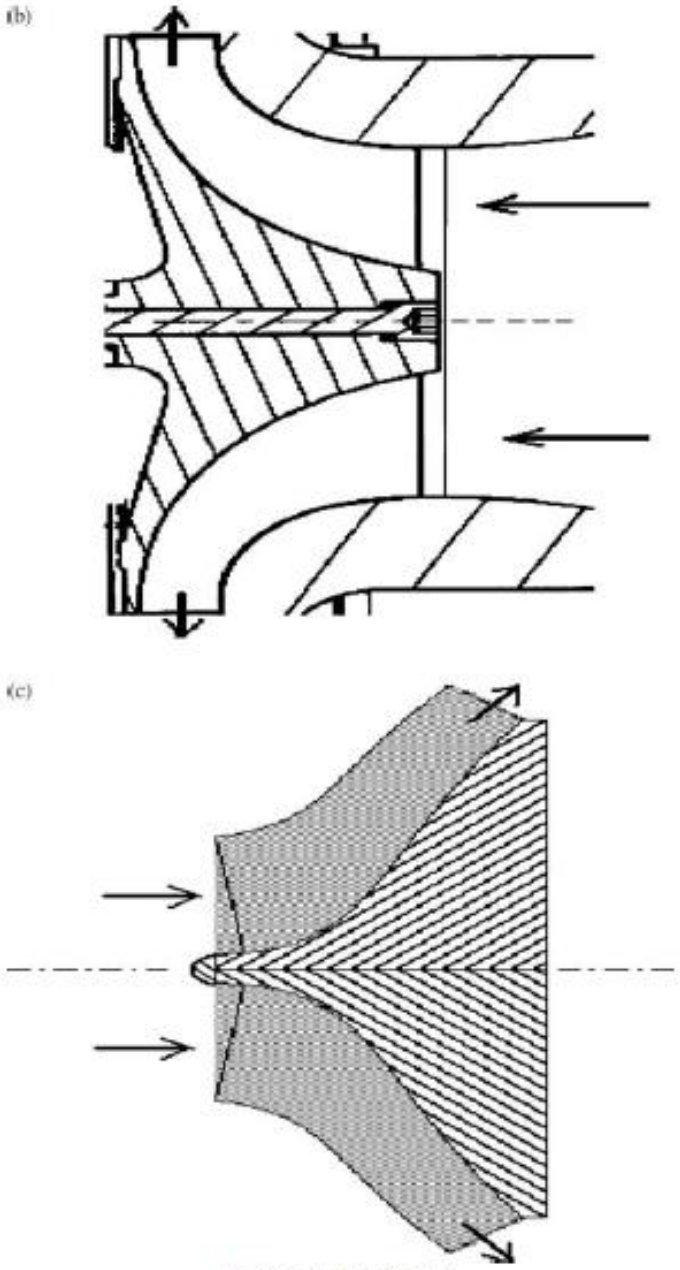

Figure 1: Continued

in determining the airfoil section, angle of attack, and the spacing between blades to be used for compressor blade design. The blade must be designed to withstand the high centrifugal forces as well as the aerodynamic loads to which they are subjected. The clearance between the rotating blades and their outer case is also very important. The rotor assembly turns at a high speed and must be rigid, well

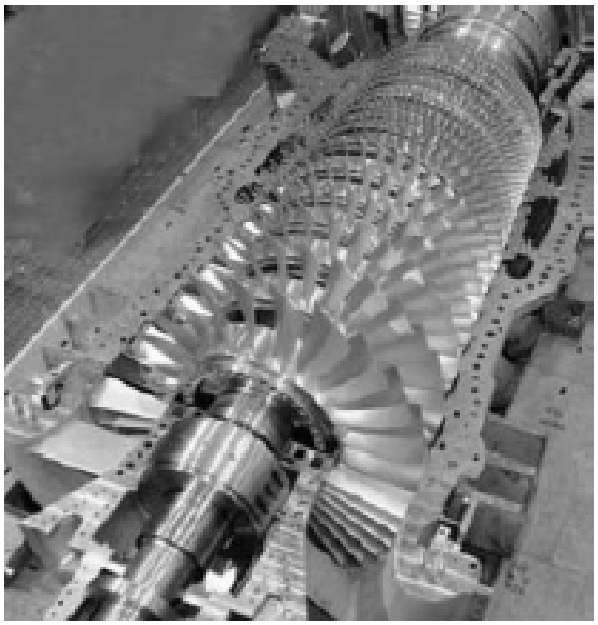

Figure 2: Axial compressors.

aligned and well balanced. Axial compressors have more benefits than centrifugal compressors at high flow and low-pressure ratio compressions. The flow range for most axial compressors is from 10,000 CFM (4.7 m^3/s) to 2,000,000 CFM (943 m^3/s) and the pressure ratio range is from 1.05 to 15. Some high-pressure ratio multistage compressors can produce pressure ratio over 30 with more than 20 stages.

Centrifugal compressor development was stimulated by aircraft propulsion. Frank Whittle and Hans Joachim Pabst von Ohain built their turbojet engines independently [1]. On August 27, 1939, Hans von Ohain's engine first time powered an aircraft flight. Shortly later, the Whittle turbojet engine was first flown on May 15, 1941. Both engine designs incorporated a centrifugal compressor to increase the gas pressure. After systematic studies [1], when researchers noticed that for the increasingly larger powered engines required for aircraft propulsion, the axial compressors were preferred. Axial compressor offered a smaller frontal area and relative better efficiency for large gas flow compression. However, centrifugal compressors still offer the advantages for low gas flow rate compressors.

The fluid comes into the centrifugal compressor through an inlet duct and can be given a prewhirl by the IGVs. The IGVs give circumferential velocity to the fluid before it flows inside of the compressor inlet. A positive vane angle produces prewhirl in the direction of the impeller rotation, and a negative vane angle produces prewhirl in the opposite direction. The positive prewhirl decreases the relative inlet Mach number. One purpose of installing the IGVs is to decrease the relative Mach number at the induce tip inlet because the highest relative velocity at induce inlet is

1.3 Aerodynamic design

The design of the turbo compressor begins with a specification and proceeds through preliminary design to blade design and analysis using design tools. The design process begins with mainline calculation, which is based on the required design flow, and stage pressure ratio or head rise to select the compressor type, number of stages and find the velocity triangles at inlet and outlet of each components of the compressor. Then the performance and basic flow parameters of each component of the compressor are analyzed based on mean line information, then the two-dimensional airfoil sections are designed and stacked up, and finally three-dimensional flow analyses are performed to do further optimization. The objective of aerodynamic design of the turbo machines is to obtain both maximum overall machine efficiency and wide operating range within the limitations imposed by stress, cost, manufacturing and other considerations. Before the 1970s, compressors were mainly designed by empirical methods, based on the accumulated experience of designers and their company. The compressors some were successful design and some time, the designed compressor could not meet efficiency and operating range target. After 1970s, CFD had played an important rule in designing the turbo machinery. Significant improvements in efficiency and operating range have been achieved. Improved experimental measurements have become available over the last three decades [30]. The combinations of the numerical predications

and detail flow measurements had led to a great improvement in flow physics in the centrifugal compressors.

Recently, a competitive product demands a high level of design optimization of compressor and involves several different disciplines considerable historical design experience and a variety of design tools. Although most of the compressor design systems allow the efficient transfer of design information, how to obtain the design information especially three-dimensional flow field information is still a big challenge. Most of the compressor design involves considerable iterations between aerodynamics, structure and manufacturing cost. During the compressor design, the knowledge of the designers and experience still play an important role. Although many integrated design system and optimization codes permit some design optimizations, many design correlations still need designers' input based on designers' experience. Part II introduces an aerodynamic design and optimization procedure. Part III summarizes the authors' centrifugal compressor design experience to help compressor designers who are in the initial stages of their careers to perform aerodynamic design.

2 Part II: Blade design and optimization

2.1 Introduction

With the development of the CFD, it has been implemented in the turbo machine design process. Great efforts are devoted to improving the efficiency of the gas turbine components. The airfoil designs for turbine and compressor airfoils plays an important role in increasing the turbine efficiency. In the airfoil design, there are two types of implements the aerodynamic design engineer often considers. One is to design and employ custom-design blade profiles with minimum losses and controlled blade boundary layers. The second and even more complex part is to minimize losses resulting from secondary flows near hub and casing. Recently, three-dimensional blade design concepts were proposed to help control secondary flows [31]; however, the complex flow is difficult; to simulate even by using fully three-dimensional Navier–Stokes flow solvers. And the validation of the Navier–Stokes solvers needs lot of experimental data and it is time consuming and expensive. Therefore, almost all the aerodynamic designs are based on the two-dimensional design. The inviscid analyses of the two dimensional airfoil sections still play an important role in the design process. Authors recently developed an airfoil design process based on the Bezer curves to produce the custom airfoil sections based on the flow field requirements of the airfoil [2]. In this study, the airfoil design process was implemented with optimization based on the two-dimension viscous turbulent code.

It was known that for a blade row in an annulus, the stream surface between two annular walls is twisted for most cases. These twists are induced by either shed vorticity or by secondary from arising from inlet vorticity. Stream surface twist can arise in an irrotational flow owing to either span wise components of velocity or span wise blade forces. Many efforts had been adopted to reduce the stream

surface twist and reduce the secondary flow losses, such as sweep [32], lean [33], bow [34] and twist [35, 36] the blades or design a non-axis symmetric end wall. However, there is little information in the available literature for using three-dimensional design and almost no information is available to show how to integrate the three-dimensional features into design process. Most of the study was still on the academic research and was based on the particular machines or blades. Moreover, most of the studies were based on the particular blade and flow situations. For example, Singh *et al*. [35] argued that closing the blade throat near the end walls could obtain significant efficiency improvements and Wallis and Denton [36] also obtained an efficiency increase from almost the opposite type of blade twist near the end wall. For different machines and different designs, may different techniques should be used according to the flow field nature of the designs. It is very important to design a blade design procedure and optimize the design.

The increased use of CFD tools has been driven mainly by two factors. First

The increased use of CFD tools has been driven mainly by two factors. First, from performance standard point of view, efficiency has steady increased. Second, the turbo machinery industry as a whole has been pushed toward reduced cost designs. The cost reduction is in terms of development, modification, production and operating costs. The cost reduction drives a turbo machine toward high loading in order to reduce stage count, while maintaining or exceeding past performance goals. The current design of the new stage is already outside of the standard airfoil database. Most of the airfoil needs to be designed and the development of the design tools to meet this requirement becomes critical. The application of CFD methodology to improve the turbo machinery design is becoming established within the turbo machinery community. However, only a limited number of publications suggest how to use CFD to help design and modify processes especially during the blade design. This paper serves to present a design process, which contains a novel two- and three-dimensional viscous turbulent code and optimization process.

2.2 Design system

Expensive manpower is invested to find configurations that are stable and efficient in the work range in the turbine and compressor design. One of the most important methods is so called stream-surface balding where two-dimensional blade profiles are to be found that insures the desired working range stability and efficiency. During the design, the constraints arising from aerodynamics, aeromechanical, mechanical, heat transfer, and manufacturing considerations have to be satisfied.

The design of turbine and compressor blade had made a great progress [31–36]. Many advanced design method and CFD tools had been incorporated into design procedure. However, most of the design procedures only focus on the flow predication and there are few papers that describe the design's overall processes and design implements. For example, Wellborn and Delaney [34] described a compressor design system used by Rolls-Royce plc, which comprise three tools, through-flow, 3D isolated blade row calculation and 3D multistage predication. The turbo machinery design is an integrated process, which contains a process

from mean line, through-flow, airfoil design and analysis. This study developed a design process, which can be easily adapted by industry.

The aerodynamic design procedures for turbo machinery airfoil used in this study are shown in Fig. 3. The design system consists of the mean line analysis, through flow analysis, airfoil section design, airfoil stackup, 3D blade row and multistage flow analysis. For obtaining the highest design efficiency, the optimizer was used to do the section optimization. The three-dimensional CFD code was used for blade stack up optimization. The optimizer may be used for three-dimensional balding although authors do not encourage to use optimizer for 3D optimization. The discussion about issues regarding to 3D optimization will be given in section of optimization.

Mean line analysis determines the loading of the stage and annular area. It plays an important role in the turbo machinery design. The mean line design for the first-stage compressor and last stage turbine is critical. The enthalpy rise for compressor and drop for turbine are fixed by the mean line analysis. The overall machine character is determined by meanline analysis. The compressor and turbine efficiency is strongly influenced by mean line design.

Through flow analysis is one of the preliminary design modules. The streamline curvature calculations can be used to optimize the overall parameters of a multistage turbo machine. This module establishes the definitions of the flow path and work distributions in radio direction. The velocity diagrams at design point for different blade row and different streamlines are determined. The optimization code can be used to do the optimization for selecting the best design parameters, for example, stage loading, and stage enthalpy change.

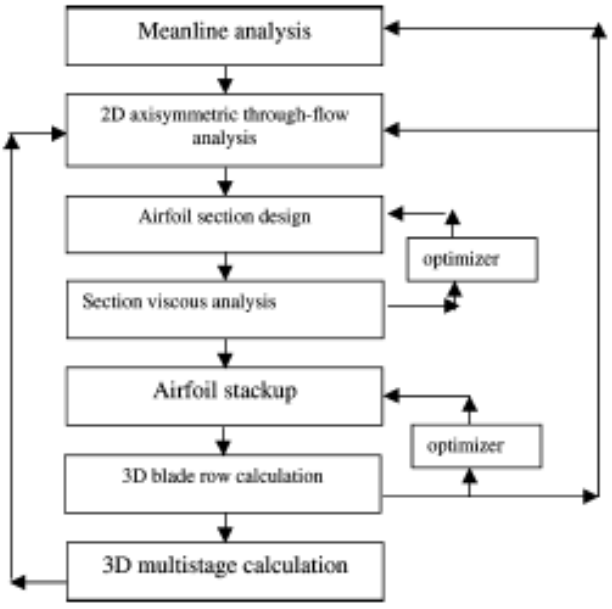

Figure 3: Blade design and optimization procedure.

The airfoil section design is a very important step for the aerodynamic design. All the airfoils are designed by the section design and reasonable stack up. In this design system, authors [2] developed a blade profile design system in which airfoil consist of four segments where tangent slopes as well as curvature are supposed to be continuous at the segment joints.

A three-dimensional blade method was developed in this study as shown in Fig. 3. It can be seen that CFD code for both section analysis and three-dimensional blade row analysis is very important. Development of the efficient and wide range application CFD codes is very important. In this study, an effective numerical method was developed for both two-dimensional and three-dimensional code. In this study, a brief introduction for the numerical method developed for two-dimensional incompressible and compressible flows was made. Details for the three-dimensional method and applications are given in reference [37].

2.3 Flow solver for section analysis

A time-marching algorithm [27, 36–41] was used in the present cascade flow computations. The computation starts with a rough perturbation, which develops under certain boundary conditions. In this approach, the governing equations are replaced by a time-difference approximation with which steady or time-dependent flows of interest can be solved at each time-level.

Assume that passage-averaging plane, where the through-flow solution is calculated, is located at the radius r with the constant angular velocity Ω. The quasi-three -dimensional time-dependent Navier–Stokes equations on the passage-averaging plan can be written as:

$$Q_t + E_x + F_y = R_x + S_y + H \tag{1}$$

where E_x, F_y, R_x, and S_y are the flux vectors.

In the above equation, the effective viscosity is the sum of the molecular viscosity and turbulent viscosity, i.e.

$$\mu_{\text{eff}} = \mu + \mu_t \tag{2}$$

Incorporating artificial dissipation terms into the time-derivatives [27, 41, 42], eqn (1) is modified as:

$$\left[\Delta t\left(\frac{\partial \Lambda_E^+}{2\partial x} - \frac{\partial \Lambda_E^-}{2\partial x} + \frac{\partial \Lambda_F^+}{2\partial y} - \frac{\partial \Lambda_F^-}{2\partial y}\right) + I\right] Q_t + E_x^+ + E_x^- + F_y^+ + F_y^- = R_x + S_y \tag{3}$$

where Λ_E and Λ_F are matrix-valued dissipation terms with respect to positive or negative values of λ_1, λ_2, and λ_3. Matrix Λ_E can be written as:

$$\Lambda_E = \lambda 3I + \left(\frac{\lambda 1 + \lambda 2}{2} - \lambda 3\right) \times \left(\frac{\gamma - 1}{a^2} E1 + E2\right) + \frac{\lambda 1 - \lambda 2}{2a} \times \left[E_3 + (\gamma - 1)E_4\right] \tag{4}$$

where

$$
\begin{aligned}
E_1 &= \left[1, u, v, C_P T\right]^T \left[(u^2+v^2)/2, -u, -v, 1\right] \\
E_2 &= \left[0,1,0,u\right]^T \left[-u,1,0,0\right] \\
E_3 &= \left[1, u, v, C_P T\right]^T \left[-u,1,0,0\right] \\
E_4 &= \left[0,1,0,u\right]^T \left[(u^2+v^2)/2, -u, -v, 1\right]
\end{aligned} \tag{5}
$$

and where

$$
\begin{aligned}
\lambda_1 &= u + a \\
\lambda_2 &= u - a \\
\lambda_3 &= u
\end{aligned} \tag{6}
$$

However, in the calculations, we cannot choose the values of λ_1, λ_2, λ_3 according to eqn (6) because near the stagnation points λ_3 approaches zero, whereas the flow in sonic condition, λ_1 and λ_2 both approach zero. To solve this problem, we limit these values in the following manner:

$$
\begin{aligned}
\lambda_1 &= \max(u + a, u/M_r^2) \\
\lambda_2 &= \max(u - a, u/M_r^2) \\
\lambda_3 &= \max(u, u/M_r^2)
\end{aligned} \tag{7}
$$

and

$$
M_r = \begin{cases} 0.001 & M \le 0.001 \\ M & 0.001 < M \le 1 \\ 1 & M > 1 \end{cases} \tag{8}
$$

where M is the calculated Mach number.

By integrating eqn (1) over space to form the hybrid scheme, we have

$$
\begin{aligned}
&\iiint \left[\Delta t \left(\frac{\partial \Lambda_E^+}{2\partial x} - \frac{\partial \Lambda_E^-}{2\partial x} + \frac{\partial \Lambda_F^+}{2\partial y} - \frac{\partial \Lambda_F^-}{2\partial y} \right) + I \right]^n \frac{Q^{n+1} - Q^n}{\Delta t} dV \\
&+ \iiint \left(\frac{\partial E^+}{\partial x} + \frac{\partial E^-}{\partial x} + \frac{\partial F^+}{\partial y} + \frac{\partial F^-}{\partial y} \right)^{n+1} dV = \iiint \left[\frac{\partial R}{\partial x} + \frac{\partial S}{\partial y} \right]^n dV + \iiint H dV
\end{aligned} \tag{9}
$$

The evaluation of viscous terms R_x and S_y of eqn (1) requires first derivatives of the velocities and the energy value at each cell face. These are achieved by evaluating the gradient of every required flow quantity at the cell center from the known primitive variables at each time step. The terms can be written as

$$
\iiint \left(\frac{\partial R}{\partial x} + \frac{\partial S}{\partial y} \right) dV = \int (R_x \mathbf{n}_x + S_y \mathbf{n}_y)\, dS \tag{10}
$$

In the present study, the second order approximation form was used as:

$$\delta Q_{i,j}^{n+1} = Q_{i,j}^{n+1} - Q_{i,j}^{n} \tag{11}$$

Defining $A = \partial E/\partial Q$ and $B = \partial F/\partial Q$, we have

$$(E^{\pm})^{n+1} = (E^{\pm})^{n} + (A^{\pm})^{n}(Q^{n+1} - Q^{n}) \tag{12}$$

$$(F^{\pm})^{n+1} = (F^{\pm})^{n} + (B^{\pm})^{n}(Q^{n+1} - Q^{n}) \tag{13}$$

and the implicit Jacobians, $A^{\pm}$, can be written as:

$$A^{+} = (A + \rho_A I)/2 \tag{14}$$

$$A^{-} = (A - \rho_A I)/2 \tag{15}$$

where ρ_A is the spectral radius of the Jacobian matrix A.

Finally, we can obtain,

$$\begin{aligned} &C_{i-1,j}\delta Q_{i-1,j}^{n+1} + C_{i,j-1}\delta Q_{i,j-1}^{n+1} + C_{i,j}\delta Q_{i,j}^{n+1} + C_{i+1,j}\delta Q_{i,j+1}^{n+1} \\ &\quad + C_{i,j+1}\delta Q_{i+1,j}^{n+1} = \Delta Q_{i,j}^{n+1} \end{aligned} \tag{16}$$

where

$$C_{i-1,j} = \frac{\Delta t}{2}(\Lambda_E^{-})_{i-1,j}^{n} S_{y\,i-1/2,j} - \Delta t(A_{i-1,j}^{-})^{n} S_{y\,i-1/2,j}$$

$$C_{i,j-1} = \frac{\Delta t}{2}(\Lambda_F^{+})_{i,j-1}^{n} S_{x\,i,j-1/2} - \Delta t(B_{i,j-1}^{+})^{n} S_{xi,j-1/2}$$

$$\begin{aligned} C_{i,j} = \Delta V_{i,j} &- \frac{\Delta t}{2}(\Lambda_E^{+})_{i,j}^{n} S_{y\,i-1/2,j} \\ &- \frac{\Delta t}{2}(\Lambda_E^{-})_{i,j}^{n} S_{y\,i+1/2,j} \\ &- \frac{\Delta t}{2}(\Lambda_F^{+})_{i,j}^{n} S_{x\,i,j-1/2} - \frac{\Delta t}{2}(\Lambda_F^{-})_{i,j}^{n} S_{x\,i,j+1/2} \\ &+ \Delta t(A_{i,j}^{-})^{n} S_{y\,i-1/2,j} - \Delta t(A_{i,j}^{+})^{n} S_{y\,i+1/2,j} \\ &+ \Delta t(B_{i,j}^{-})^{n} S_{x\,i,j-1/2} - \Delta t(B_{i,j}^{+})^{n} S_{x\,i,j+1/2} \end{aligned}$$

$$C_{i+1,j} = \frac{\Delta t}{2}(\Lambda_E^{-})_{i+1,j}^{n} S_{y\,i+1/2,j} + \Delta t(A_{i+1,j}^{-})^{n} S_{y\,i+1/2,j}$$

$$C_{i,j+1} = \frac{\Delta t}{2}(\Lambda_F^{+})_{i,j+1}^{n} S_{x\,i,j+1/2} + \Delta t(B_{i,j+1}^{+})^{n} S_{xi,j+1/2}$$

Since eqn (16) is an implicit scheme, it can improve the numerical stability even with a large time step. In this numerical scheme, $C_{i-1,j}$, $C_{i+1,j}$, $C_{i,j}$, $C_{i,j-1}$, and $C_{i,j+1}$ are all scalars, which are calculated using integration combined with the flux vectors. In this way, the computational efforts are greatly reduced as compared with other coefficient matrix implicit schemes for all time-steps [27, 41]. The implicit equation (eqn (16)) can be solved by using two sweeps along i and j directions as follows:

$$C_{i,j-1}\delta Q^{n+1}_{i,j-1} + C_{i,j}\delta Q^{n+1}_{i,j} + C_{i,j+1}\delta Q^{n+1}_{i,j+1} = \Delta Q^{n+1}_{i,j} - C_{i-1,j}\delta Q^{n+1}_{i-1,j} - C_{i+1,j}\delta Q^{n}_{i+1,j} \tag{17}$$

Since the present scheme consists of an explicit part to calculate $\Delta Q_{i,j}$ and an implicit part to calculate $\delta Q_{i,j}$, which possesses the advantage of both schemes.

In this study, the time-step is selected according to the CFL number constraints as:

$$\Delta t = \min(\Delta t_x, \Delta t_y) \tag{18}$$

where

$$\Delta t_x \le \frac{CFL \cdot \Delta x}{|u| + a + (2\omega/\Delta x \rho)}$$

$$\Delta t_y \le \frac{CFL \cdot \Delta y}{|v| + a + (2\omega/\Delta y \rho)}$$

where $\omega = \max(\mu/Re, \mu_t + 2\mu/Re, \mu\gamma/P_r Re)$.

The choice and development of a turbulence model remain important points to reproduce the flow features. However, there is still no such kind of turbulence model, which can well represent a true flow situation. The Baldwin–Lomax [27, 41] model has several good features, such as its usefulness in separated flows with a small separation region, its relatively smooth and continuous length-scale from transition of the boundary layer into the far wake region, and its ability to accurately predict the wall effect near the trailing edge. For these reasons, the above-mentioned Baldwin–Lomax turbulence model was employed in this study to handle the turbulent flow computing cascade flows around the turbine. The boundary conditions play an important role in determining accurate solutions and rapid numerical convergence. Several types of boundary conditions have been used which are similar to the previous studies [27].

The discussion has been extended for many years for the discussion of best type mesh, which should be used, for turbine or compressor blade flow calculation [43, 44]. The more orthogonal the grid, the smaller will be the numerical errors due to the discretization of governing equations. However, no one type of grid is ideal for blade-to-blade flow calculation. In this study, the H-type mesh was used. Another problem for the blade-to-blade mesh is the trailing edge mesh and trailing edge Kutta condition [45]. The author has noticed that the number of the mesh point near the trailing edge points strongly influences the loss calculation. Here, a realistic method is proposed, i.e. when the mesh on the trailing edge

boundary conditions have been used which are similar to the previous studies [27].

The discussion has been extended for many years for the discussion of best type mesh, which should be used, for turbine or compressor blade flow calculation [43, 44]. The more orthogonal the grid, the smaller will be the numerical errors due to the discretization of governing equations. However, no one type of grid is ideal for blade-to-blade flow calculation. In this study, the H-type mesh was used. Another problem for the blade-to-blade mesh is the trailing edge mesh and trailing edge Kutta condition [45]. The author has noticed that the number of the mesh point near the trailing edge points strongly influences the loss calculation. Here, a realistic method is proposed, i.e. when the mesh on the trailing edge

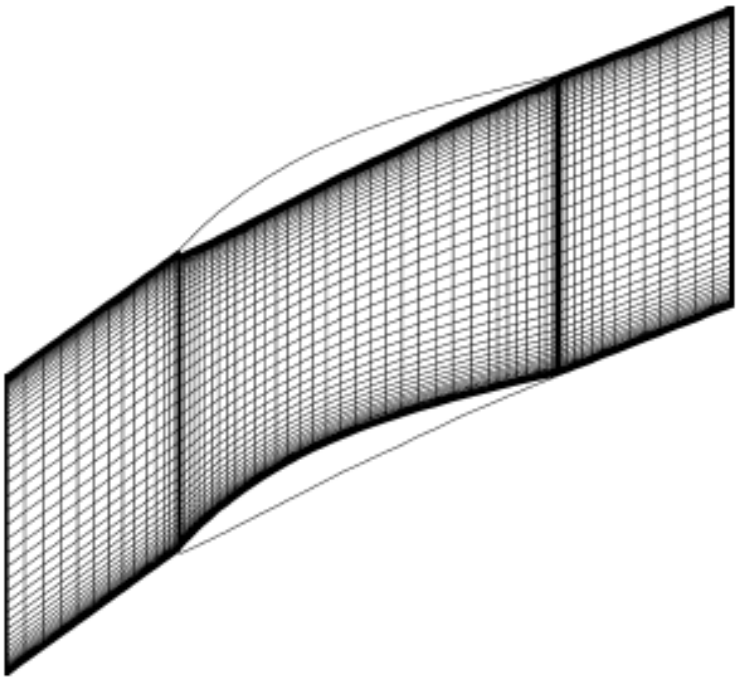

Figure 4: Computational mesh.

circle is more than 10 points, an explicit viscous Kutta condition [45] is applied on the trailing edge circle which flow can leave the blade smoothly.

The mesh refinement study was conducted prior to the calculations; as reported by Xu and Amano [27, 37, 41], the mesh size of 110×45 with 80 nodes on blade is sufficient. The H-mesh was used in all the computations. The computational mesh is shown in Fig. 4. A typical convergence history of the calculation is shown in Fig. 5. It is demonstrated that the present code has a good convergence. In this study, this code was used in the two dimensional airfoil section analysis and optimization.

2.4 Optimization

Read

Page 335 to 360

CHAPTER 10

Advances in understanding the flow in a centrifugal compressor impeller and improved design

A. Engeda
Turbomachinery Lab, Michigan State University, USA.

Abstract

The last 60 years have seen a very high number of experimental and theoretical studies of the centrifugal impeller flow physics at government, industry and university levels, which have been extensively documented. As Robert Dean, one of the well-known impeller aerodynamists stated, "The centrifugal impeller is probably the most complex fluid machine built by man". Despite this, it is still the widest used turbomachinery and continues to be a major research and development topic. Computational fluid dynamics has now matured to the point where it is widely accepted as a key tool for aerodynamic analysis. Today, with the power of modern computers, steady-state solutions are carried out on a routine basis, and can be considered as part of the design process. The complete design of the impeller requires a detailed understanding of the flow in the impeller and aerodynamic analysis of the flow path and structural analysis of the impeller including the blades and the hub. This chapter discusses the developments in the understanding of the flow in a centrifugal impeller and the contributions of this knowledge towards better and advanced impeller designs.

it is not surprising that the centrifugal compressor continues to command a great deal of attention, both from compressor designers and from those engaged in understanding the underlying engineering science.

Industrial applications require stage pressure ratios of 1.5:1 or even less, whereas helicopter gas turbines require the highest pressure ratios, with 6:1 being commonplace and the latest engines demanding 10:1 or more from a single compressor stage. Table 1 and Fig. 1 summarize the application areas of turbocompressors.

The wide range of demands on centrifugal compressors brings many design considerations. Most of the design requirements need solutions to two major problems: stress and aerodynamics. The stress problems are caused by the material strength limitations and the capability to accurately predict blade and impeller steady state and vibrational stress for complex impeller shapes and at high rotational speeds. The aerodynamic problem is to efficiently accomplish large air deflections and diffusion at high flow velocity, with the added difficulty of very small passage flow areas required to get good efficiency and high pressure ratio.

Table 1: Application areas of turbocompressors.

Types of compressors	Pressure ratio			Efficiency	Operating range
	Industrial	Aerospace	Research		
Positive displacement	Up to 30	–	–	78–82%	–
Centrifugal	1.2–1.9	2.0–7.0	13	75–87%	Large 25%
Axial	1.05–1.3	1.1–1.45	2.1	80–91%	Narrow 3–10%

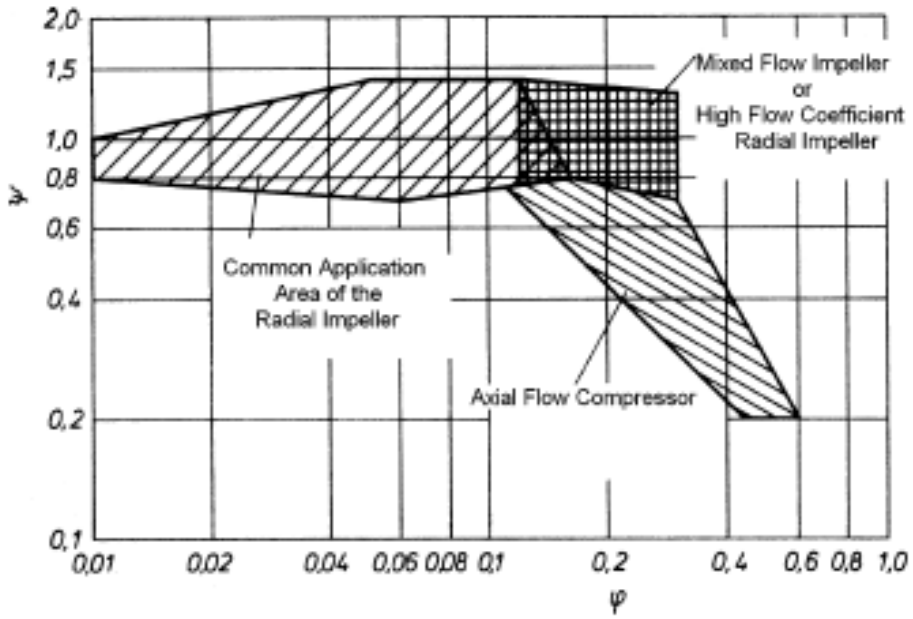

Figure 1: Application areas of turbocompressors.

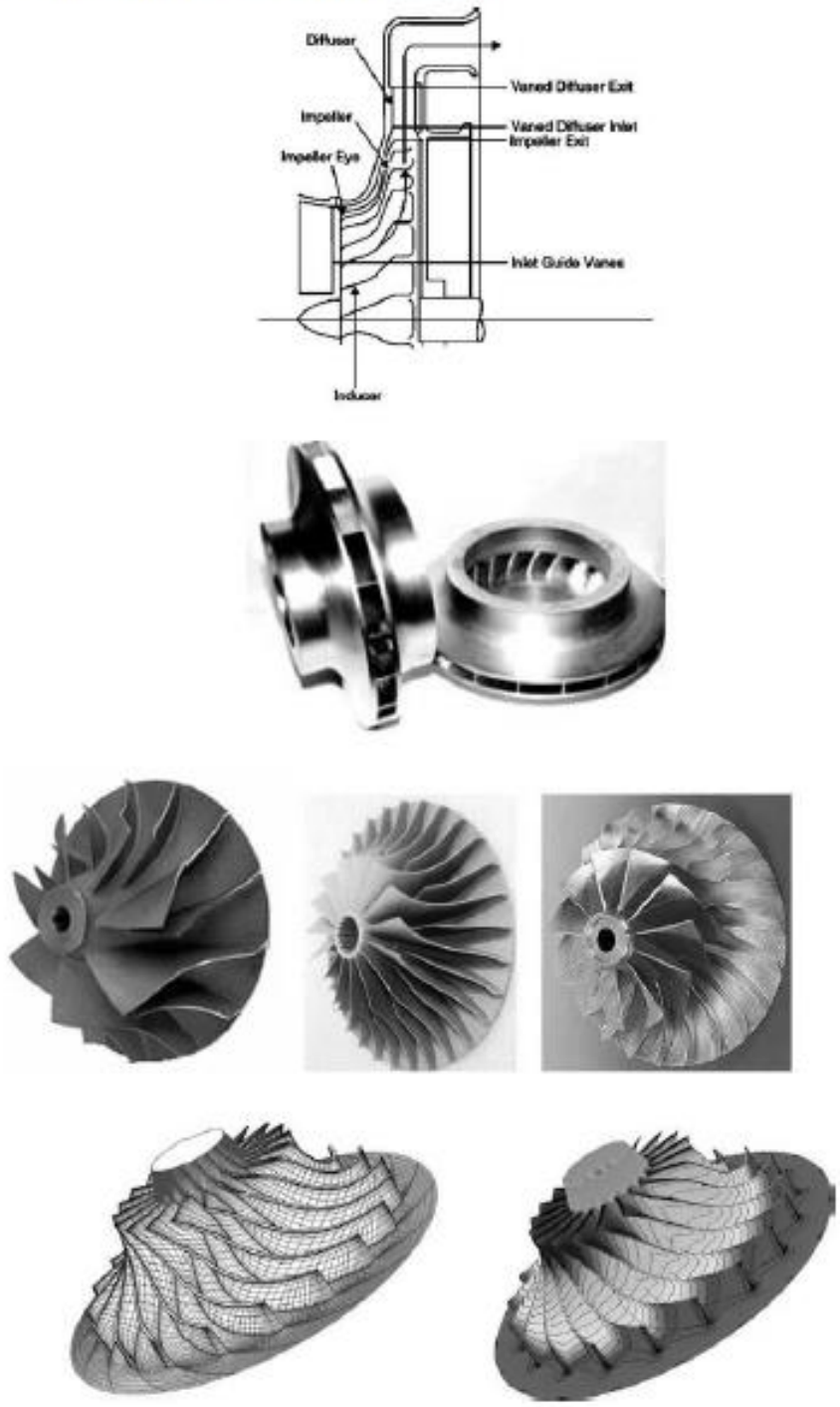

Figure 2: Examples of centrifugal impellers and modeling.

3 The centrifugal compressor stage

As shown in Fig. 3, a simple centrifugal compressor stage consists of four basic components:

- inlet,
- impeller,
- vaneless or vaned diffuser, and
- collector or a volute.

The fluid is drawn in through the inlet into the eye of the impeller parallel to the axis of rotation. To add angular momentum, the impeller whirls the fluid outward and turns it into a direction perpendicular to the rotation axis.

As a result, the energy level is increased, resulting in both higher pressure and velocity. The purpose of the following diffuser is to convert some of the kinetic energy of the fluid into static pressure. Outside the diffuser is a scroll or volute whose function is to collect the flow from the diffuser and deliver it to the discharge pipe. It is possible to gain a further deceleration and thereby an additional pressure rises within a volute.

An example of the contribution of each component of the compressor is shown in Fig. 4. The solid line represents the static pressure rise while the dotted line indicates the total pressure change for the individual component in a single stage of centrifugal compressor.

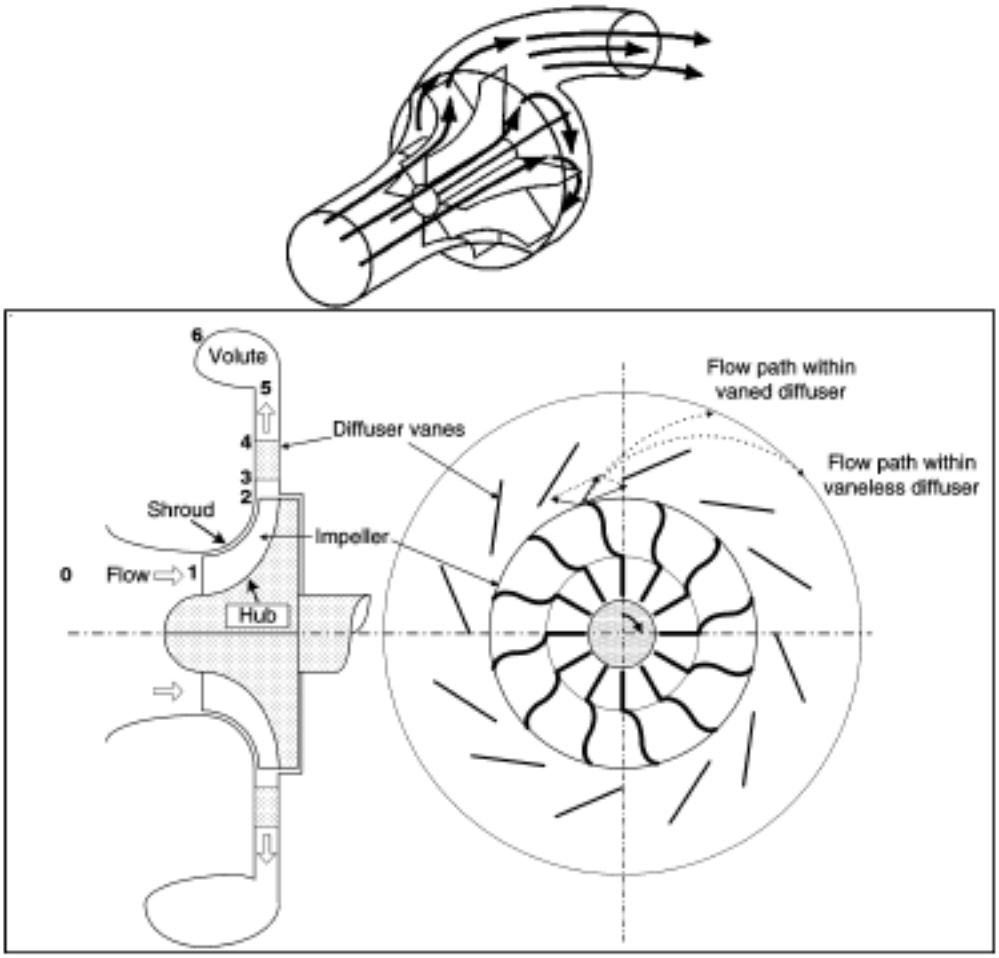

Figure 3: Example of configuration for a single-stage centrifugal compressor.

pressure rises within a volute. Figure 4 shows the typical flow characteristics in a centrifugal compressor stage on an enthalpy–entropy diagram (h–s).

The impeller is the only rotating component of a centrifugal compressor stage, and the energy is transferred to the fluid by the mechanical work of the driving motor.

4 Similitude, dimensional analysis and control volume analysis

Based on 1D streamline theory, the aerodynamic design of the centrifugal impeller has significantly advanced in the last 60 years without knowledge about the detailed internal flow in the impeller. This practice has led to very successful impeller designs simply by using:

- Similitude,
- Dimensional analysis,
- Empirical knowledge, and
- Control volume analysis.

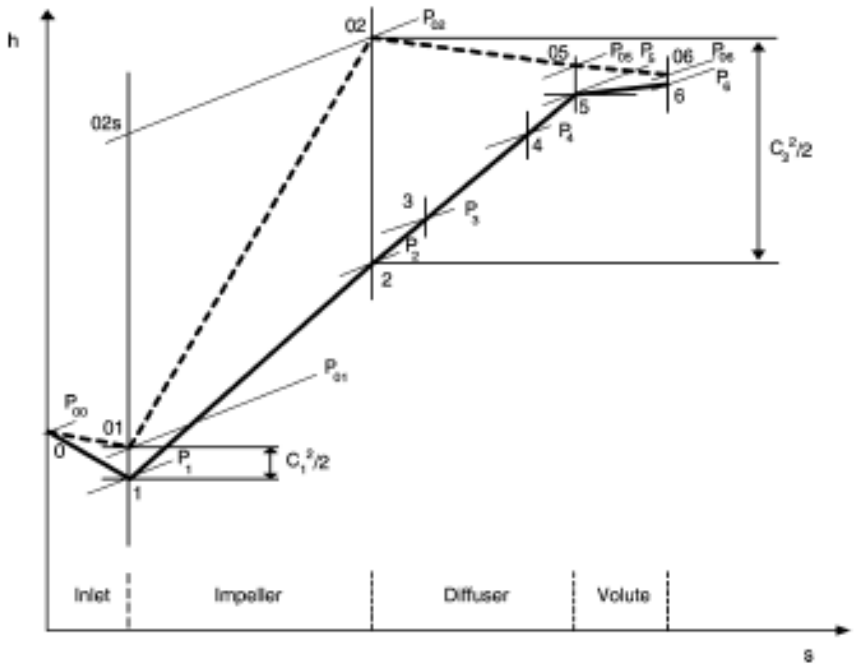

Figure 4: Example of *h*–*s* diagram for a centrifugal compressor stage.

4.1 Similitude

If similar flow patterns exist in the passages of two impellers then the polytropic efficiencies of the impellers are equal. Flow similarity requires that:

- The two impeller passages be geometrically similar;
- Velocities at corresponding points in each impeller bear a constant ratio to each other;
- The velocities at corresponding points in each impeller have the same direction relative to some reference direction; and
- The ratio of the forces of any two types acting upon the fluid at any point in one impeller equals the ratio of the same types of force acting on the fluid at the corresponding point in the second impeller.

4.2 Dimensional analysis

Using dimensional analysis, the characteristics of the impeller can be illustrated using dimensionless parameters involving all relevant variables. For impeller diameter *(D)*, inlet stagnation pressure (P_{01}), inlet stagnation temperature (T_{01}), mass flow rate ($\dot{m}$), rotational speed (N), fluid properties: the universal gas constant (R), kinematic viscosity (ν), and the ratio of specific heats (γ), the performance of the impeller, may be represented by:

$$P_{02} = f\left(\dot{m}, P_{01}, R, T_{01}, \gamma, N, \nu, D\right)$$

$$\eta = f\left(\dot{m}, P_{01}, R, T_{01}, \gamma, N, v, D\right)$$

The mass flow rate ($\dot{m}$), the efficiency (η) and the stagnation temperature rise $\Delta T_{01} = T_{02} - T_{01}$ of an impeller can be expressed as functions of the independent variables:

$$\dot{m}\,;\eta : \Delta T_0 = f\left(P_{01}, P_{02}, R, T_{01}, \gamma, N, v, D\right)$$

These can be reduced to a set of non-dimensional groups:

$$\frac{\dot{m}\sqrt{RT_{01}}}{P_{01}D^2}; \eta; \frac{\Delta T_0}{T_{01}} = f\left(\frac{ND}{\sqrt{\gamma RT_{01}}}, \frac{P_{02}}{P_{01}}, \frac{\dot{m}}{vD}, \gamma\right)$$

Since the impeller operates on a specific gas, the values of R and γ are specified. Hence the non-dimensional groups become:

$$\frac{\dot{m}\sqrt{RT_{01}}}{P_{01}D^2}; \eta; \frac{\Delta T_0}{T_{01}} = f\left(\frac{ND}{\sqrt{\gamma RT_{01}}}, \frac{P_{02}}{P_{01}}, \frac{\dot{m}}{vD}\right)$$

The Reynolds number of the gas has little effect on the performance of the machine, and can usually be ignored. Hence:

$$\frac{\dot{m}\sqrt{RT_{01}}}{P_{01}D^2}; \eta; \frac{\Delta T_0}{T_{01}} = f\left(\frac{ND}{\sqrt{\gamma RT_{01}}}, \frac{P_{02}}{P_{01}}\right)$$

For the impeller efficiency a relationship between η, $\Delta T_0/T_{01}$, and P_{02}/P_{01} can be established out of the definition of isentropic efficiency as:

$$\eta_{\text{imp-TT}} = \frac{\left(P_{02}/P_{01}\right)^{(\gamma-1/\gamma)} - 1}{\left(\Delta T_0 / T_{01}\right)}$$

For a particular machine, the diameter (D) is constant and therefore may be ignored. Thus, the complete performance of the compressor may be represented by the relationships (for a particular fluid, such as air)

$$\frac{\dot{m}\sqrt{T_{01}}}{P_{01}}; \eta = f\left(\frac{N}{\sqrt{T_{01}}}, \frac{P_{02}}{P_{01}}\right)$$

$$\frac{\dot{m}\sqrt{T_{01}}}{P_{01}}; \frac{\Delta T_0}{T_{01}} = f\left(\frac{N}{\sqrt{T_{01}}}, \frac{P_{02}}{P_{01}}\right)$$

By plotting η and P_{02}/P_{01} against the mass flow parameter $\dot{m}\sqrt{T_{01}/P_{01}}$ for a series of values of $N/\sqrt{T_{01}}$, the complete performance of the machine is determined.

4.3 Control volume analysis

Using a control volume analysis (Fig. 5), for any N total amount of some property: mass, energy or momentum, the n per unit mass amount of N is expressed as:

$$N = n\rho dv$$

The time rate of change of N, can be expressed as:

$$\frac{dN}{dt} = \frac{\partial}{\partial t}\int_{cv} n\rho dv + \int_{cs} n\rho \overline{C} \cdot d\overline{A}$$

The equation states that the time rate of change N is equal to the time rate change of the property within the control volume plus the net rate of efflux of N across the boundary. For N is momentum:

$$N = m \cdot \overline{C} = n \cdot \rho \cdot dv \qquad n = \frac{m \cdot \overline{C}}{\rho \cdot dv} = \overline{C}$$

$$\sum \overline{F} = \frac{d\left(m\overline{C}\right)}{dt} = \frac{\partial}{\partial t}\int_{cv} \rho \overline{C} dv + \int_{cs} \rho \overline{C}\overline{C} \cdot d\overline{A}$$

Applying this equation for the momentum component in the x direction:

$$\sum F_x = \frac{\partial}{\partial t}\int_{cv} \rho C_x dv + \int_{cs} \rho C_x \overline{C} \cdot d\overline{A}$$

Applying this for the torque exerted by any force on the control volume, in this case an impeller and for steady state case:

$$T_{z-z} = \overline{r}x\overline{F} = \frac{\partial}{\partial t}\int_{cv} (\rho \overline{r})x\left(\overline{C}dv\right) + \int_{cs}\left(\rho \overline{r}x\overline{C}\right)\left(\overline{C} \cdot d\overline{A}\right)$$

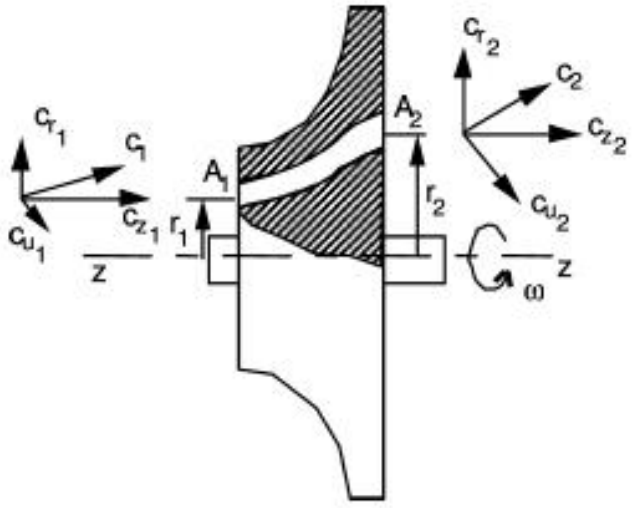

Figure 5: An impeller as a control volume.

$$T_{z-z} = \int_{A2}(r_2 C_{u2})(\rho_2 C_{r2} dA) - \int_{A1}(r_1 C_{u1})(\rho_1 C_{r1} dA)$$

$$T = \dot{m}(r_2 C_{u2} - r_1 C_{u1})$$

The impeller is the rotating component of the centrifugal compressor stage, where energy transfer of the compressor stage occurs, stagnation enthalpy change across the impeller ($\Delta h_{0\text{-imp}}$).

$$\Delta h_{0\text{-imp}} = h_{02} - h_{01}$$

Thus, the overall energy transfer is given by:

$$\dot{m}\ \Delta h_{0\text{-imp}} = -\dot{W} = \omega T = \dot{m}\ (U_2 C_{u2} - U_1 C_{u1})$$

From velocity triangles (Fig. 6) at impeller exit and inlet, it can be shown:

$$U_2 C_{u2} = \tfrac{1}{2}\left(U_2^2 + C_2^2 - W_2^2\right) \quad \text{and} \quad U_1 C_{u1} = \tfrac{1}{2}\left(U_1^2 + C_1^2 - W_1^2\right)$$

Thus,

$$\Delta h_{oc} = \tfrac{1}{2}\left[\left(U_2^2 - U_1^2\right) + \left(W_1^2 - W_2^2\right) + \left(C_2^2 - C_1^2\right)\right]$$

The sum of the first and the second terms on the right hand side represents the increase in static pressure and the kinetic energy increase is shown in the last term. In an axial compressor machine, there is no impeller tip speed variation ($U_2 = U_1$constant) explaining a higher enthalpy rise in a radial compressor. If the impeller inlet flow is purely axial (i.e. $C_{u1} = 0$) the theoretical total enthalpy reduces to:

$$\Delta h_{0c} = \frac{\dot{W}}{\dot{m}} = U_2 C_{u2}$$

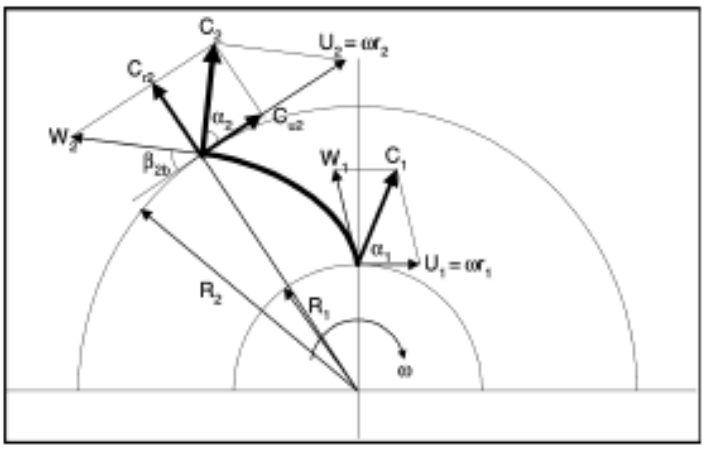

Figure 6: Velocity triangles.

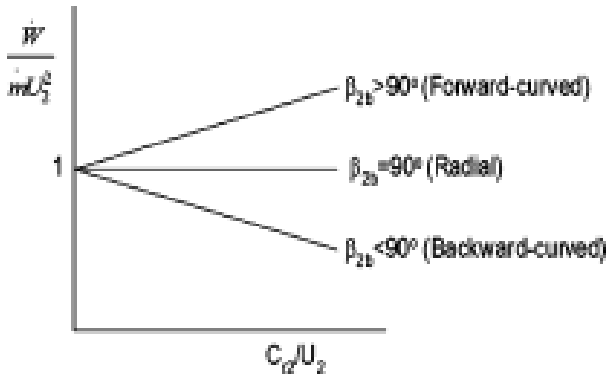

Figure 7: Linear relationship between specific energy transfer and flow rate for a given β_{2b}.

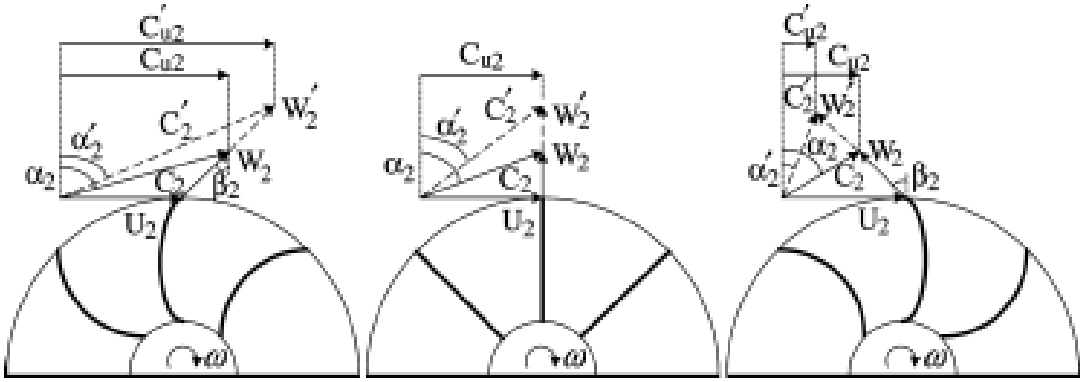

Figure 8: Exit velocity triangles for the three exit conditions.

Then the effect of impeller exit blade angle, β_{2b} on the theoretical enthalpy rise becomes

$$\frac{\dot{W}}{\dot{m}} = U_2^2\left(1 - \frac{C_{r2}}{U_2}\cot\beta_{2b}\right), \text{ since } C_{u2} = (U_2 - C_{r2}\cot\beta_{2b})$$

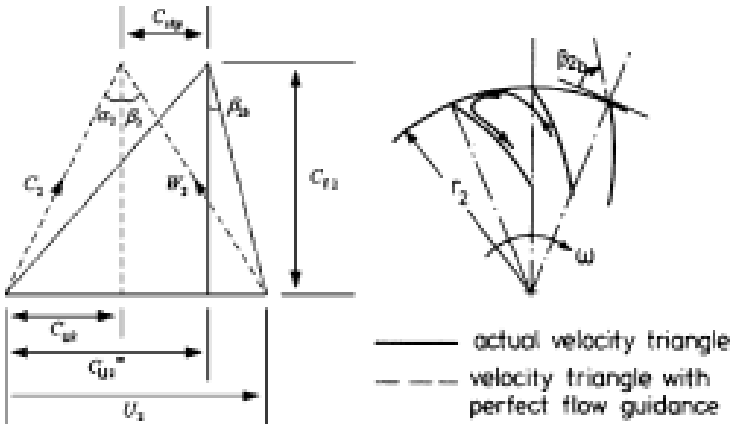

Figure 9: Definition of slip.

channels (defined by blade shape and hub and shroud profiles) should be chosen to give a smooth change in the relative Mach number along the mean flow path in the meridional plane. Consider the backswept impeller shown in (Fig. 9) rotating clockwise. The body of air passing through the channel between the two blades has inertia and will resist the turning effect of the impeller. The air therefore tends to rotate relative to the impeller channel, but in the opposite direction. Near the tip, this relative rotation causes the tangential component of absolute velocity (c_{u2}) to be less than the fluid leaving the impeller at the blade angle. Thus, the relative flow leaving an impeller is not perfectly guided by a finite number of blades, which is called *slip*, leading to the modified velocity triangle as shown in the figure below. The effect of slip is to reduce the magnitude of the tangential component of velocity, resulting in the reduction of the pressure ratio as well as compressor power consumption. Therefore, the slip effect requires a higher impeller rotating speed to obtain the same pressure ratio as the case of no slip, and this causes increased stress levels and relative velocities in the impeller, which finally leads to increased friction losses and reduced efficiency.

A slip factor in general form is defined by

$$\sigma = 1 - \frac{C_{\text{slip}}}{U_2} = 1 - \frac{C_{u2}^{\infty} - C_{u2}}{U_2}$$

From the velocity triangle (Fig. 9), the tangential component of velocity is reevaluated by

$$C_{u2} = \sigma U_2 + C_{r2} \tan \beta_{2b}$$

The calculation method in each of these groups can be further classified on the basis of the computational scheme used:

- singularity methods,
- streamline curvature methods,
- finite difference methods, or
- finite element methods.

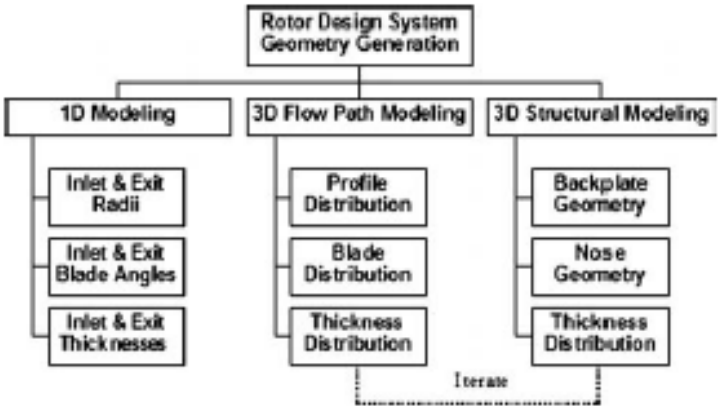

Figure 10: CAD system approach.

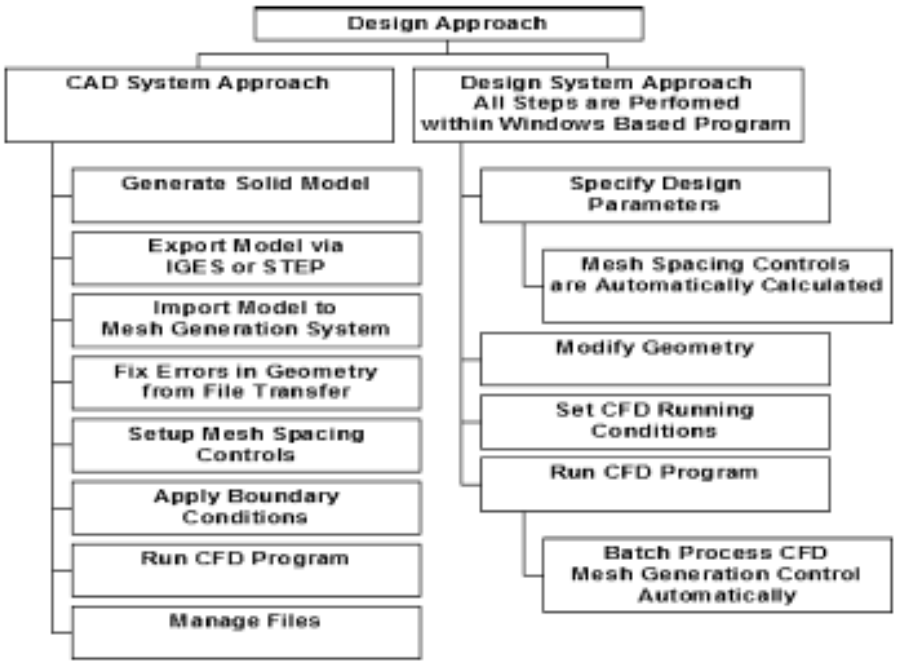

Figure 11: Design system approach.

CHAPTER 11

Thermal engineering in hybrid car systems

K. Suga
Department of Mechanical Engineering,
Osaka Prefecture University, Japan.

Abstract

To understand thermal engineering aspects in the recent hybrid cars, this chapter summarizes modern hybrid car systems and their thermal management issues. Since the recent commercial hybrid cars employ a gasoline/diesel–electric hybrid system, thermal issues related to internal combustion engines and electric systems are major factors for improving their tank to wheel efficiency. Although the combustion issues are important, this chapter focuses on the thermal management of the electric systems including batteries, traction/generation motors and inverters. Topics on heat sinks and combined thermal management of several electric parts are also discussed.

1 Introduction

The "hybrid car" system uses multiple power generation for providing propulsive force Although it has a history of over 100 years and although there are several hybrid car systems, the recent commercial hybrid cars employ the gasoline/diesel–electric hybrid system, which uses an internal combustion (IC) gasoline/diesel engine and electric motors. In order to enhance the system efficiency and to maintain its superior performance, thermal engineering is very important for developing the hybrid car systems. In fact, the modern hybrid car systems require highly sophisticated thermal management since their power electronic systems generate a large amount of heat and their performance is greatly affected by their surrounding temperature. In order to understand thermal engineering aspects in the hybrid car systems, this chapter introduces a brief history, system configurations and thermal engineering aspects of the modern hybrid car systems.

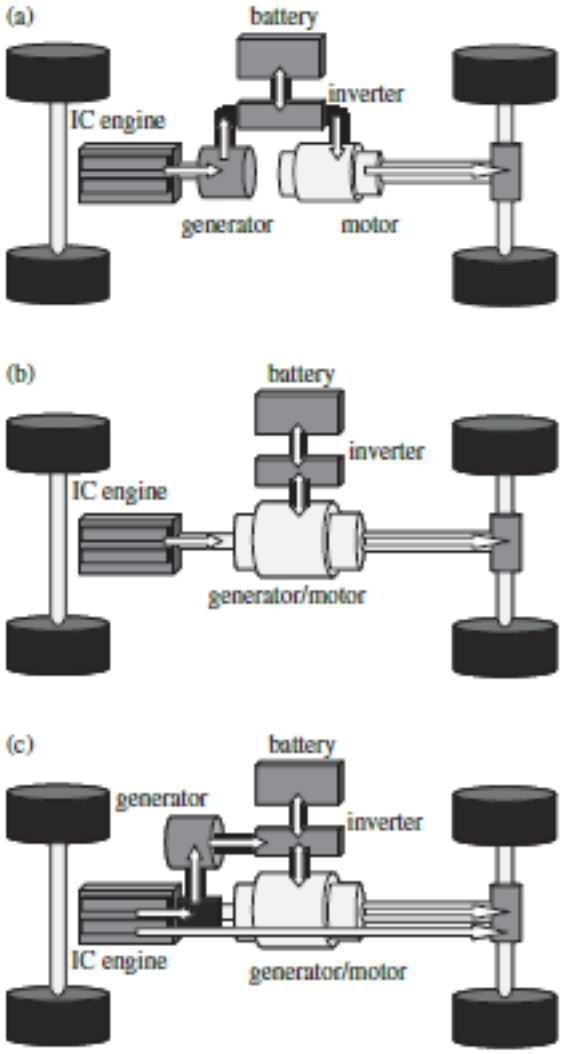

Figure 2: Powertrain configurations of hybrid cars: (a) series hybrid; (b) parallel hybrid; (c) series–parallel hybrid.

3.3 Series–parallel hybrid

This powertrain system combines the advantages of the parallel and series powertrain systems as in Fig. 2c. The engine can drive the wheels directly as in the

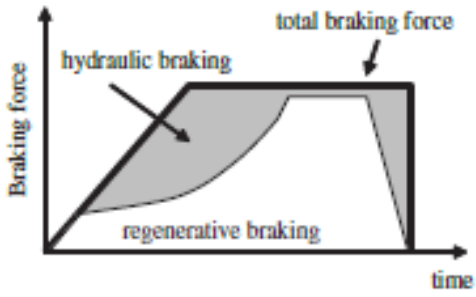

Figure 3: Cooperative regenerating brake system.

parallel powertrain and can also be effectively disconnected from the wheels so that only the electric motor powers the wheels as in the series powertrain in some occasions. The Toyota Prius employs this mechanism and so do some others. Consequently, the engine can almost always operate at near the optimum condition. At lower speeds, it operates more as a series hybrid, while at high speeds, where the series powertrain is less efficient, the engine takes over and energy loss is minimized. Although this system costs higher than the pure parallel hybrid due to its generator, larger battery pack, and more sophisticated controlling unit, the series-parallel powertrain has the highest potential to perform among the systems referred to.

It is clear that thermal management of the main components such as the battery, the electric motor, the DC–AC inverter, and the IC engine (which are common in any design configurations) is essential to achieve high performance of the hybrid car powertrain systems.

3.4 Regenerative braking system

In any power train configuration, a regenerative/recharging braking system is equipped in a modern hybrid car. When the vehicle is decelerated or braked, the system generates electricity by using the motors as generators. As illustrated in Fig. 3, the total braking force is obtained by both the regenerative braking and the conventional hydraulic braking. To obtain the maximum regenerating, the cooperative controlling system is optimized.

4 Technologies and challenges for thermal management of hybrid car system components

4.1 Battery pack

Although nickel-metal hydride (NiMH) batteries are normally used, Lithium ion batteries are expected to replace NiMH batteries in the near future. Irrespective of the battery types, the charging level is controlled within a designed range as in Fig. 4.

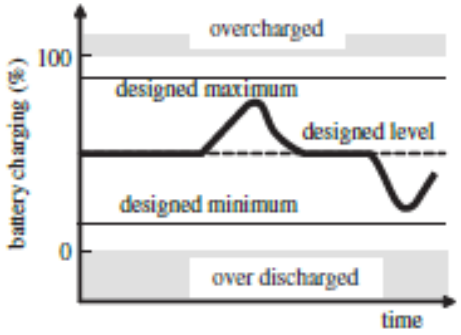

Figure 4: Example of a time history of battery charging in a hybrid car system.

Table 1: Permanent capacity loss (Δ_C) of a Li-ion battery after 1 year usage.

T	Δ_C at 40% charging	Δ_C at 100% charging
0°C	2%	6%
25°C	4%	20%
40°C	15%	35%
60°C	25%	40% (after 3 months)

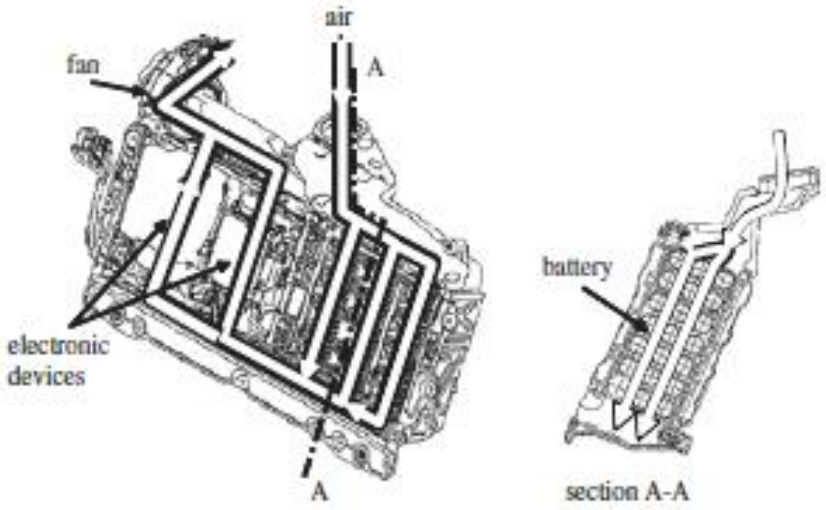

Figure 5: Battery cooling system of the Honda Insight.

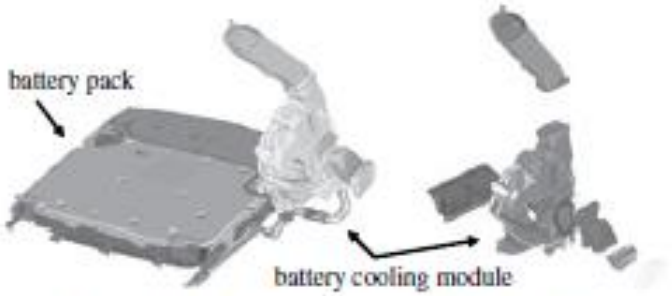

Figure 6: Auxiliary battery cooling unit [6].

4.2 Traction/generator motor

The thermal management of an electric traction/generator motor itself is for keeping its temperature under the limits, which are normally given by electric insulating materials used in the components. For example, the limit temperature of the coil is about 180°Cand that of the rotor magnet is about 120°C. A high-performance electric motor is estimated to produce heat of about 2500, 300 and 400 W due to its stator iron, copper and rotor losses under its design condition of 20 W/cm.[3]

One of the main issues of cooling motors is reducing the thermal resistance between the stator coil and the iron core to remove heat from the coil. For reducing the thermal resistance, the coil needs to be tightly packed after wiring to increase the contact surface area between the coated wire and the iron core. In fact, by doing so, the thermal resistance can be reduced to 15 K/kW from the standard value 50 K/kW.

Another more important issue is designing direct cooling system for the stator and

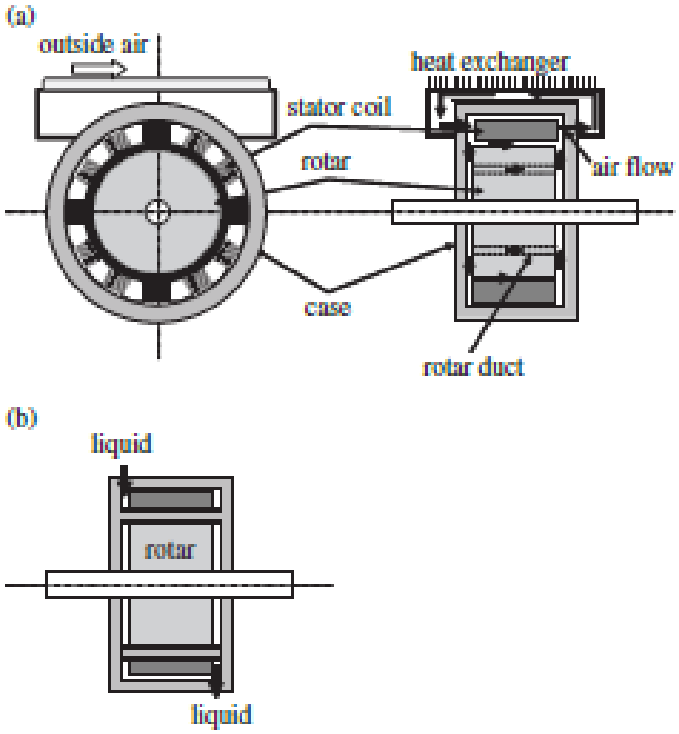

Figure 7: Cooling system of a radial type motor.

the heat exchanger mounted on the case. For a high performance motor/generator issuing much more heat, a liquid cooling system is coupled as in Fig. 7b.

An axial type motor has higher power density compared with that of the radial type and thus requires a liquid cooling system as shown in Fig. 8. The stator and the rotor are cooled by oil flows. Since heat generation from the rotor is <20% of the stator's, the required oil flow rate for the rotor is lower than that for the stator.

4.3 Inverter

Inverters and converters compose a power control unit (PCU) of hybrid cars. Currently, the volume of the PCU is about 9500 cm^3 due to the available space for it in engine rooms of sedans. Thus, one can see a linear relation between the motor output and the power density of the inverter [7] shown as the solid line in Fig. 9. However, the bigger and the more powerful motors are required, the smaller space remains for the PCU. Consequently, it is readily expected that a much higher power density (>10 W/cm^3) is required in the near future (shown as the broken line in Fig. 9) since required motor outputs are expected to be at least 100 kW. (In fact, the latest very powerful Toyota's hybrid sports utility vehicle (SUV) employs a motor whose maximum output is 123 kW [8] though there is a bigger PCU space in the SUV than those in sedans.)

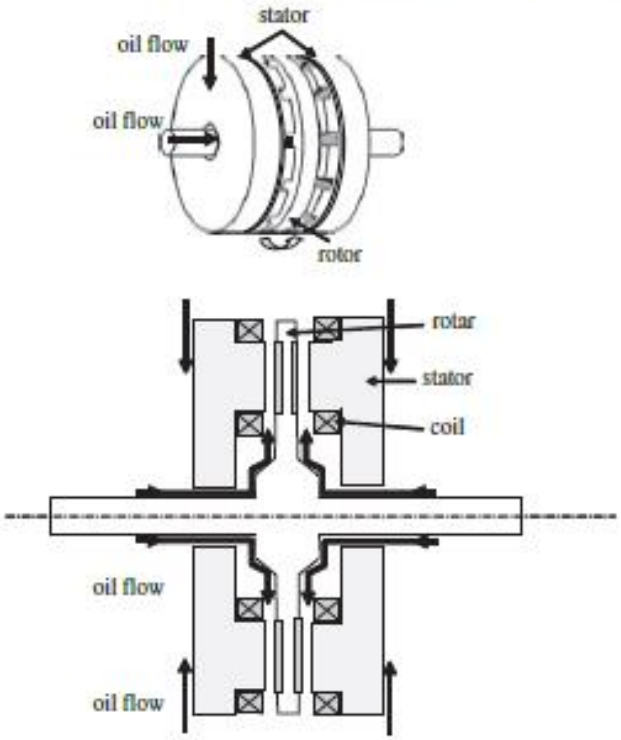

Figure 8: Cooling system of an axial type motor.

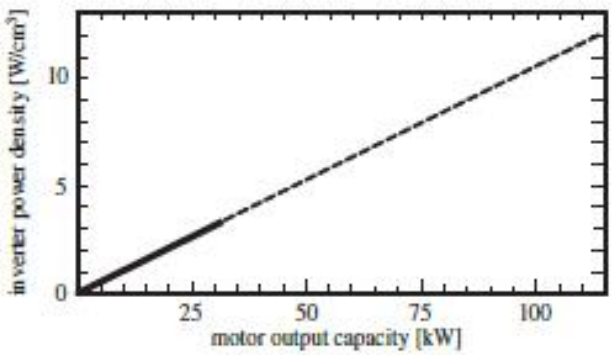

Figure 9: Relation between inverter power densities and motor outputs.

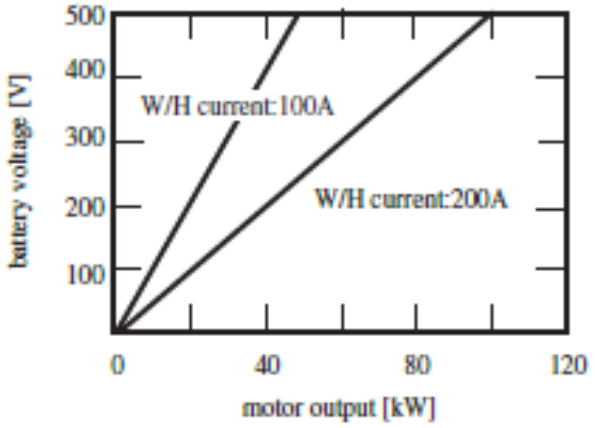

Figure 10: Relation between battery voltages and motor outputs.

4.3.1 Packaging architecture and its thermal issues

The currently applied package architecture of the power devices such as the inverters is illustrated in Fig. 11a. It consists of the insulated gate bipolar transistor (IGBT) chip soldered onto a direct bond copper (DBC) ceramic substrate that in tern is soldered onto a metallic baseplate. The ceramic substrate works as an electrical insulator for the device from the baseplate. The metallic baseplate is for spreading the heat generated at the IGBT chip out to the larger heat sink area. The heat sink is generally bolted onto the baseplate with an intervening thermal grease layer. Due to heating up and cooling down of the IGBT chip during its on/off cycle processes, each packaging layer expands and contracts at a rate proportional to its temperature. The coefficient of thermal expansion (CTE) is significantly different between the silicon of the die ($\simeq$ 4 ppm/K), the ceramic substrate ($\simeq$ 4–8 ppm/K) and the metal baseplate ($\simeq$ 17–24 ppm/K) and thus it leads to high stresses at the solder interfaces between the layers. Consequently, such repeated stresses bring about severe damage to the bonding, which causes higher electric and thermal resistance eventually leading to total failure. To reduce the thermally induced stresses, instead of using a pure metal baseplate, a composite material of Al and SiC whose CTE is 7.2 ppm/K is employed in Toyota's hybrids [9]. In such a case, however, thermal conductivity of the baseplate is also reduced to the half of copper's.

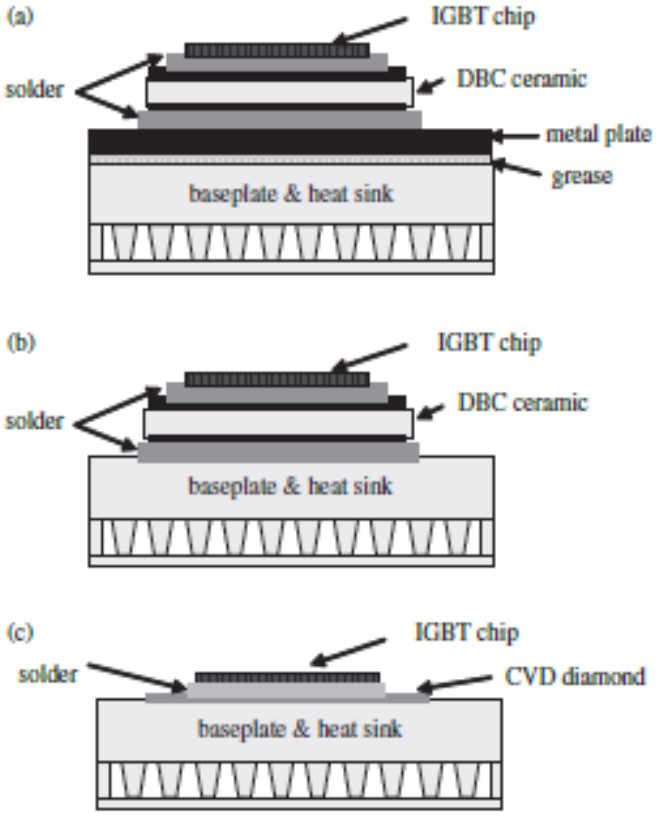

Figure 11: Chip-heat sink configurations: (a) standard architecture; (b) latest architecture; (c) future architecture.

Figure 11c is the ultimate packaging architecture currently considered [10]. It is an application of a thin diamond layer on the top of the baseplate surface by chemical vapor deposition (CVD). Diamond has the highest thermal conductivity (1–2 kW/(mK)) [12], which is 2.5–5 times as high as that of copper and 5–12 times as high as that of AlSiC. The use of CVD diamond would allow the heat from the silicon chip to spread out over the entire area of the baseplate with higher efficiency than is possible with either the first or second generation architectures shown in Figs11a and b. In addition, diamond is an electrical insulator and thus replaces the ceramic substrate, which exists exclusively to electrically insulate the power die from the rest of the package. This eliminates another layer from the packaging, providing additional enhancement of the thermal and mechanical performance.

4.3.2 Thermal analysis of the power devices

In order to predict temperature distribution of a power device module, the finite element method (FEM) or the thermal resistance network analysis is usually applied. Since one can find many textbooks on the FEM, only the latter is reviewed here.

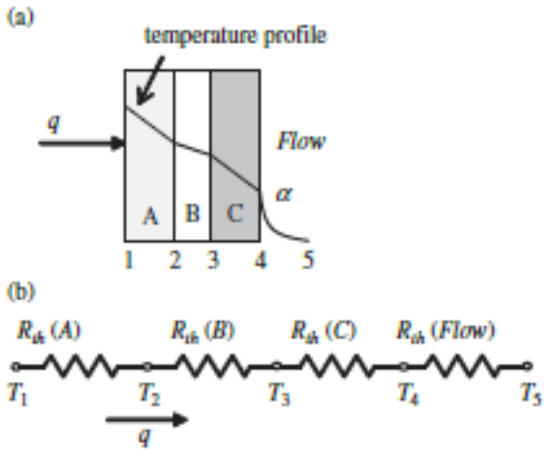

Figure 12: One dimensional heat transfer through a composite wall and its electrical analog.

When one considers one-dimensional heat transfer through a composite wall as shown in Fig. 12a, the heat flux q may be written as

$$q = \frac{T_1 - T_5}{\delta_A/\lambda_A + \delta_B/\lambda_B + \delta_C/\lambda_C + 1/\alpha}, \tag{1}$$

where δ_x, λ_x and α are, respectively, the thickness and the thermal conductivity of material x and the heat transfer coefficient at the wall boundary. This form can be rewritten defining thermal resistance R_{th} as

$$qS = \frac{\Delta T_{overall}}{R_{th}(A) + R_{th}(B) + R_{th}(C) + R_{th}(\text{Flow})}, \tag{2}$$

where

$$\begin{aligned} R_{th}(A) &= \delta_A/(\lambda_A S) \\ R_{th}(B) &= \delta_B/(\lambda_B S) \\ R_{th}(C) &= \delta_C/(\lambda_C S) \\ R_{th}(\text{Flow}) &= 1/(\alpha S), \end{aligned} \tag{3}$$

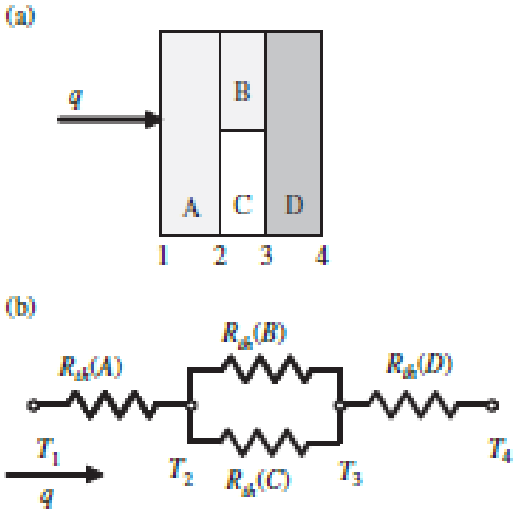

Figure 13: Parallel one dimensional heat transfer and its electrical analog.

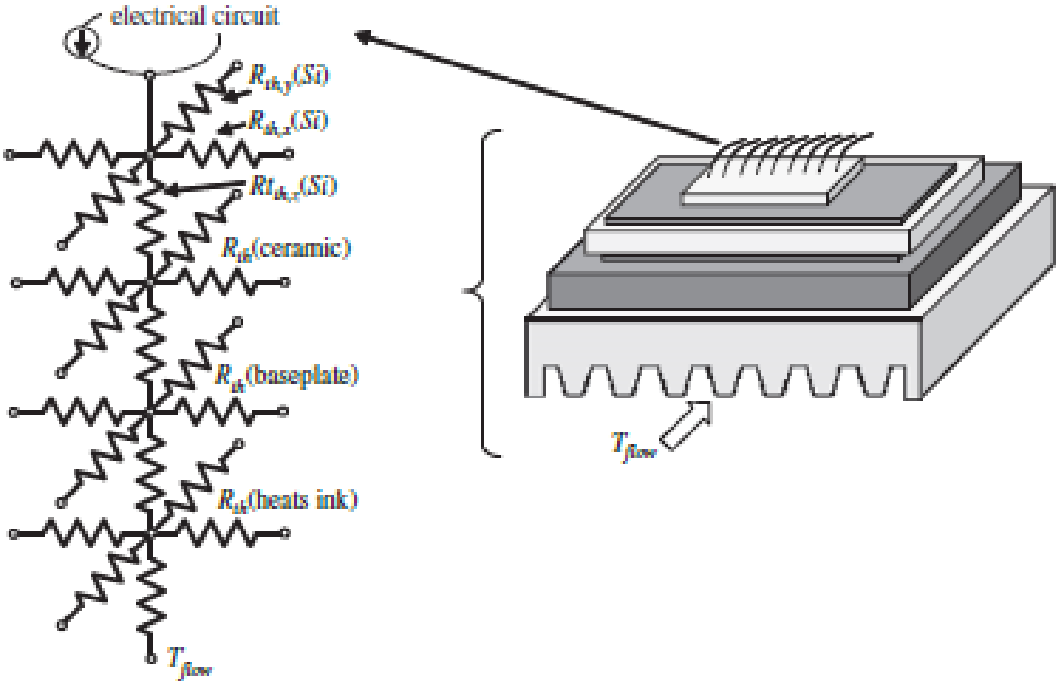

Figure 14: Thermal network analysis of a chip-heat sink configuration.

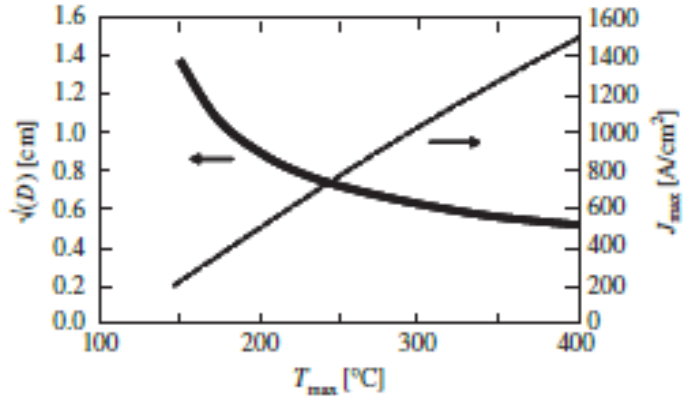

Figure 15: Estimated relation between the maximum chip temperature and chip size/current density of SiC inverter.

density would be $D = 0.9 \times 0.9$ cm^2 and J_{max} = 500 A/cm^2, respectively. These values are well in the scope of manufacturing a PCU of over 100 kW power in a reasonable size.

4.4 Heat sink

To illustrate the relation between the power dissipation and the required performance of heat sinks, Fig.16 describes representative trends of an electronic device: the increase of CPU power dissipation by year [13]. It also shows the required thermal resistance of heat sinks to accommodate the power dissipation. Following the increase of the power density of the inverters, their power dissipation is also getting higher. Since 100 kW SiC inverters are estimated to dissipate about 1.2 kW, which is 10 times as high as that of the CPU, a much more effective heat sink is eagerly required. Liquid cooled heat sinks are thus usually applied to the inverters rather than air cooled ones.

4.5 Combined thermal management

Since an available space for the hybrid system components is getting smaller, many of them are required to be combined together and form an assembly unit. Figure 20 shows the Aisin AW's HD-10 hybrid transmission [15, 16], which is employed in the Ford Escape hybrid. Traction and generator motors, a capacitor, a PCU and etc. are combined together to form a transmission unit there. In such a system, integral thermal management is required rather than for each component. In fact, in the HD-10, to cool the power electronics and electric motors by a single water cooling system, a system consisting of an automatic transmission fluid (ATF)/water heat exchanger and a water cooled heat sink is equipped. The ATF, circulated by an oil pump, cools the two electric motors and provides lubrication for the gear train. The number of fins of each water and ATF channels was optimized considering the balance of heat generation from each component in real world usage.

5 Conclusion

In this chapter, some of important thermal engineering issues and related technologies for designing components of the hybrid car systems are presented. As shown in Table 2, the current gasoline hybrid system enhances the tank to wheel efficiency of the conventional gasoline engine cars to 2.3 times higher. Therefore, the hybrid car systems are very effective technology to cope with the issues on

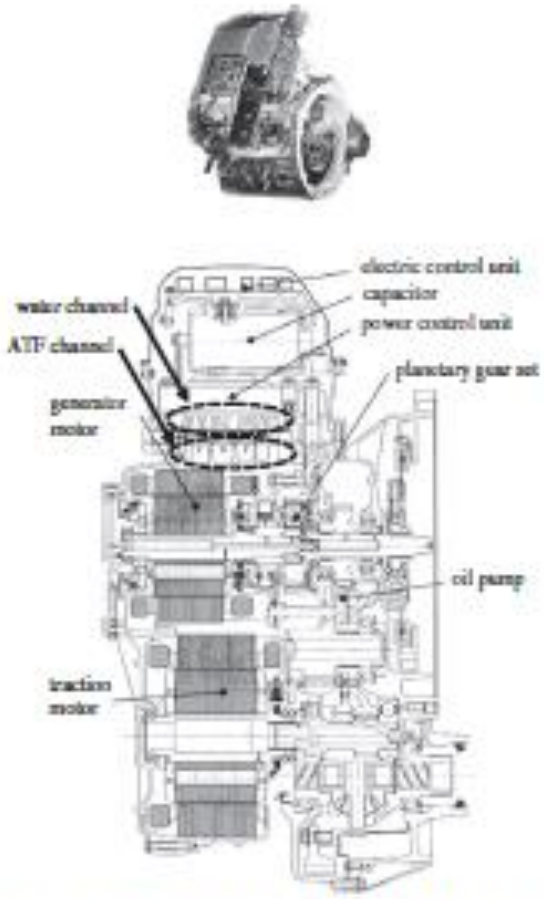

Figure 20: Cross-section of the Aisin AW's HD-10 hybrid transmission.

Table 2: Well to tank/wheel efficiency of hybrid systems.

	Well to tank	Tank to wheel	Well to wheel
Gasoline engine car	88%	16%	14%
Gasoline hybrid car	88%	37%	32%
Hydrogen FCEV	58%	38%	22%
FCHV	58%	50%	29%

the global environment and natural resources as well as economy. As discussed in this chapter, thermal engineering is certainly important to enhance the system efficiency and to maintain its performance for long term usage.